MÁSTER UNIVERSITARIO EN INGENIERÍA INDUSTRIAL
(MII)

TRABAJO FIN DE MÁSTER

STRUCTURE - PROPERTY RELATIONS IN ALIGNED SUPRAMOLECULAR POLYETHYLENE MATERIALS

Autor: Alicia Vivas Hernando

Director: Prof. Holger Frauenrath

Madrid

Agosto de 2021

Declaro, bajo mi responsabilidad, que el Proyecto presentado con el título

Structure-property relations in aligned supramolecular polyethylene materials

en la ETS de Ingeniería - ICAI de la Universidad Pontificia Comillas en el curso académico **2020 - 2021** es de mi autoría, original e inédito y no ha sido presentado con anterioridad a otros efectos. El Proyecto no es plagio de otro, ni total ni parcialmente y la información que ha sido tomada de otros documentos está debidamente referenciada.

Fdo: ALICIA VIVAS HERNANDO   Fecha: 11/08/2021

Autorizada la entrega del proyecto

EL DIRECTOR DEL PROYECTO

Fdo: PROF. HOLGER FRAUENRATH   Fecha: 20/08/2021

MÁSTER UNIVERSITARIO EN INGENIERÍA INDUSTRIAL
(MII)

TRABAJO FIN DE MÁSTER

STRUCTURE - PROPERTY RELATIONS IN ALIGNED SUPRAMOLECULAR POLYETHYLENE MATERIALS

Autor: Alicia Vivas Hernando

Director: Prof. Holger Frauenrath

Madrid

Agosto de 2021

STRUCTURE - PROPERTY RELATIONS IN ALIGNED SUPRAMOLECULAR POLYETHYLENE MATERIALS

Autor: Vivas Hernando, Alicia

Director: Frauenrath, Holger

Entidad Colaboradora: École Polytechnique Fédérale de Lausanne (EPFL)

RESUMEN DEL PROYECTO

Introducción

Las fibras UHMWPE (polietileno de muy alto peso molecular) son fibras de alto rendimiento con propiedades deseables para aplicaciones de ingeniería. Sin embargo, debido a su elevada red de entrelazamiento, precisan métodos de procesamiento que requieren tiempo y coste adicionales y que utilizan disolventes orgánicos perjudiciales para el medio ambiente. El HDPE (polietileno de alta densidad), por otro lado, es altamente reprocesable pero no tiene las propiedades mecánicas suficientes para cumplir con exigencias a nivel industrial, ya que no posee la capacidad de orientación que tiene el UHMWPE.

La modificación supramolecular del PE se ha desarrollado en el pasado para obtener propiedades termomecánicas adaptables y una procesabilidad mejorada, y la incorporación de aditivos semejantes del el laboratorio anfitrión ha desbloqueado la posibilidad de utilizar polietilenos de mayor peso molecular. En particular, se ha observado una ventana de temperatura donde estos materiales se comportan de una manera similar a la goma, abriendo nuevas posibilidades de procesamiento.

Este proyecto pretende aprovechar esta ventana de temperatura para producir fibras de HDPE orientadas que imitan el comportamiento de las fabricadas a partir de UHMWPE, evitando al mismo tiempo los problemas técnicos y ambientales asociados a ellas. Por un lado, el uso de la química supramolecular y el concepto del laboratorio huésped abren una nueva ventana de procesamiento en la que el polímero está totalmente fundido, pero el aditivo todavía puede agregarse. Por lo tanto, la hipótesis es que la presencia de este aditivo influirá en la forma en que el material se oriente, bajo métodos de procesamiento específicos. Por otro lado, el uso de HDPE, así como la formación de enlaces de hidrógeno, asegurará que el material sea fácilmente procesable.

En última instancia, el objetivo del proyecto es investigar un HDPE adecuado para aplicaciones de ingeniería, a través de técnicas de procesamiento específicas que influyen en su orientación.

Metodología

Para el desarrollo del proyecto, las mezclas de polímeros se hicieron a partir de un polietileno modificado y un aditivo. La modificación del polímero se hizo a través de la química supramolecular, mediante la

fijación de grupos finales auto-ensamblables basados en oligopéptidos a ambos extremos de las cadenas de polietileno. Luego, se incorporó un aditivo al polímero para promover la formación de redes supramoleculares dentro del material. Este aditivo se basó en los mismos segmentos autoensamblables. La reacción que intervino en esta mezcla fue una reacción de acoplamiento peptídico. Estas mezclas sintetizadas se llamaban materiales concepto. Se compararon las mezclas prístinas (PE comercial) y de referencia (PE comercial más el aditivo).

En primer lugar, las mezclas se hicieron con dos polietilenos de peso molecular diferente (30K y 100K) y dos aditivos diferentes (cadena corta y cadena larga). Se realizó un cribado preliminar, seleccionando el polímero 30K y el aditivo de cadena corta, por tener las propiedades más adecuadas. Para el desarrollo del resto del proyecto se eligió una concentración del 1% en peso de aditivo.

Las mezclas se caracterizaron con DSC, reología y microscopia óptica dependiente de la temperatura. Los dos primeros experimentos se realizaron para evaluar el perfil de temperatura y el comportamiento fluido de los materiales. El último se realizó para investigar la estructura macro y microscópica del material, así como la posible separación de fases entre el polímero y el aditivo dentro del material.

Cuando las mezclas se caracterizaron correctamente, se produjeron las muestras alineadas. Éstas se hicieron mediante el uso de una extrusora y una rueda giratoria, y luego se midieron utilizando un microscopio óptico. Las fibras se produjeron a tres temperaturas diferentes: 220ºC (AS220), 190ºC (AS190) y temperatura ambiente (estirado en frío, CS190).

Las muestras alineadas se caracterizaron por DSC, difracción de rayos X y ensayos de tracción. Se realizaron experimentos de DSC para evaluar tanto la cristalinidad como las estructuras cristalinas de las muestras orientadas, en comparación con las relajadas, así como la separación de fase. Se realizaron experimentos de difracción de rayos X, tanto en ángulo corto como ancho, para evaluar la orientación de las muestras, así como las distancias y estructuras supramoleculares. Se realizaron pruebas de tracción para analizar la resistencia al rendimiento, el alargamiento, la resistencia y el módulo de Young de los diferentes grupos de muestra.

Resultados

Estudio del material bruto

La Figura 1 muestra los experimentos de DSC y reología realizados en mezclas de polietileno a diferentes concentraciones de aditivos.

Por un lado, una mayor concentración de aditivo dio lugar a la formación de una nueva "meseta gomosa". Los resultados de DSC indicaron un aumento de las temperaturas de agregación y desagregación del aditivo con una mayor concentración de aditivo, lo que finalmente abrió la ventana de temperatura de estos con las temperaturas de fusión y cristalización del polímero. Como se observa en los resultados de reología, esta ventana demostró ser una etapa en la que el material se comportaba como un sólido blando, dando lugar a nuevas oportunidades de procesamiento, por ejemplo, la extrusión de fibras en una etapa donde el polímero se encontrara completamente fundido, pero el aditivo todavía estaba en proceso

de agregación. Esta meseta gomosa aumentó con la concentración de aditivo, y se relacionó con la fuerza de las redes supramoleculares co-ensambladas.

Por otro lado, los experimentos de DSC demostraron el inicio de la separación de fase alrededor del 4% en peso, lo que se evidencia por la aparición de picos dobles en las transiciones del aditivo. Esto se demostró, además, a través de resultados de microscopia óptica, como se puede ver en las mezclas de 8% en peso en la Figura 1.
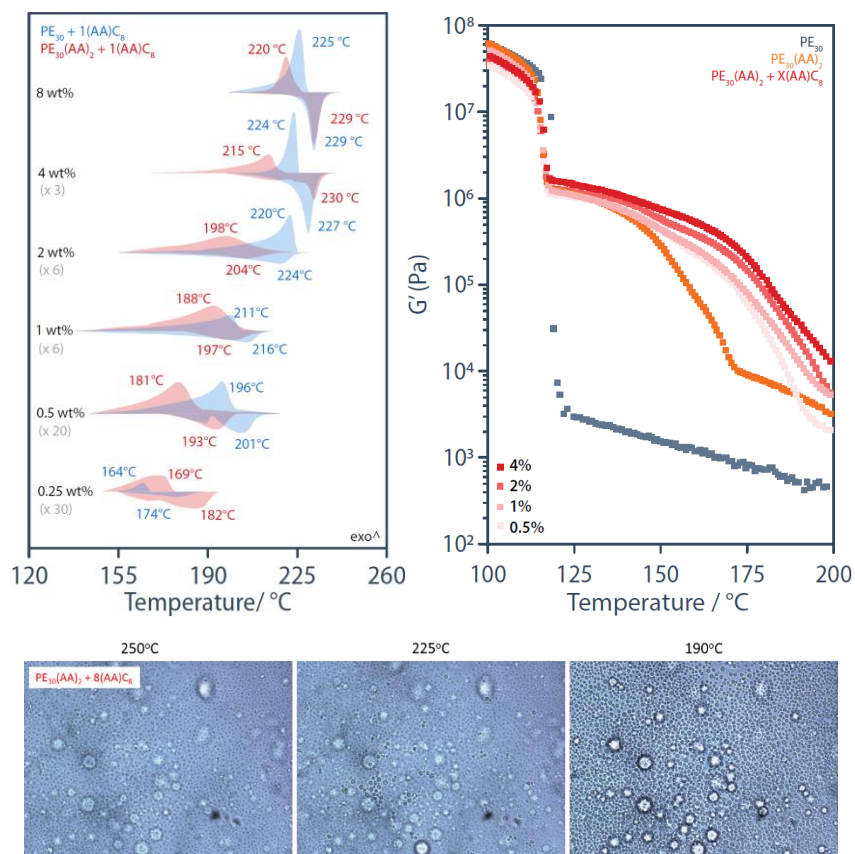

Figura 1. DSC (izquierda), reología (derecha) y miscoscopía óptica (debajo) de las mezclas de polímeros en diferentes conceptraciones de aditivo

Estudio de las muestras alineadas

La Figura 2 muestra los resultados de DSC para las fibras AS220, AS190 y CS190, en un primer ciclo (muestra orientada) y un segundo ciclo (muestra relajada).

Los experimentos de DSC mostraron picos de polímero que tenían un pico predominante a la izquierda para las fibras estiradas en caliente, y a la derecha para las fibras estiradas en frío. Este pico fue tomado como indicativo de dos especies cristalinas diferentes: en el primer caso, una cristalización laminar; en el segundo caso, una cristalización fibrilar. Esto se acentuó aún más por el cambio en las temperaturas máximas del polímero de las fibras estiradas en frío, que representaban un mecanismo de cristalización diferente. Además, el PE mostró una disminución de la cristalinidad en las fibras extruidas en caliente, mientras que esta cristalinidad aumentó para las estiradas en frío.

En cuanto a los picos de aditivo, la observación más notable fue el aumento de la cristalinidad en las fibras extruidas en caliente, en comparación con la muestra relajada. Este efecto no se observó en las fibras estiradas en frío.
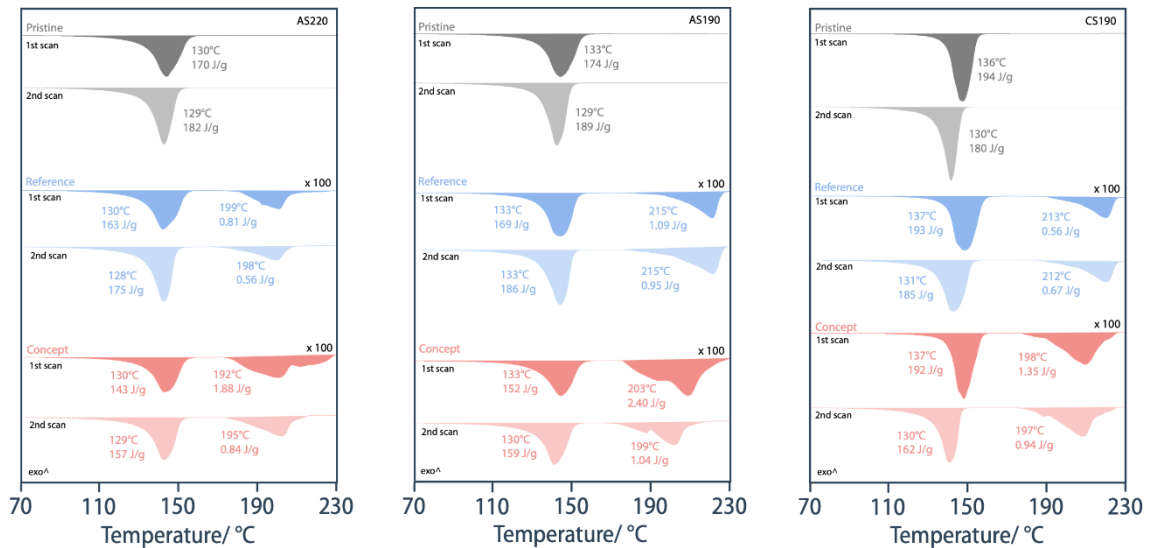

Figura 2. Experimentos de DSC para AS220 (izquierda), AS190 (centro) y CS190 (derecha), tanto orientadas (1er scan) como relajadas (2º scan).

Figura 3 muestra los experimentos de difracción de rayos X de las muestras.

Para las fibras extruidas en caliente, se obtuvo una periodicidad a lo largo del eje de la fibra, como se revela en las integraciones azimutales. Esto sería representativo de láminas apiladas, demostrando la explicación tomada a partir de los resultados del DSC. Sin embargo, las fibras AS220 mostraron distancias interlaminares más bajas que las fibras AS190, lo que indica que estas últimas podrían estar evolucionando hacia estructuras más largas, como los cristales fibrilares. En cuanto al grado de orientación, las fibras AS220 mostraron la mayor orientación en materiales prístinos, seguido por el concepto y luego la referencia. AS190 mostró la mayor orientación en los materiales conceptuales, seguido por la prístina y luego la referencia.

Las fibras estiradas en frío mostraron una periodicidad perpendicular al eje de la fibra, que sería representativa de los cristales fibrilares. Las integraciones azimutales mostraron una orientación similar en todos los materiales, como también se puede observar en las distancias interlaminares.
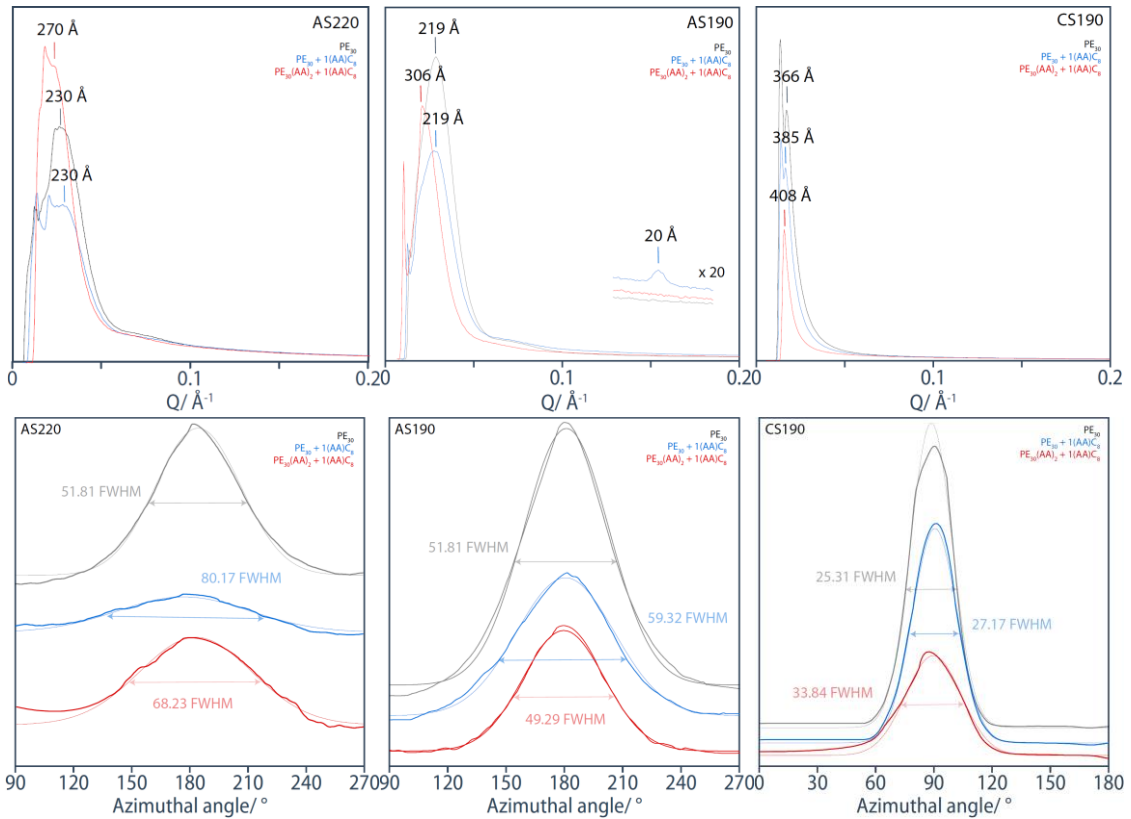
Figura 3. Experimentos SAXS de AS220 (izquierda), AS190 (centro) y CS190 (derecha) para la integración 2-theta (arriba) y azimuthal (debajo)

La Figura 4 muestra las propiedades mecánicas obtenidas para los diferentes grupos de muestras.

La elongación se incrementó considerablemente en el material concepto extruido en caliente, y el límite elástico no pareció verse muy afectado en este caso. De hecho, para las fibras AS190, en realidad aumentó en comparación con las fibras prístinas.

La tenacidad aumentó en los materiales conceptuales independientemente del método de procesamiento, y el módulo de Young no parecía verse afectado por los grupos de muestras.

Más notablemente, las fibras AS190 tuvieron un aumento simultáneo en tenacidad, límite elástico y alargamiento, lo que es significativo de un mejor rendimiento y potencial.
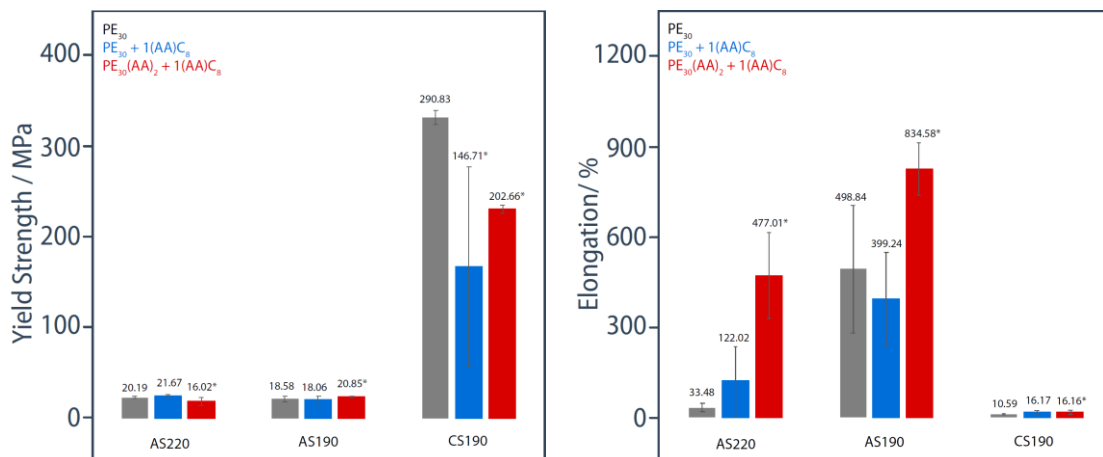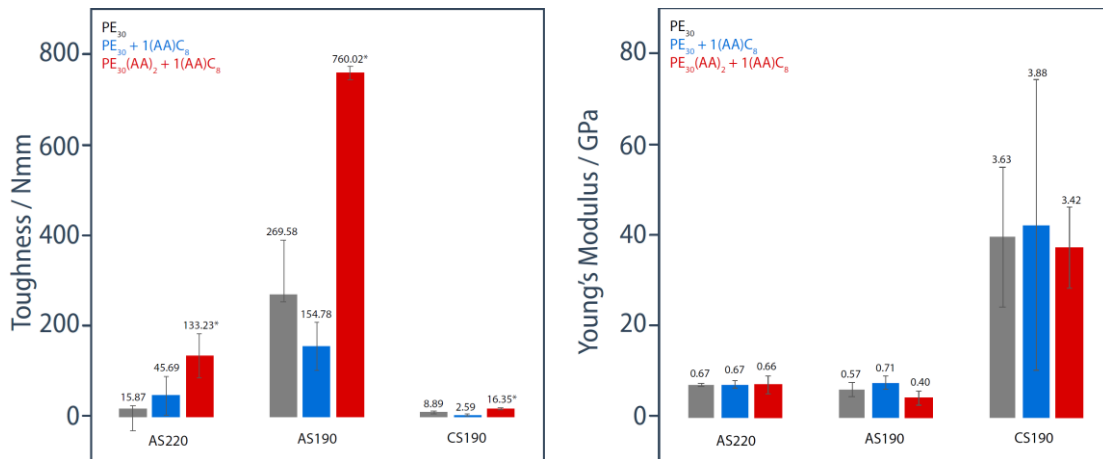
Figura 4. Propiedades mecánicas de las fibras alineadas.

Conclusiones

Por un lado, en cuanto a los materiales en bruto, se confirmó la formación de una nueva meseta gomosa debido a la presencia de la modificación del polímero y la incorporación de aditivo. Esta meseta gomosa permitió que el material se comportara como un sólido blando, y estaba presente entre las temperaturas de transición del polímero y las del aditivo. La longitud de esta meseta se amplió con el aumento de la concentración de aditivo, pero la incorporación de demasiado aditivo llevó a la segregación de fase, como se demostró a través de los experimentos de microscopia óptica.

Por otro lado, con respecto a las muestras alineadas, los resultados de DSC insinuaron la presencia de dos mecanismos de cristalización competidores dentro de los materiales, dando lugar a dos superestructuras cristalinas diferentes dependiendo de si el proceso se realizó a altas temperaturas o en condiciones ambiente. Se hipotetizó que estas dos estructuras eran cristales laminares y fibrilares, y estaban representados por un pico predominante izquierdo o derecho, respectivamente. Los resultados de XRD confirmaron esta hipótesis cuando las integraciones azimutales de muestras estiradas en caliente mostraron periodicidad a lo largo del eje de fibra, representativa del apilamiento laminar, mientras que las integraciones azimutales de muestras estiradas en frío mostraron periodicidad perpendicular a este eje, representando cristales fibrilares. Particularmente en las fibras AS190, los materiales conceptuales mostraron la mayor orientación, como se indica en las integraciones azimutales. Los ensayos de tracción mostraron una mayor tenacidad independientemente del método de procesamiento en las fibras conceptuales, con fibras AS190 teniendo el mejor rendimiento y sin *tradeoff* de la tenacidad y el límite elástico. Este mayor rendimiento mecánico se atribuyó al efecto sinérgico de la modificación de las cadenas y la metodología de procesamiento. En otras palabras, la modificación del polímero y la incorporación del aditivo no modificaron las propiedades mecánicas *per se* de los materiales, sino que dieron lugar a oportunidades de procesamiento que podrían hacerlo. Estas oportunidades de procesamiento consistían en fundir el material a una temperatura cercana a la temperatura de agregación del aditivo, de modo que una secuencia de roles de carga, primero del entrelazamiento del polímero y luego de las nanofibras del aditivo solidificado, fuera promovida.

STRUCTURE - PROPERTY RELATIONS IN ALIGNED SUPRAMOLECULAR POLYETHYLENE MATERIALS

Author: Vivas Hernando, Alicia

Director: Frauenrath, Holger

Collaborating Entity: École Polytechnique Fédérale de Lausanne (EPFL)

PROJECT SUMMARY

Introduction

UHMWPE fibers are high-performance fibers with desirable properties for engineering applications. However, because of their high entanglement network, they require time- and cost-intensive processing methods that use environmentally detrimental organic solvents. HDPE, on the other side, is highly reprocessable but does not have the sufficient mechanical properties to fulfill industrial applications, as it does not possess the ability to orient as UHMWPE does.

Supramolecular modification of PE has been developed in the past to obtain tailorable thermomechanical properties and enhanced processability, and the incorporation of matching additives by the host laboratory has unlocked the possibility to use higher molecular weight polyethylenes. In particular, a temperature window has been observed where these materials behave in a rubber-like manner, opening up new processing possibilities.

This project aims to take advantage of this temperature window to produce oriented HDPE fibers that mimic the behavior of those made from UHMWPE, whilst avoiding the technical and environmental issues associated to them. On the one hand, the use of supramolecular chemistry and the concept of the host laboratory brings a new processing window in which the polymer is fully molten but the additive may still aggregated. Therefore, the hypothesis is that the presence of this additive will influence the way in which the material orients, under specific processing methods. On the other hand, the use of HDPE, as well as hydrogen-bonding ligands, will ensure that the material is easily processable.

Ultimately, the goal of the research project is to investigate a HDPE material that is suitable for engineering applications, through specific processing techniques than influence its orientation.

Methodology

For the development of the project, polymer blends were synthesized from a modified polyethylene and an additive.The modification of the polymer was done through supramolecular chemistry, by attaching oligopeptide-based self-assembling end groups to both ends of the polyethylene chains. Then, an additive was incorporated to the polymer in order to promote the formation of supramolecular networks within the material. This additive was based on the same self-assembling segments. The reaction intervening in

this blend was a peptide coupling reaction. These synthesized blends were called concept materials. Pristine (commercial PE) and reference (commercial PE plus the additive) blends were made for comparison.

First, the blends were made with two different molecular weight polyethylenes (30K and 100K) and two different additives (short chain and long chain). A preliminary screening was performed, deciding on the 30K polymer and the short chain additive, because of desirable properties. For the development of the rest of the project, a concentration of 1 wt% of additive was chosen.

The blends were first characterized by DSC, rheology and temperature-dependent optical microscopy. The first two experiments were performed to assess the temperature profile and flow behavior of the materials. The latter was performed to investigate the macro and microscopic structure of the material, as well as the possible phase separation of polymer and additive within the material.

When the blends were correctly characterized, the aligned samples were developed. These were done by the use of an extruder and a spinneret, and then measured using an optical microscope. The fibers were produced at three different temperatures: 220ºC (AS220), 190ºC (AS190) and room temperature (cold-stretched, CS190).

The samples were characterized by DSC, X-ray diffraction and tensile testing experiments. DSC experiments were performed to assess both the crystallinity and crystalline structures of the oriented samples, compared to relaxed ones, as well as the phase separation. X-ray diffraction experiments were performed, both at short and wide angle, to evaluate the orientation of the samples, as well as the supramolecular distances and structures. Tensile testing was performed to analyze yield strength, elongation, toughness and Young's modulus of the different sample groups.

Results

Study of the bulk material

Figure 1 shows the DSC and rheology experiments performed on polyethylene blends at different additive concentrations.

On the one hand, a higher concentration of additive resulted in the formation of a new rubbery plateau. DSC results indicated increased additive aggregation and disaggregation temperatures with increased additive concentration, which ultimately opened up the temperature window of these with the polymer melting and crystallization temperatures. As seen in the dynamic shear rheology results, this window proved to be a stage in which the material behaved like a soft solid, giving rise to new processing opportunities, for instance, fiber drawing at a stage where the polymer was fully molten, but the additive was still in the process of aggregating. This rubbery plateau increased with the amount of additive, and so it was related to the strength of the co-assembled supramolecular networks.

On the other hand, DSC experiments proved the initiation of phase separation at around 4 wt%, which is evidenced by the appearance of double transition peaks. This was further proved through optical microscopy results, as can be seen in the 8 wt% blends in Figure 1.
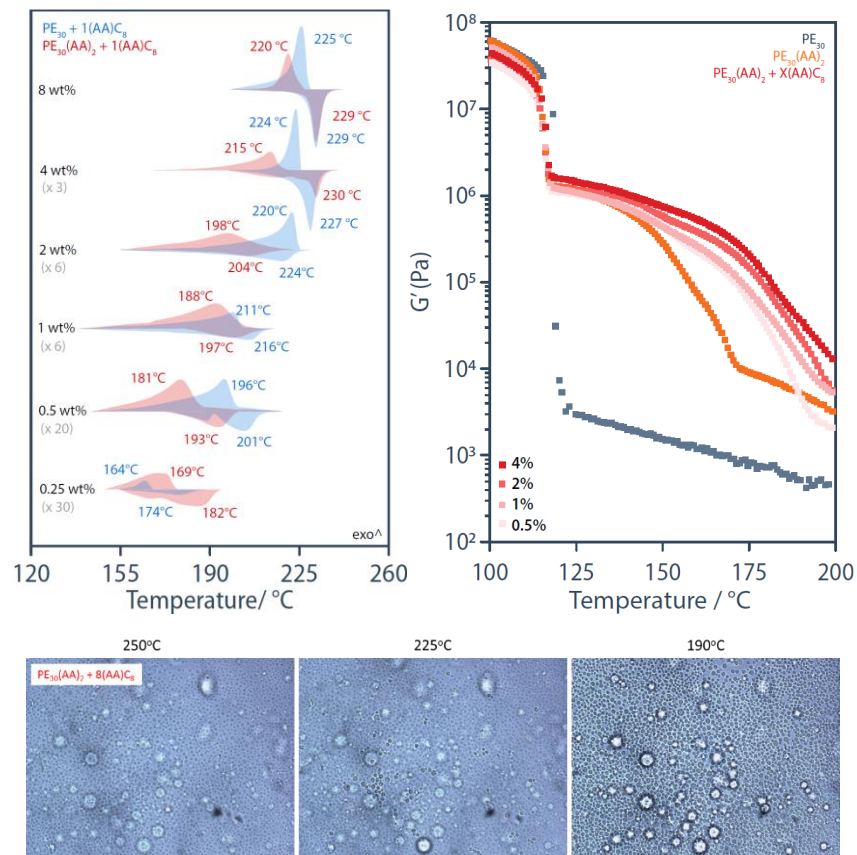

Figure 1. DSC (left), dynamic shear rheology (right) and optical micrographs (bottom) of polymer blends at different additive concentrations.

Study of the aligned samples

Figure 2 shows the DSC results for AS220, AS190 and CS190 fibers, on a 1st scan (oriented sample) and a 2nd scan (relaxed sample).

DSC experiments showed polymer peaks that had a predominant shoulder to the left for the melt-spun fibers, and to the right for cold-stretched fibers. This shoulder was taken as an indicative of two different crystalline species: in the first case, a lamellar crystallization; in the second case, a fibrillar crystallization. This was further emphasized by the shift in polymer peak temperatures of the cold-stretched fibers, which represented a different crystallization mechanism. Moreover, PE showed decreased crystallinity in melt-spun fibers, whereas this crystallinity increased for the cold-stretched ones.

As for the additive peaks, the most notable observation was the increased crystallinity in the melt-spun fibers, compared to the relaxed sample. This effect was not observed in the cold-stretched fibers.
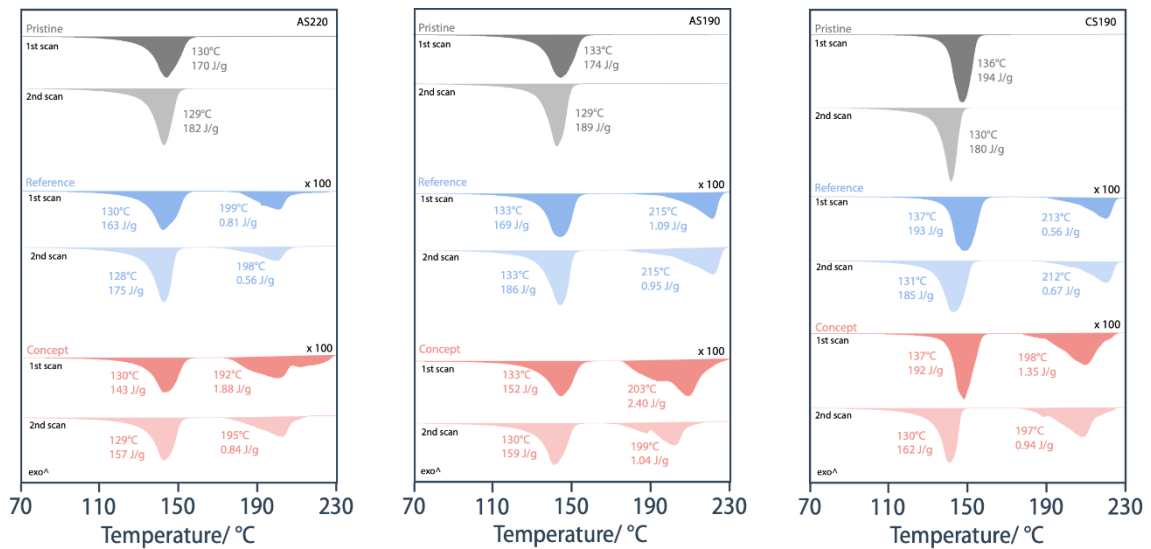
Figure 2. DSC experiments of AS220 (left), AS190 (middle) and CS190 (right) fibers, when oriented (1st scan) and relaxed (2nd scan).

Figure 3 shows the X-ray SAXS experiments for the aligned samples.

For both melt-spun fibers, a periodicity along the fiber axis was obtained, as revealed in the azimuthal integrations. This would be representative of stacked lamellae, therefore proving the point made from the DSC results. Still, the AS220 fibers showed lower interlamellar distances than the AS190 fibers, indicating that the latter may be evolving into longer structures, such as fibrillar crystals. As for the degree of orientation, AS220 fibers showed the most orientation in pristine materials, followed by concept and then reference. AS190 showed the most orientation in concept materials, followed by pristine and then reference.

The cold-stretched fibers showed periodicity perpendicular to the fiber axis, which would be representative of fibrillar crystals. Azimuthal plots showed similar orientation in all materials, as can be also observed in the interlamellar distances appearing through the 1D plotted peaks.
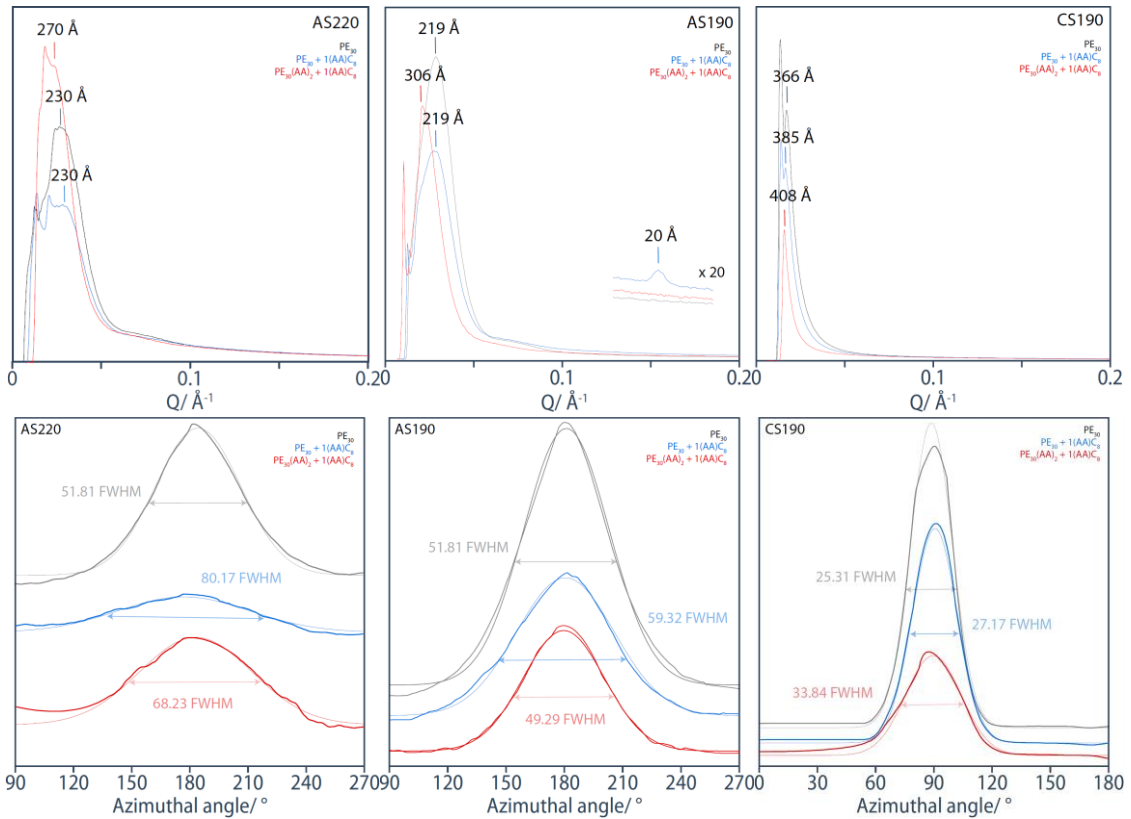
Figure 3. SAXS experiments of AS220 (left), AS190 (middle) and CS190 (right) samples, for both 2-theta (top) and azimuthal (bottom) integrations.

Figure 4 shows the mechanical properties obtained for the different sample groups.

Elongation was greatly increased in the concept melt-spun fibers, and the yield strength did not seem to be greatly affected in this case. In fact, for the AS190 fibers, it actually increased in comparison to the pristine fibers.

Toughness increased in the concept materials regardless of the processing method, and Young's modulus did not seem to be affected by sample groups.

Most notably, AS190 fibers had a simultaneous increase in toughness, yield strength and elongation, which is significative of improved performance and potential.
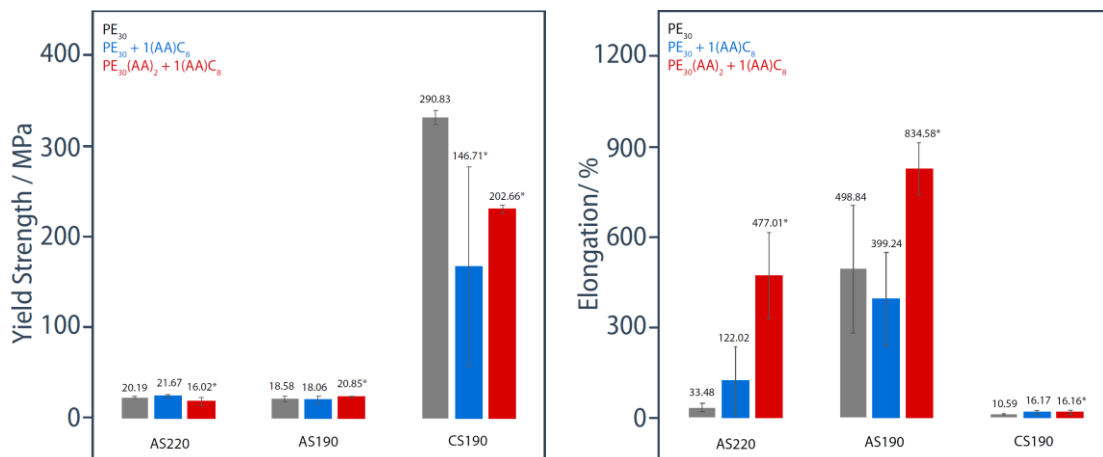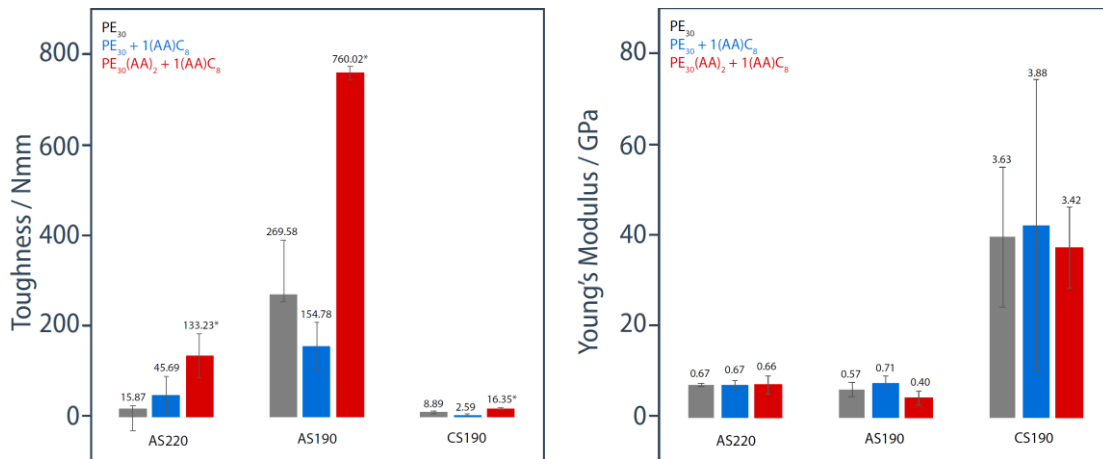
Figure 4. Mechanical properties of aligned samples.

Conclusions

On the one hand, regarding the bulk materials, it was confirmed that a new rubbery plateau was formed due to the presence of the end-modification and incorporation of additive. This rubbery plateau enabled the material to behave as a soft solid, and was present between the transition temperatures of the polymer and those of the additive. The length of this plateau was extended with increasing additive concentration, but incorporating too much additive led to phase segregation, as proved through the optical microscopy experiments.

On the other hand, regarding the aligned samples, DSC results hinted on the presence of two competing crystallization mechanisms within the materials, leading to two different crystalline superstructures depending on if the process was done at high temperatures or at ambient conditions. It was hypothesized that these two structures were lamellar and fibrillar crystals, and were represented by a predominant left and right shoulder in the polymer peak, respectively. XRD results confirmed this hypothesis when the melt-spun sample azimuthal plots showed periodicity along the fiber axis, representative of lamellar stacking, whereas the cold stretched sample azimuthal plots showed periodicity perpendicular to this axis, representing fibrillar crystals. Particularly in the AS190 fibers, the concept materials showed the most orientation, as indicated in the azimuthal plots. Tensile testing experiments showed increased toughness regardless of the processing method in concept fibers, with AS190 fibers having the best performance and no trade-off of toughness and yield strength. This enhanced mechanical performance was attributed to the synergistic effect of the end-modification and the processing methodology. In other words, the end-modification and incorporation of additive did not change the mechanical properties per se of the materials, but gave rise to processing opportunities that could do so. These processing opportunities involved melt-spinning the material at a temperature close to the aggregation temperature of the additive, so that a sequence of load-bearing roles, first from the polymer entanglement and then from the just solidified additive nanofibrils, was promoted.

ACKNOWLEDGEMENTS

INDEX

LIST OF ABBREVIATIONS

ε	strain
σ	stress
Ac	acetyl
Ala	L-alanine
$CHCl_3$	chloroform
DCM	dichloromethane
DIPEA	N,N - diisopropylethylamine
DMSO	dimethyl sulfoxide
DSC	differential scanning calorimetry
exo	exothermic
G'	shear storage modulus
G''	shear loss modulus
GPC	gel permeation chromatography
HDPE	high-density polyethylene
M	molar
MeOH	methanol
M_n	number-average molecular weight
M_w	weight-average molecular weight
MW	molecular weight
NMR	nuclear magnetic resonance
PE	polyethylene
ppm	parts per million
PyBOP	benzotriazole-1-yloxy-tris(pyrrolidino)phosphonium hexafluorophosphonate
ROMP	ring opening metathesis polymerization
r.t.	room temperature
rpm	revolutions per minute

SAXS	small-angle X-ray scattering
tan δ	loss factor
T_c	crystallization temperature
THF	tetrahydrofuran
T_m	melting point
Tol	toluene
wt %	weight percentage
WAXS	wide-angle X-ray scattering
XRD	X-ray diffraction

CHAPTER 1

INTRODUCTION

MOTIVATION

Polyethylene (PE) is the world's most used polymer [1]. With an annual production of nearly 100 million tons in 2018 [2], it accounts for over 30% of the total plastic use [3]. This prevalence, mainly due to desirable properties such as toughness, resistance to moisture and chemical inertness, enables it to be manufactured in a broad range of grades, which are classified mostly by density and chain branching [4].

The main application of polyethylene is packaging [3], either in "softer" applications with lower density PE, like plastic bags and films, and more "rigid" applications, such as bottles, for higher density PE. A common end-of-life treatment is reprocessing [5], which is straightforwardly done from the melt for these PE grades [6]. Other applications include construction, automotive, electrical, electronic, agricultural, medical and ballistics. Still, engineering applications are vastly underexploited due to lack of appropriate combinations of strength, stiffness and toughness, and they are mostly dominated by ultra-high molecular weight polyethylene (UHMWPE). This grade of polyethylene, with unbranched polymer chains and molecular weights of up to 6 million g/mol, is mostly used in industrial applications because of its excellent mechanical properties, as well as for its chemical inertness, lubricity and abrasion resistance [7]. Moreover, it has an intrinsic ability to orient into fibrils when processed correctly, allowing for the production of high-performance fibers with yield strengths comparable to high-strength steels [7]. A major drawback of this material is its processability. Because of its high chain entanglement, UHMWPE is too viscous to be processed from the melt, and thus is usually processed from a gel state, using organic solvents [6]. Therefore, one of the biggest challenges regarding polyethylene materials stems from the tradeoff between their mechanical properties and their processability. For engineering applications, where these mechanical properties need to satisfy more demanding constraints, the required polyethylene grades have poor processability and disadvantages both at an economic level, as they involve specific techniques, and at an environmental level, as they require the use of organic solvents [8]. Hence, the challenge is to create a polyethylene grade that has an appropriate combination of strength, stiffness and toughness for engineering applications but remains easily processable.

A common strategy for the development of high-performance plastics is polymer blending, where the combination of different properties results in novel materials with enhanced mechanical properties [9]. In particular, an approach that enables the tailoring of the processability and properties of polymers is the use of thermoplastic elastomers, which are materials composed of soft and hard segments that behave as elastomers at room temperature but have thermoreversible non-covalent crosslinks [10]. Fields such as supramolecular chemistry capitalize on these existing crosslinks by adding matching fillers that form hydrogen bonds with the hard segments, extending these crosslinks into networks [11]. Similar strategies can be applied to polyethylene materials [69], where a supramolecular modification could lead to tailored thermomechanical properties. What is more, this technique could open up new frontiers in polyethylene processing, as well as influence orientation and subsequent improvement of mechanical properties.
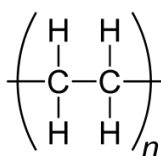
STATE OF THE ART

POLYETHYLENE MATERIALS

Polyolefins are polymers derived from olefins, also called alkenes (C_nH_{2n}). In particular, polyethylene (PE) is a type of polyolefin defined by the formula $(C_2H_4)_n$, corresponding to the molecular structure that is shown in Figure 5.

Figure 5. Molecular structure of polyethylene.

Polyethylene is produced through the polymerization of ethene ($CH_2=CH_2$), which is usually obtained from petrochemical sources, although it can also be made by dehydration of ethanol. The specific polymerization methodology used will determine the different polyethylene grades, which can be classified either by their density or their chain branching on the molecular level. Amongst the branched grades, the most common one is low-density polyethylene (LDPE), whereas the linear grades are mostly dominated by high-density polyethylene (HDPE), ultra-high molecular weight polyethylene (UHMWPE) and linear low-density polyethylene (LLDPE). Still, there other less common grades that cover other density ranges or molecular weights.

Polyethylene is a thermoplastic material and, as such, its temperature behavior is characterized by softening or melting upon heating and solidification upon cooling. In fact, it is a semi-crystalline type of thermoplastic material, meaning it has amorphous and crystalline domains within its internal structure, in varying compositions. At a molecular level, the crystalline areas are composed of densely packed PE chains, ordered in an orthorhombic unit cell, and typically folded into hairpin folds to form 2D crystalline lamellae with a thickness on the order of a few nanometers. The amorphous regions are formed by randomly oriented, entangled chains [38]. These crystalline and amorphous fractions can then arrange into different superstructures. On the one hand, if the crystallization of polyethylene begins at a single nucleus point, the resulting structure consists of the crystalline lamellae arranged in a star-like structure, called a spherulite [39]. This can be observed in Figure 6.
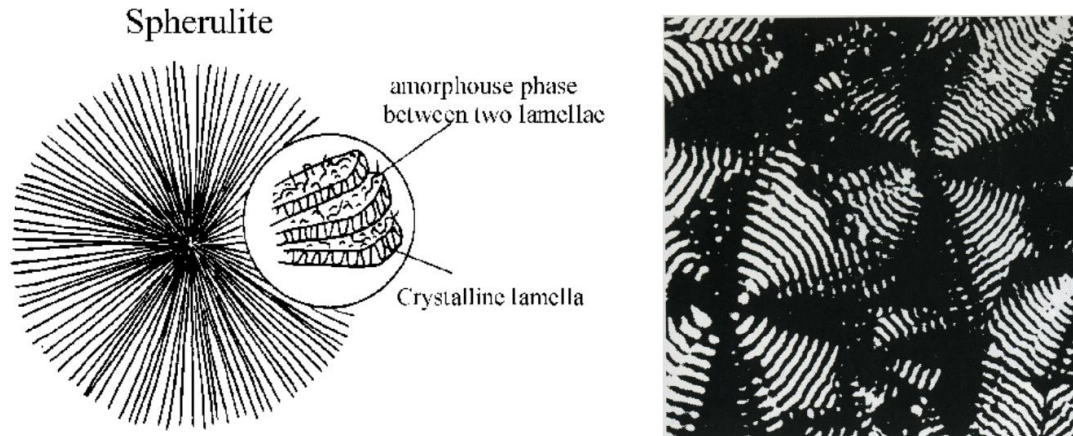
Figure 6. Schematic representation (left) [39] and optical micrograph (right) [40] of a spherulite structure.

On the other hand, according to the Hosemann-Bonart model [41], the crystalline regions in PE can aggregate into lamellar structures that are tied together by amorphous regions. These layers are characterized by crystalline layer thickness, d_c, and amorphous layer thickness, d_a, adding up to the long period d_{ac}. Alternating layers of these become fibers, and then these bundle into fibrils, as shown in Figure 7 [42]. These superstructures appear mostly under deformation, especially in higher molecular weight polyethylene materials, as they are usually a product of chain orientation [43].
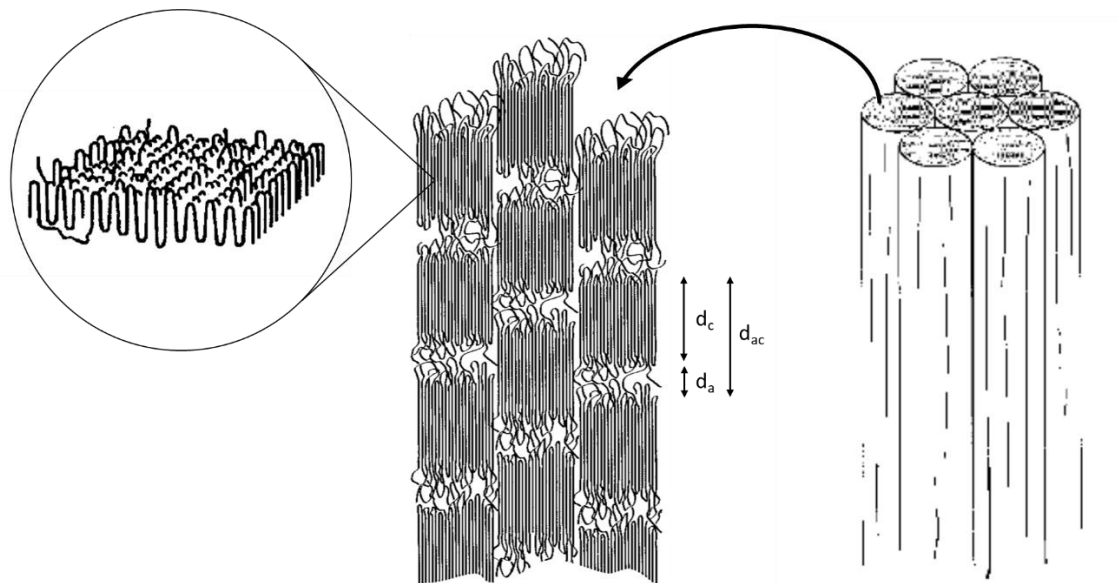
Figure 7. Schematic representation of polyethylene according to the Hosemann- Bonart model [42], with crystalline lamellae (left), fibers (middle) and firbils (right).

Finally, there can exist a combination of fibrillar and spherulite structures, resulting in so-called shish-kebab structures [44]. In this case, the main element, or "shish", is a fibril, and the "kebab" part consists of crystalline lamellae arranged as spherulites, as is portrayed in Figure 8.
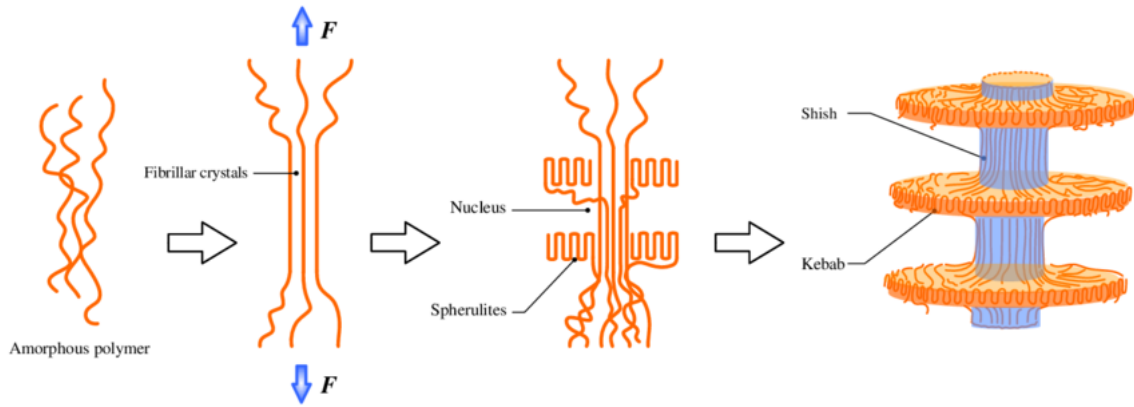
Figure 8. Schematic representation of the formation of a shish-kebab structure [45].

The mechanical and physical properties of polyethylene are strongly affected by both branching and molecular weight, which are directly related to chain density and crystallinity. As for the physical properties, a highly crystalline polyethylene involves densely packed chains that therefore require a low degree of branching. A high branching ratio hampers chain packing, resulting in lower crystallinity. As for the mechanical properties, they are mostly influenced by the fraction and arrangement of the crystalline and amorphous fraction. A high degree of crystallinity will result in higher stiffness, tensile strength and hardness, as well as chemical resistance [46]. However, it will also decrease impact strength and tensile crack resistance. As for the amorphous domains, a larger amount will result in higher elasticity [47]. The basic thermomechanical properties of common polyethylene materials are summarized in Table 1.

Table 1. Properties of LDPE and HDPE [48].

Property	LDPE	HDPE
Density [g/cm³]	$0.915 - 0.935$	$0.942 - 0.965$
Degree of crystallinity [%]	40 - 50	60 - 80
Young's modulus (23 ºC) [GPa]	0.2	1
Tensile strength [MPa]	8 - 15	20 - 30
Ultimate elongation [%]	600	400 - 800
Shear modulus [GPa]	$0.1 - 0.2$	$0.7 - 1.0$
Bending strength [MPa]	10	35
Thermal expansion coefficient [1/K]	$1.7 \cdot 10^{-4}$	$2.0 \cdot 10^{-4}$
Melting temperature [ºC]	105 - 110	130 - 135

HIGH-DENSITY POLYETHYLENE (HDPE)

High-density polyethylene (HDPE) is an unbranched grade of polyethylene with a density of 0.942 to 0.965 g/cm^3 and a characteristically high strength-to-density ratio [48]. The lack of branching is achieved by the type of polymerization performed, which is done using catalysts such as homogeneous organometallic (metallocene) catalysts, heterogeneous Ziegler-Natta catalysts or Phillips-type catalysts. The resulting reaction is exothermic, with an average standard enthalpy of around 105 kJ/mol [49]. Other properties of HDPE are summarized in Table 1. Its uses generally include hard packaging, such as bottles, although it is also used in pipe systems and other applications that require harder materials. Still, the use of HDPE remains mostly restricted to commodity uses, and it does not have great presence in structural or engineering applications.

Deformation mechanisms

Upon drawing, HDPE has the ability to orient, that is, to acquire a fibrous structure in which most of the polymer chains are aligned along the orientation direction and stack in planar, chain-folded crystals (see Figure 7) [50]. As represented in Figure 9, there are several mechanisms that take place during this deformation, namely [51]:

- *Fibrillar slip*. It involves the fibrils shearing relative to each other.

- *Lamellar slip*. It entails lamellar crystals shearing over each other, and it accounts for most of the elastic deformation of the material under cold drawing [51].

- *Chain slip*. It results in the deformation of the crystals by crystallographic slip parallel to the chain direction, and it accounts for the plastic deformation of the material under cold drawing [51].
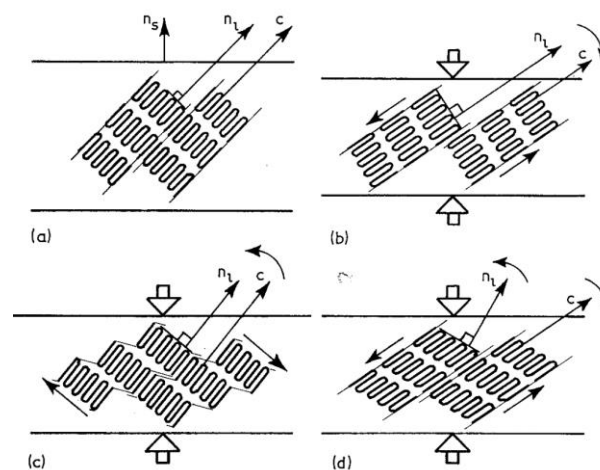

Figure 9. Schematic diagram of (a) the structure before deformation; (b) after fibrillar slip; (c) after lamellar slip and (d) after chain slip. c represents the chain direction, n_c is the surface normal of the lamella crystals and n_s is the surface normal of the specimen (parallel to compression direction) [51].

The degree of orientation of HDPE is greatly influenced by the cold draw ratio, theoretically achieving higher orientation at higher draw ratios [52]. In fact, there is a strong correlation of this strain rate with the Young's modulus, and this correlation was even found to translate to hot-drawing processes [53]. Moreover, when the process is performed at an elevated temperature rather than at ambient conditions, the long spacing, d_{ac}, is affected, increasing with increased draw temperature [54].

ULTRA-HIGH MOLECULAR WEIGHT POLYETHYLENE (UHMWPE)

Ultra-high molecular weight polyethylene (UHMWPE) is a linear homopolymer with a viscosity-average molecular weight of up to 6 million g/mol (compared to a 200,000 g/mol for a typical HDPE grade) [7]. It is characterized by a notable impact resistance and toughness, as well as chemical inertness, lubricity and abrasion resistance.

With regards to its structure, UHMWPE has crystalline lamellae that result from the folding of the polymer chains during the cooling process, and these lamellae are embedded in amorphous regions and connected through tie molecules [55]. The degree and orientation of these crystalline regions depend on factors such as the molecular weight, processing conditions and environmental conditions of the polymer. The high crystallinity is what gives this material its good mechanical properties. However, because of the high chain entanglement, UHMWPE is too viscous to be processed from the melt, as it decomposes before it is able to flow [56]. Therefore, the usual approach to UHMWPE processing involves the use of organic solvents to uncoil the polymeric chain and spin filaments from the gel state [57].

High-performance fibers

UHMWPE has an intrinsic ability to orient into fibrillar crystals if correctly processed, resulting in extremely long chains of polyethylene that are aligned in the same direction and linked to one another through many van der Waals bonds [57]. UHMWPE fibers, such as the commercially available Dyneema® fibers, are highly oriented gel-spun strands that can achieve orientation of over 95% and a level of crystallinity of around 85%. Moreover, they allow yield strengths up to 15 times higher than steel, for the same weight [57], making these fibers extremely useful in industry. The excellent mechanical properties of UHMWPE fibers are attributed to the high orientation and crystallinity of their molecular structure and the high bond energy of C-C [7]. Moreover, they are resistant to water and moisture, most chemicals, ultraviolet radiation and microorganisms [57]. However, because of the weak bonding between molecules, local thermal excitations may disrupt the crystalline structure of UHMWPE fibers, causing these materials to have lower heat resistance than other high-strength fibers. In fact, although their melting point lies around 144 to 152ºC, they cannot be used at temperatures exceeding 80 to 100ºC for extended periods of time [57].

UHMWPE materials are normally structured as stacked lamellae. When gel-spun, these lamellae start to slip, decreasing their lateral sides, while the amorphous layers between them elongate to create fibrillar

crystals ("shish"), resulting in what has been referred to as a "shish-kebab" structure. Upon further strain, the lamellae completely stretch to exclusively form fibrillar crystals [55]. Therefore, when stretching UHMWPE, a highly oriented material can be obtained. Figure 10 illustrates the process from the usual shish-kebab structures of UHMWPE to the fibrillar crystals that form upon high-strain hot stretching. The manufacturing of these fibers requires specialized, high-cost processes such as gel-spinning. To do so, the polymer is first dissolved into a dilute solution which is then melt-spun to form a solvent-containing gel fiber. This solvent-rich fiber needs to either be treated with a second solvent to eliminate the first one, or at least dried or left to evaporate in order to form the solid fiber [58]. In addition to the high cost and time-consuming process, a great disadvantage in the manufacturing of UHMWPE fibers is the negative environmental impact caused by the organic solvents used in the process.
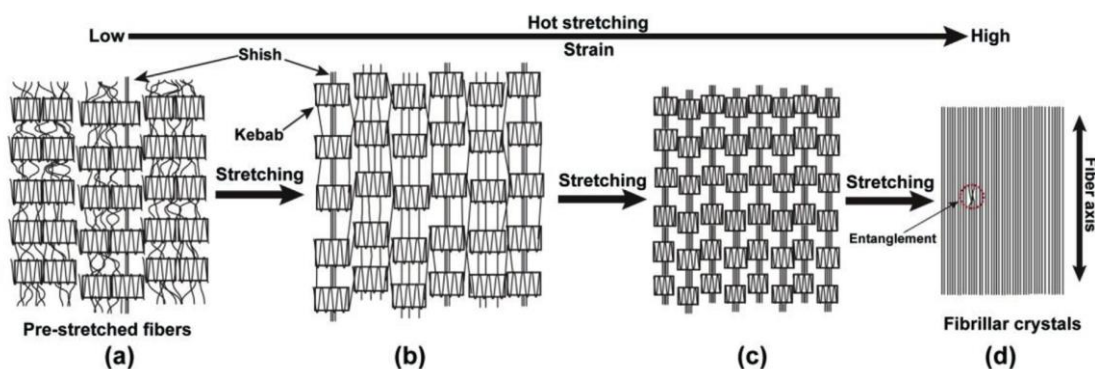

Figure 10. Schematic diagram of the structural evolution of UHMWPE fibers upon hot stretching [55].

UHMWPE fibers are used in applications such as armors, where they are woven and layered at various angles to create composite materials. Other uses include cut-resistant gloves, climbing equipment, vehicle armors or, in general, any type of application that requires high abrasion, chemical or moisture resistance.

THERMOPLASTIC ELASTOMERS

The concept of thermoplastic elastomers (TPEs) was commercially introduced by the Shell Chemical Company (U.S.A.) in 1965 as a material that possessed the properties of rubber at room temperature, but with the ability to be processed by rapid thermoplastics processing techniques instead of chemical vulcanization [12].

On the one hand, rubbers are high-resilience, high-tensile strength, and abrasion-resistant materials formed by covalently crosslinked polymer chains. This crosslinking occurs during the curing process of elastomers through vulcanization, which is irreversible. On the other hand, thermoplastics are polymers that soften or melt upon heating, allowing for multiple reprocessing cycles. A block copolymer A-B-A structure, where A is a "hard" glassy-amorphous or crystalline segment and B is a "soft", extensible segment, enables thermoplastic elastomers to behave as vulcanized rubber at room temperature but to flow like a thermoplastic when heated above the glass transition or melting temperature of the "hard"

segments [10]. This behavior is possible due to the nature of their crosslinks. While conventional rubbers are crosslinked through primary valence bonds, thermoplastic elastomers rely on secondary valence bonds such as Van der Waals interactions, dipole interactions or hydrogen bonds [13]. At high temperatures or under the influence of specific solvents, these bonds break down; upon cooling or disappearance of the solvent, they are restored with no damage to the material.

Depending on the polymers that compose these segments, there are six generic classes of commercially available TPEs, namely:

- *Styrenic block copolymers (SBCs)*. Styrenic block copolymers are formed by polystyrene end blocks and polybutadiene, polyisoprene, poly(ethylene-butylene), poly(ethylene-propylene) or, most recently, isobutylene mid-blocks [14]. SSBCs are most commonly used in footwear, adhesives and seals or grips with low specifications.

- *Thermoplastic polyolefins (TPOs)*. Thermoplastic polyolefins are formed by blends of impact-modified polypropylene and other polyolefins, such as polyethylene; they possess high impact resistance, low density and good chemical resistance [15]. TPOs are most commonly used in automotive applications.

- *Thermoplastic vulcanizates (TPVs)*. Similar to TPOs, thermoplastic vulcanizates are composed of blends between dynamically vulcanized elastomers and a continuous thermoplastic matrix [16]. TPVs are usually employed in applications requiring heat resistance and weight-saving, such as automotive or pipe seals.

- *Thermoplastic polyurethanes (TPUs)*. Thermoplastic polyurethanes are formed through a polyaddition reaction between diisocyanate and one or more diols, resulting in high-modulus, high-strength, drawable and tough materials [17]. Within the material, phase separation arises from the incompatibility between the hard and soft segments. This phase separation increases with chain length of soft segments. Whereas the hard segments tend to aggregate because of the formation of hydrogen bonds between the C=O and N–H groups of the urethane functions, the soft segments form amorphous domains [18]. These hydrogen bonds, as well as dipole-dipole interactions between hard segments, result in a network of physical crosslinks between flexible soft segments. TPUs are commonly used as a soft engineering polymer or to replace hard elastomers.

- *Thermoplastic copolyesters (TPCs)*. Thermoplastic copolyesters are composed of multi-block structures where the hard segment is a crystalline copolymer, such as poly(butylene terephthalate), while the soft segment is a copolymer of a higher molecular weight diol and terephthalic acid [10]. TPCs are most commonly used in automotive parts or in sealing applications.

- *Thermoplastic polyamides (TPAs).* Thermoplastic polyamides are composed of multi-block structures where the hard segment is a crystalline polyamide and the soft segment is a polyether or polyester [10].

POLYETHYLENE-DERIVED THERMOPLASTIC ELASTOMERS

Early work on polyolefin-derived thermoplastic elastomers dates back to the 1950s, where development was made on blends using polypropylene and polyethylene [22]. Gessler *et al*. [23]conducted experiments on isotactic polypropylene and polyisobutylene, ultimately discovering what he called "dynamic curing". Also called dynamic vulcanization, this process entailed vulcanizing the rubber during the melt-mixing with the molten plastic, resulting in the crosslinking of one of the phases of the polymer blend whilst still maintaining flow behavior above the melting point [24]. Hartman *et al*. [25] later experimented on blends containing linear and branched polyethylene, as well as polyisobutylene.. With the discovery of the Ziegler-Natta catalyst, several attempts were made to directly polymerize thermoplastic elastomers from ethylene and propylene [26][27][28][29].

Nowadays, most polyethylene-derived thermoplastic elastomers are based on block copolymers of ethylene and α-olefin comonomers arranged into alternating soft and hard segments, generally using metallocene catalysts [30]. In fact, The Dow Chemical Company patented these olefin block copolymers in 2013 under the name of INFUSE^{TM} [31]. In this case, crystalline polyethylene blocks act as the "hard" segment, whilst copolymers of ethylene and higher α-olefins act as amorphous "soft" segments with a low glass transition temperature, T_g. Recent advances have also developed multiple-step strategies using α-diimine nickel catalysts that require higher α-olefins [32][33] and even single-step strategies using only ethylene as feedstock [34][35].

A material of interest that could be replaced by PE-based TPEs is PEX, which is a commercially available cross-linked polyethylene mostly aimed at solving the high-temperature limitations of conventional polyethylene [36]. However, the crosslinking not only improves thermal resistance but also results in enhanced properties such as impact strength, stress crack resistance and abrasion resistance [36]. This makes it useful as an alternative to PVC, CPVC or copper in applications such as pipework systems, as well as in radiant heating/cooling systems or high-tension insulation [37]. PEX can be prepared from different grades of polyethylene, although the most commonly used grade is HDPE. As for the crosslinking methods, a distinction can be made between peroxide or silane crosslinking, which are forms of chemical crosslinking in which initiators are employed to generate free radicals, and irradiation crosslinking, which is a form of physical crosslinking involving the use of high-energy radiations to generate these free radicals [37]. Disadvantages of crosslinked polyethylene involve its high viscosity, the need of more controlled processes and its inability to re-melt, which impedes its recyclability [37].

SUPRAMOLECULAR POLYMERS BASED ON HYDROGEN-BONDED LIGANDS

Supramolecular polymers, as pioneered by Meijer *et al*., are materials formed by repeating units that are held together by reversible and highly directional non-covalent bonds, such as hydrogen bonds [11]. Much like thermoplastic elastomers, these polymers emerge from the need to combine good mechanical properties with facile processability.

Supramolecular chemistry relies on the concept of molecular self-assembly, that is, the formation of systems or networks with no external guidance. Applied to polymers, this is achieved by the synthesis of polymers with self-assembling segments [59]. Particularly, systems based on hydrogen bonding offer great advantages because of the high strength and easy reversibility of these bonds, as well as for their unidirectionality, which helps avoid unwanted interactions in other directions [11].

Different units have been used as self-assembling segments, as shown in Figure 11. Meijer *et al*. used self-complementary 4-ureido-2-pyridinone (UPy) units that were able to form dimers connected by four hydrogen bonds [60]. These were used to end-functionalize poly(dimetylsiloxane) (PDMS), resulting in an increased virtual molecular weight and rubber-like behavior at room temperature [59]. Still, the reversibility of the bonds provided low melt viscosity above the deaggregation temperature, improving the processability of the material. Other approaches involved the use of benzene-1,3,5-tricarboxamide (BTA) as the self-assembling unit, which results in a helical arrangement of three hydrogen bonds in column-like aggregates because of its ditopic nature [61]. Frauenrath et al. reported the use of oligo(L-alanine) end groups of different lengths in the functionalization of poly(isobutylene) derivatives, resulting in the formation of one-dimensionally extended β-sheet tapes and nanofibrils [62]. Depending on the number of repeat units in the oligopeptide, the aggregates obtained varied. For peptides with one amino acid unit formed small aggregates, whilst 2 to 3 amino-acid peptides formed single, antiparallel β-sheet tapes and longer oligopeptides gave rise to rigid β-sheet nanofibrils formed by stacked β-sheet tapes. Moreover, blends of monofunctional and difunctional polymers with either matching or different-length oligopeptide end groups were produced, resulting in different material properties. With matching end groups, blends formed elastic rubbers with tailorable shear moduli; with non-matching units, interpenetrating supramolecular networks with good damping properties were formed.
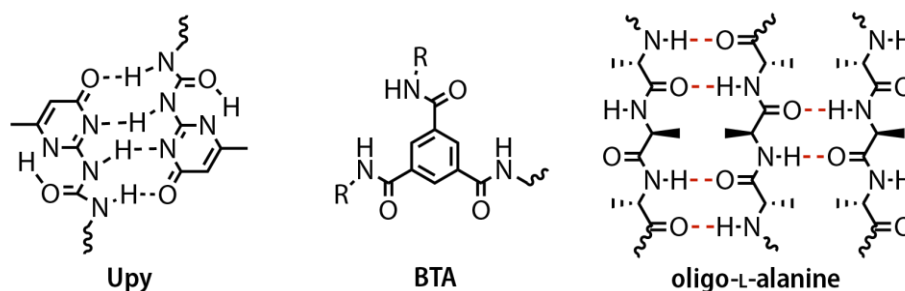

Figure 11. Molecular structures of UPy, BTA and oligo-L-alanine hydrogen-bonging units.

Supramolecular polyethylene

Concepts of supramolecular chemistry, applied to the aforementioned polymers, can also be applied to polyethylene derivatives to produce materials with tailorable thermal and mechanical properties. Lacombe *et al*. [63] reported the use of thymine (Thy) and 2,6-diamino-1,3,5-triazine (DAT) end groups to functionalize low molecular weight polyethylene materials, resulting in lamellar morphologies due to microphase separation of polar supramolecular segments and non-polar PE chains. They found that Thy-functionalized PE structural organization was driven by end-group crystallization, whilst the DAT-functionalized material was driven by PE crystallization. Moreover, they conclude that molecular weights of at least 2 times the entanglement MW should be used for their supramolecular modification in order to obtain enhanced mechanical properties, as they observed that longer polymer chains would promote less phase separation. Indeed, at low molecular weights the polymer chains remained confined within their own lamellae, and so the end groups would be acting as boundaries rather than bonds between these chains. However, they do bring attention to the fact that too long polymer chains could decrease the probability of aggregation of end-groups, because of the smaller concentration of these within the material. Also, they conclude that non-crystallizable end-groups should be employed to allow the driving force to be the crystallization of the polymer.

In conclusion, previous work in difunctionalized low molecular weight PE has proved that (a) the molecular weight should be at least two times over the entanglement weight, (b) the end groups used should be non-crystallizable and (c) a too high molecular weight can result in loss of end-group association.

PRELIMINARY WORK IN THE HOST LABORATORY

Frauenrath and coworkers took the challenge of applying concepts of supramolecular polymers, that had worked for lower molecular weights, into high molecular weights. In order to do so, they developed a strategy based on using blends of oligopeptide-modified high molecular weight polymers and matching additives to form reinforced nanostructures based on the co-assembly of these segments. This concept is represented in Figure 12.
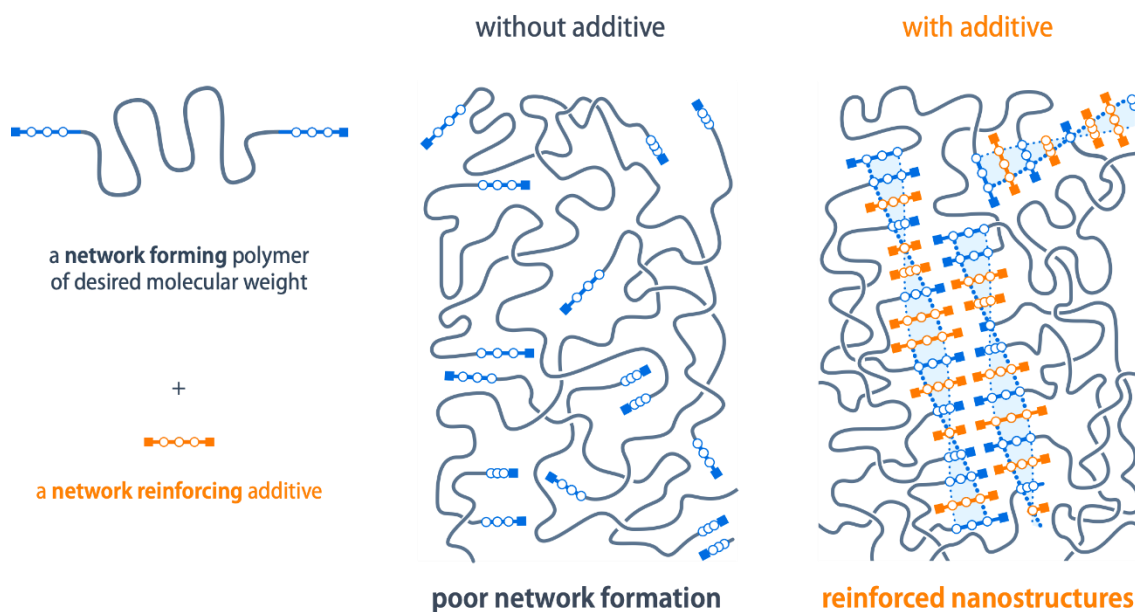
Figure 12. Schematic representation of the host laboratory concept.

This way, the amount of self-assembling oligopeptide units (additive plus end groups) could be adjusted independent of the desired molecular weight, with the only constraint being not to incorporate too much additive so that microphase segregation would occur. In particular, this concept was preliminarily applied to polyethylene materials of molecular weights of 30,000 g/mol and 100,000 g/mol, using tri-alanine-based oligopeptides and matching additives. These have a higher deaggregation temperature than the melting temperature of polyethylene, therefore providing a temperature window in which the polymer behaves rubber-like. This opens up new doors in terms of processing, both by enabling easier approaches and because of the opportunities that arise in terms of structure reconfiguration or orientation in, for instance, melt-spinning.

STATEMENT OF THE PROBLEM

UHMWPE fibers are high-performance fibers with desirable properties for engineering applications. However, they require time- and cost-intensive processing methods that use environmentally detrimental organic solvents. HDPE, on the other side, is highly reprocessable but does not have the mechanical property profile to address engineering applications similar to the ones that UHMWPE is used for.

The supramolecular modification of PE has been developed in the past to obtain tailorable thermomechanical properties and enhanced processability, and the incorporation of matching additives by the host laboratory has unlocked the possibility to use higher molecular weight polyethylenes. In particular, a temperature window has been observed where these materials behave in a rubber-like manner, opening up new processing possibilities.

This current project aims to take advantage of this temperature window to produce oriented HDPE fibers that mimic the behavior of those made from UHMWPE, whilst avoiding the technical and environmental issues associated to them. On the one hand, the use of supramolecular chemistry and the concept of the host laboratory brings a new processing window in which the polymer is fully molten but the additive remains still aggregated. Therefore, the hypothesis is that the presence of this additive will influence the way in which the material orients, under specific processing methods. On the other hand, the use of HDPE, as well as hydrogen-bonding ligands, will ensure that the material is easily processable.

Ultimately, the goal of the research project is to investigate a HDPE material that is suitable for engineering applications, through specific processing techniques than influence its orientation.

RESEARCH QUESTIONS

Stemming from the previous statement of the problem, several research questions will be proposed below, all of which will be answered through the completion of this project.

BULK MATERIAL

1. Does the proposed approach of employing an end-modified polymer plus a matching low-molecular weight additive promote the formation of co-assembled supramolecular structures within the material?

2. Does the proposed solution help tailor the temperature profile of the materials?

3. What is the temperature-dependent behavior of the material, at a microscopic level?

4. Which phase diagram for the proposed materials systems can be deduced based on the findings of the project?

ORIENTED SAMPLES

1. Can the proposed material be processed into fibers?

2. Does the proposed solution promote the orientation of structures within the material?

3. How is the degree of crystallinity of the material affected by the proposed solution?

4. How are the mechanical properties of the material affected by the proposed solution?

5. How are the mechanical properties of the material affected by the processing methodology?

CHAPTER 2

RESULTS AND DISCUSSION

STUDY OF THE BULK MATERIALS

SYNTHESIS AND CHARACTERIZATION OF COMPOUNDS

The project's main focus was to characterize the structure-property relations of the defined polymer blends through the performance of experiments and tests. After previous literature research and gathering of information, the different compounds that were required to produce these blends first had to be prepared by chemical synthesis. Table 2 explains the nomenclature that will be subsequently used to refer to the described synthesized polymers.

Table 2. Nomenclature of synthesized polymers.

Polymer	Molecular weight (g/mol)	End-group	Nomenclature
Concept	30,000	Ala_2Ac	$PE_{30}(AA)_2$
	100,000	Ala_2Ac	$PE_{100}(AA)_2$

Table 3 explains the nomenclature that will be subsequently used to refer to the described synthesized additives.

Table 3. Nomenclature of the synthesized additives.

Additive	Base oligopeptide	Alkyl chain	Nomenclature
Short-chain additive	Ala_2Ac	C_2C_6	$(AA)C_8$
Long-chain additive	Ala_2Ac	C_8C_{12}	$(AA)C_{20}$

END-MODIFIED POLYETHYLENE

Amino-telechelic PE was coupled to an already available acetyl-L-alanyl-L-alanine (Ala_2Ac) through a PyBOP-promoted peptide coupling reaction to furnish the target polymers $PE_{30}(AA)_2$ and $PE_{100}(AA)_2$, which were, respectively, 30,000 and 100,000 g/mol end-functionalized PE (approximate values, according to NMR results). Figure 13 and Figure 14 show the reactions for $PE_{100}(AA)_2$ and $PE_{30}(AA)_2$, respectively.
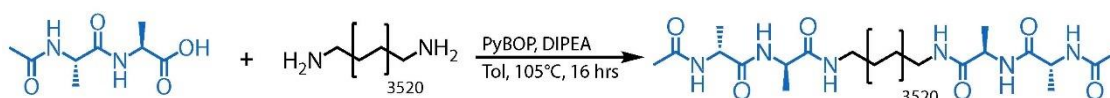

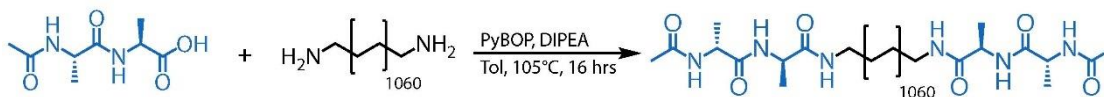*Figure 13. Peptide coupling reaction for $PE_{100}(AA)_2$.*

Figure 14. Peptide coupling reaction for PE$_{30}$(AA)$_2$.

Entanglement density greatly determines properties such as melt viscoelasticity, dynamic behavior and fracture behavior. Once a 3D entanglement network is formed within the polymer, which occurs when each polymer chain has more than one entanglement point, the properties cease to vary. For PE, the generally accepted entanglement molecular weight is 1,250 g/mol [68]. Therefore, the specific molecular weight values (100,000 and 30,000 g/mol) were chosen to be significantly over this critical point.

According to DSC measurements, PE$_{30}$(AA)$_2$ had a crystallization temperature of 114°C and a melting point of 129°C, whereas PE$_{100}$(AA) had a crystallization temperature of 111°C and a melting point of 130°C.

ADDITIVE

For the desired formation of single β-sheet tapes through self-assembly, the polymer end group had to contain an oligopeptide with at least two alanine repeat units, according to previous laboratory research. As using more alanine groups would be less cost-effective and cause solubility problems, acetyl-L-alanyl-L-alanine (Ala$_2$Ac) was chosen.

A matching additive was synthesized through an amide coupling reaction between Ala$_2$Ac and a branched alkyl chain, to enhance the solubility of the additive in the polymer matrix. With respect to the length of this alkyl chain, two different additives were synthesized, one with a longer alkyl chain (C$_8$C$_{12}$) and one with a shorter one (C$_2$C$_6$). Accordingly, the resulting reactions of the Ala$_2$Ac with each of these compounds furnished the target additives (AA)C$_{20}$ and (AA)C$_8$, respectively.
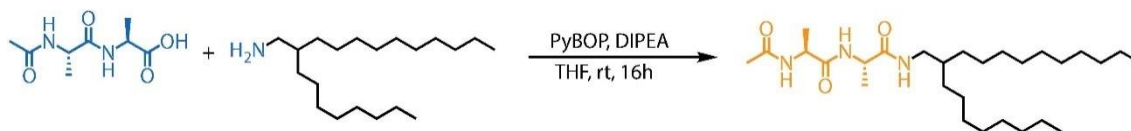

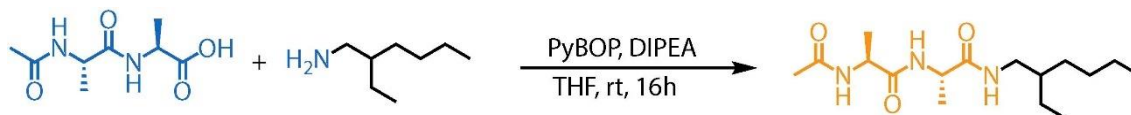*Figure 15. Peptide coupling reaction for (AA)C$_{20}$.*

Figure 16. Peptide coupling reaction for (AA)C$_8$.

Characterization of Additives

DSC measurements were performed on the (AA)C$_8$ to investigate the thermal transitions present in the bulk material, as revealed in Figure 17. The second cooling scan revealed a crystallization temperature of 227°C, and the second heating scan revealed a melting point at 228°C. As for the (AA)C$_{20}$, DSC results

showed a crystallization temperature of 175°C in the second cooling scan, as well as a melting point of 179°C in the second heating scan.
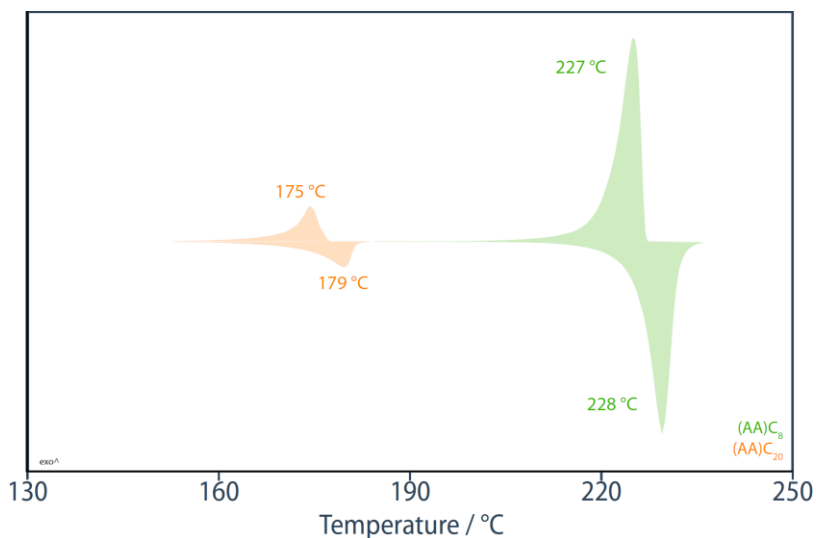

Figure 17. DSC curves of (AA)C$_8$ and (AA)C$_{20}$.

SYNTHESIS AND CHARACTERIZATION OF BULK MATERIALS

Once the end-modified polymer and the additive were synthesized, blends of the two components of the two were prepared. For the purpose of this study, control materials had to also be prepared to correctly analyze the influence of the involved parameters. Consequently, the following groups were compared:

- **Pristine material**, consisting of commercial HDPE (non-functionalized), in pellet form.

- **Reference material**, consisting of a blend of the commercial HDPE (non-functionalized) with the synthesized additive, at defined weight percentages.

- **Concept material**, consisting of a blend of the oligopeptide-functionalized polyethylene with the synthesized additive, at defined weight percentages.

Table 4 explains the nomenclature that will be subsequently used to refer to the described synthesized polymer blends.

Table 4. Nomenclature of the synthesized blends.

Sample	Polymer	Additive	Nomenclature
Pristine	Commercial HDPE	–	PE$_{30}$
Reference	Commercial HDPE	(AA)C$_8$	PE$_{30}$ + (AA)C$_8$
		(AA)C$_{20}$	PE$_{30}$ + (AA)C$_{20}$

40

Concept	PE$_{30}$(AA)$_2$	(AA)C$_8$	PE$_{30}$(AA)$_2$ + (AA)C$_8$
		(AA)C$_{20}$	PE$_{30}$(AA)$_2$ + (AA)C$_{20}$
	PE$_{100}$(AA)$_2$	(AA)C$_8$	PE$_{100}$(AA)$_2$ + (AA)C$_8$
		(AA)C$_{20}$	PE$_{100}$(AA)$_2$ + (AA)C$_{20}$

PRELIMINARY SCREENING OF MATERIALS

In the initial synthesis of these materials, there were three parameters involved, namely:

- **Molecular weight** of the polymer. The available molecular weights were 30,000 or 100,000 g/mol, and these will be subsequently referenced as PE$_{30}$ and PE$_{100}$, respectively. As they can also be functionalized or non-functionalized, the term (AA)$_2$ will be added to the nomenclature of those that are di-functionalized with the Ala$_2$Ac compound.

- **Type of additive**. The available additives comprised long alkyl residues (Ala$_2$Ac-C$_8$C$_{12}$) or short alkyl residues (Ala$_2$Ac-C$_2$C$_6$). These additives will be subsequently referenced as (AA)C$_{20}$ and (AA)C$_8$, respectively.

- **Additive content** in the polymer matrix, measured as a weight fraction. In the nomenclature, it will be referred to as a simple number just before naming the additive.

Based on DSC, dynamic shear rheology and optical microscopy results, the parameters were narrowed down to one molecular weight and one type of additive under the following considerations:

As observed in Figure 18, the DSC of the polymer of molecular weight 100,000 g/mol revealed a melting point of 130°C and a crystallization temperature of 111°C. The DSC of the 30,000 g/mol polymer revealed a melting point of 129°C and a crystallization temperature of 114°C. Additive transition peaks were observed for both of the blends, being more pronounced for the 30,000 g/mol material. For the further development of the project, this polymer (PE$_{30}$ if non-functionalized, PE$_{30}$(AA)$_2$ if di-functionalized) was selected as, at a lower chain length, there would be a higher concentration of end groups in the blend, which would result in a better co-assembly. Also, a lower molecular weight polymer would require less additive to stabilize the system. Moreover, a lower molecular weight polymer would have lower viscosity, which would facilitate the processing and handling of the material.

Regarding the two types of additive that were available, DSC data showed aggregation temperatures of 188°C for the short alkyl chain additive and 151°C for the long alkyl chain additive. As for the deaggregation temperatures, DSC results represented in Figure 18 revealed transitions at 197°C and 168°C, respectively. Therefore, in comparison to the 129°C melting point of the polymer, the short alkyl chain additive allowed for a larger temperature window. These results were confirmed through rheology results where, as observed in Figure 18, the short alkyl chain additive provides a larger temperature interval for the rubbery plateau, compared to the long alkyl chain additive. Therefore, for the further

development of the project, the short alkyl chain additive, (AA)C$_8$, was chosen because a larger temperature window would provide advantages in terms of processing and precision of future methods.
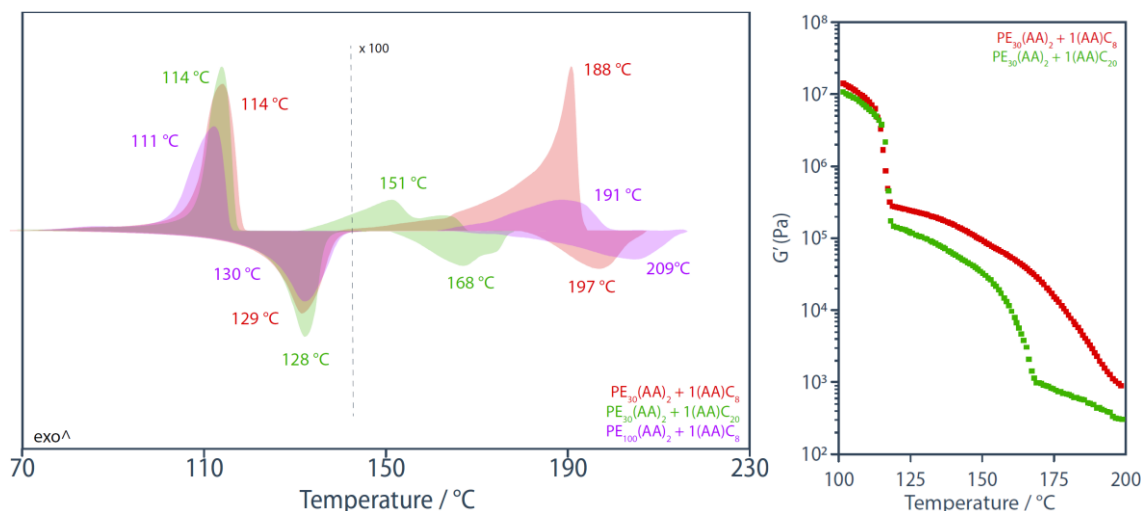

Figure 18. DSC (left) and dynamic shear rheology (right) experiments comparing long-chain and short-chain additives, with different molecular weight PEs.

Regarding the additive content, several weight percentages were used according to the specific needs of the experiments. Particularly for the study of the aligned samples, a weight percentage of 1 wt% was selected because, on one side, the concentration of additive in the blend had to be high enough to promote the creation of supramolecular networks within the system while, on the other side, the concentration of additive in the blends should not be so high as to cause macroscopic phase separation between an additive-rich phase and a polymer-rich phase. Temperature-dependent optical microscopy experiments were performed on blends at different weight fractions of the additive to assess this phase separation, as well as to investigate the structure formation within the material.

As can be observed in Figure 19, upon cooling from a fully molten temperature, the reference blends phase segregated into nanofibrils. On the contrary, the concept blends did not show this behavior, as their modification enabled the dispersion of the additive throughout the material, in the form of nanophase-segregated and polymer-tethered aggregates resulting from the co-assembly of additive and polymer end groups.
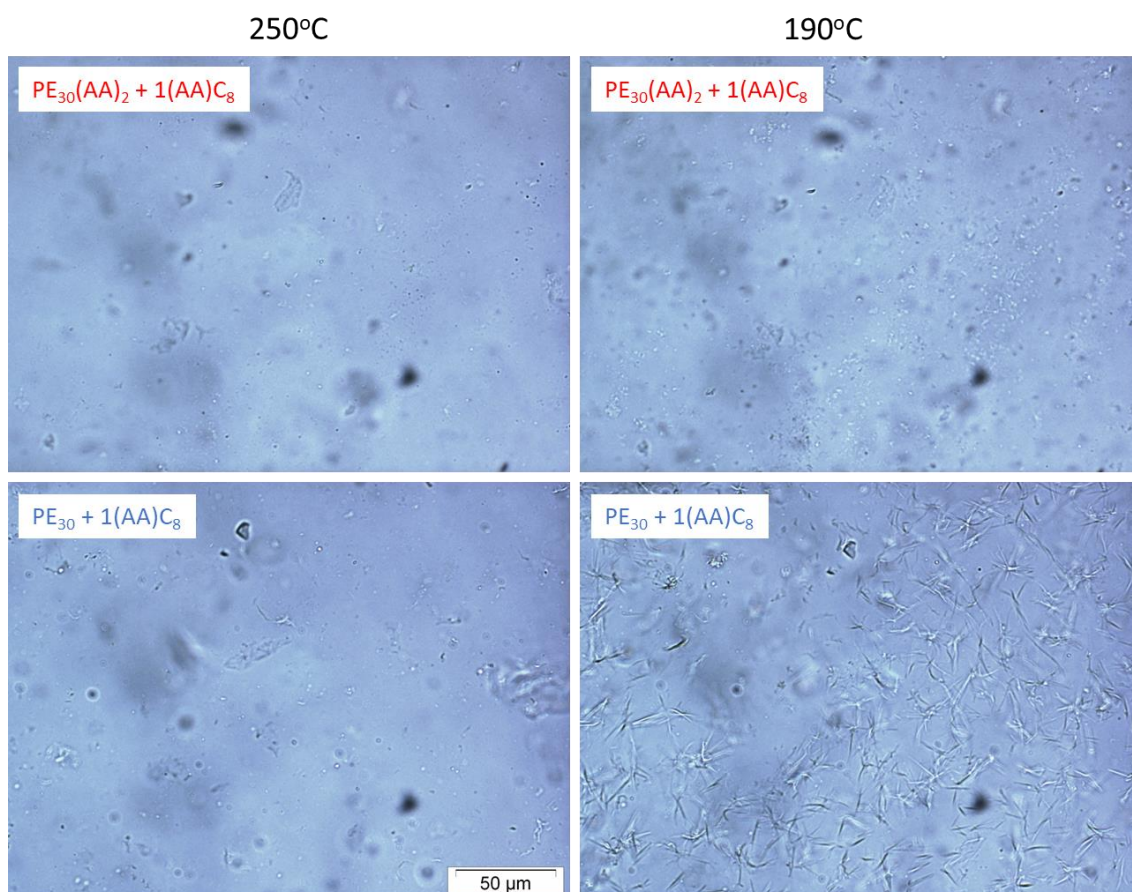
Figure 19. Micrographs of the 1% (AA)C$_8$ polymer blends cooling from 250°C (left) to 190°C (right).

When the additive content increased, as shown in Figure 20, phase separation started to occur even for end-modified materials, as the material could not stabilize the high concentrations of additive in the polymer matrix anymore.
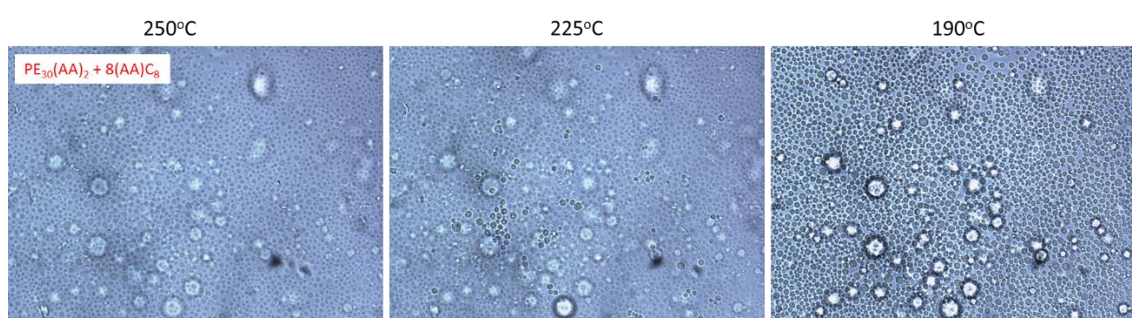

Figure 20. Micrographs of the 8% (AA)C$_8$ polymer blends cooling from 250°C (left) to 190°C (right).

As for the blends at 2 and 4 *wt*% of the additive, these showed similar behaviors as the blend containing 1 *wt*% of the additive, indicating that the phase separation started within the 4–8 *wt*% range. Still, the 1 *wt*% material was chosen in order to save material, especially additive, in view of future industrial processes and reduction of costs.

CHARACTERIZATION OF BULK MATERIALS

The selected blends were characterized both thermomechanically, through DSC and rheology techniques, and structurally, through optical microscopy. Then, their phase behavior was investigated through theoretical models based on the obtained experimental data.

Thermomechanical characterization of bulk materials

The bulk materials were further investigated by DSC and dynamic shear rheology experiments. For this purpose, different weight percentages were used in order to identify the trends within the temperature profiles and flow behavior of the material.

An important characteristic that was investigated throughout this preliminary characterization process was the phase separation which, in this case, was the microscopic separation of two immiscible phases visible in the optical micrographs: a polymer-rich phase and an additive-rich phase. A first indication of this phase separation appeared in the DSC results, in the form of two separate transition peaks suggesting two different phases within the material. As can be observed in Figure 21, the blends with lower additive concentration showed one transition peak. However, at higher concentrations, this was not the case anymore, as can be noticed in the 4 *wt*% blends. The reason why the 8 *wt*% blends did not show these double peaks is probably because these were out of the measured temperature range. A clearer understanding of the phase separation within the material can be obtained through the previous temperature-dependent optical microscopy (Figure 20), where the phases can be visualized.

Another important aspect was related to the new rubbery plateau formed with the incorporation of the additive, as revealed in Figure 21. DSC results indicated increased additive aggregation and deaggregation temperatures with increased additive concentration, which ultimately opened up a temperature window between these transitions and the polymer melting and crystallization temperatures. As seen in the dynamic shear rheology results, this window proved to be a stage in which the material behaved like a soft solid, giving rise to new processing opportunities, for instance, fiber drawing at temperatures where the polymer matrix was already fully molten, but the additive was still aggregated. The temperature range of this rubbery plateau increased with the amount of additive, and so it was related to the strength of the co-assembled supramolecular networks.
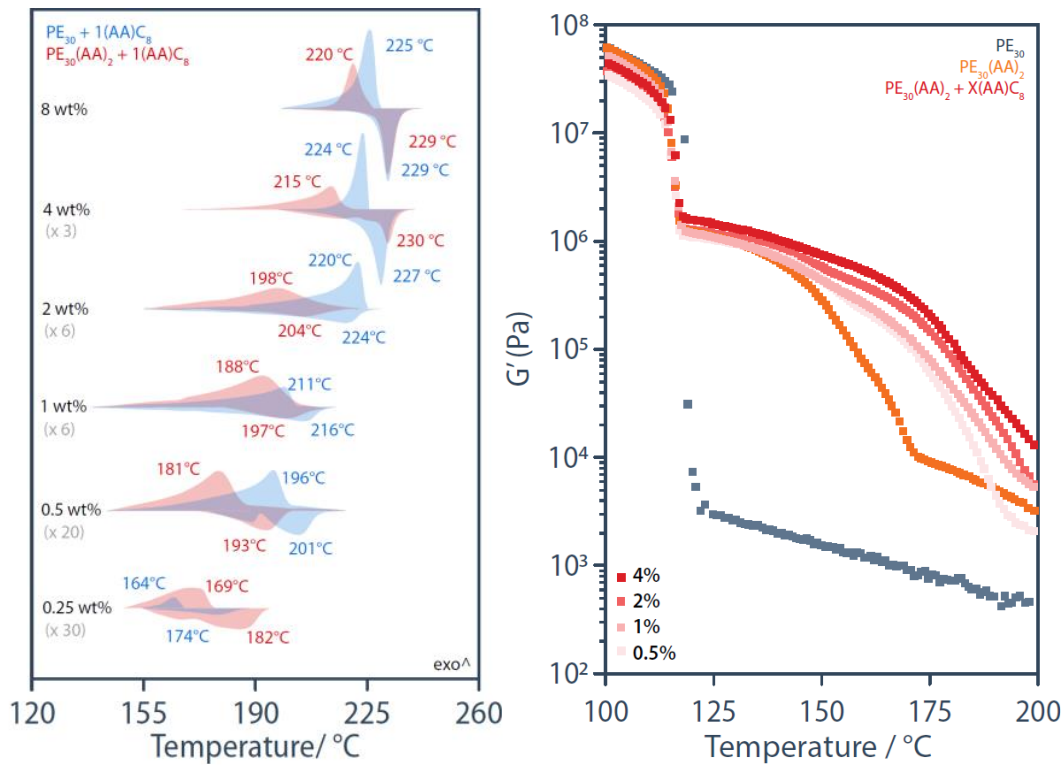
Figure 21. DSC (left) and dynamic shear rheology (right) of polymer blends at different additive concentrations.

Figure 22 represents a more close-up view of the DSC thermogram of the material containing 1 *wt%* of additive, which was the one used for the completion of the research project. The results on this specific 1 *wt%* blend served to provide a closer look into the aforementioned rubbery plateau and its boundaries. In this case, results showed a second crossover temperature of 163°C for the end-modified material, providing nearly 40°C of additional "soft-solid" state for the PE. This effect was enhanced with the incorporation of additive, where the crossover temperature increased to 181°C, that is, nearly 20°C more than the modified polymer with no extra additive.
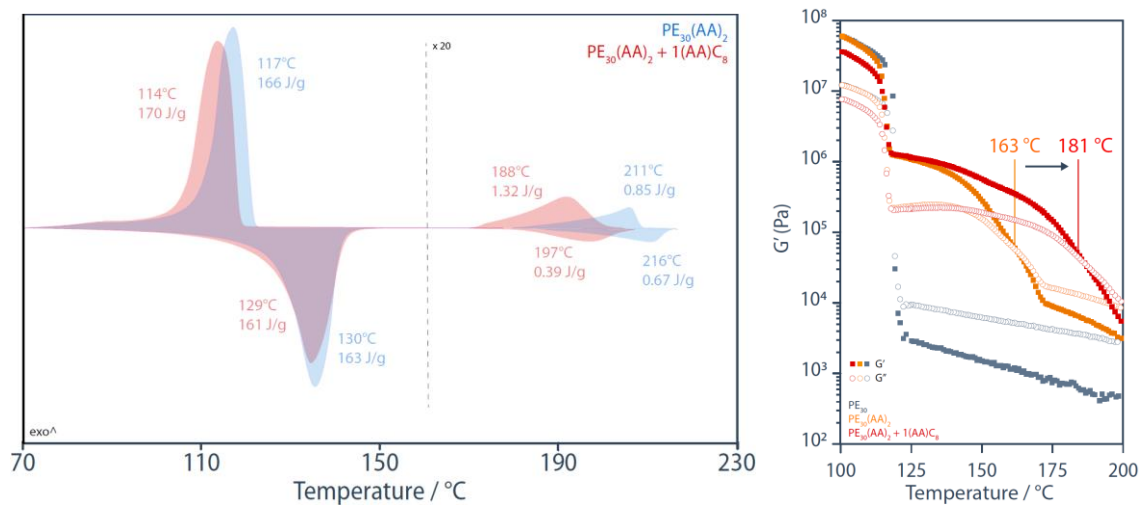

Figure 22. DSC (left) and dynamic shear rheology (right) of polymer blends at 1 wt% additive concentration.

Phase behavior of the bulk material

With the information gathered from the DSC and optical microscopy data, an approximate phase diagram of the blends was deduced.

The thermodynamics of mixing of polymer blends can be described by the Flory-Huggins theory [67], assuming some simplifications. This theory presents a lattice model that relies particularly on the Flory-Huggins parameter, χ, which describes the differences in the strength of pairwise interaction energies between species in a mixture. To get a good fit for the PE/additive systems that were studied within this research project, it was assumed that the interaction parameter was a sum of two terms: one that was independent from the temperature and one that was inversely proportional to it.

$$\chi = \chi_1 + \frac{\chi_0}{T}$$

This interaction parameter can be applied to the general Flory-Huggins equations, which take into account the Gibbs free energy change in polymer blends. Particularly, T_{sep} represents the curve that separates a single homogeneous melt phase from a two-phase system composed of molten additive and molten polymer, whereas T_m represents the curve that separates this homogeneous phase with a two-phase system with crystallized additive and molten polymer. This configuration is exemplified in Figure 23.
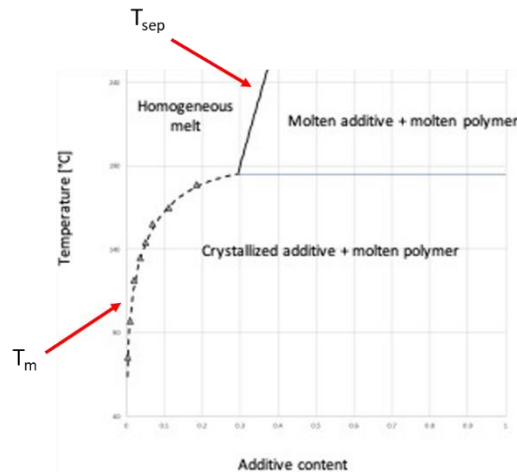

Figure 23. Example of a phase diagram derived from Flory-Huggins equations.

Applying the experimental results from the development of the research project, the following equations for these curves are obtained:

$$T_{sep} = -\frac{\chi_0(1-\phi_1)^2}{(1-\phi_1)[1+\ln\phi_1] + \left[\phi_1\ln\phi_1 + \frac{(1-\phi_1)\ln 1-\phi_1}{m_2}\right]} \approx -\frac{\chi_0(1-\phi_1)^2}{1-\phi_1+\ln\phi_1+\chi_1(1-\phi_1)^2}$$

Equation 1. Equation for the curve that separates a single homogeneous melt phase from a two-phase system composed of molten additive and molten polymer.

$$T_m = \frac{\frac{R\chi_0}{\Delta H_1}(1 - \phi_1)^2 + 1}{\frac{1}{T_{mo}} - \frac{R}{\Delta H_1}[1 - \phi_1 + \ln \phi_1]}$$

Equation 2. Equation for the curve that separates a single homogeneous melt phase from a two-phase system composed of crystallized additive and molten polymer.

From these equations, an approximate phase diagram can be obtained relying on the experimental data from DSC and rheology measurements. Figure 24 represents a segment of this phase diagram, for both the reference and concept materials, where the data points shown have been fitted into a curve using Equation 1 and Equation 2.
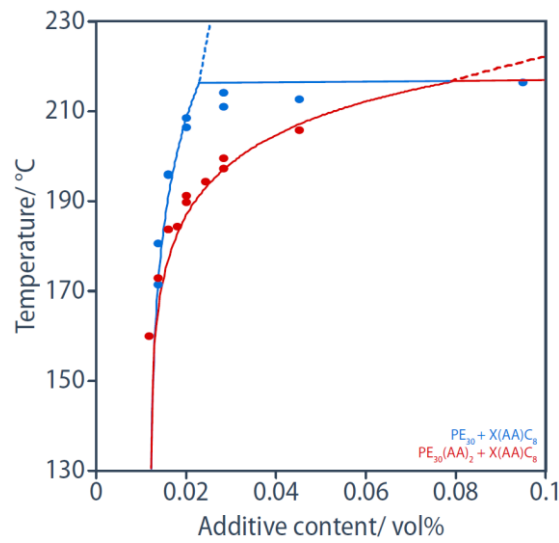
Figure 24. Theoretical phase diagram plot from approximation of Flory-Huggins equations.

STUDY OF THE ALIGNED SAMPLES

PROCESSING OF ALIGNED SAMPLES

After the blends were synthesized and characterized for their thermal properties, aligned samples were produced by creating fibers out of the material, using both melt-spinning and cold-drawing methods.

MELT-SPINNING OF FIBRES

This process involved melting the bulk materials, extruding them at a specific nozzle temperature and pulling from the extruded rod to create a fiber. To do so, a apparatus was designed in which a spinneret was placed opposite to the extruder, to collect the fiber while simultaneously pulling on it and stretching it. This apparatus can be observed in Figure 25.
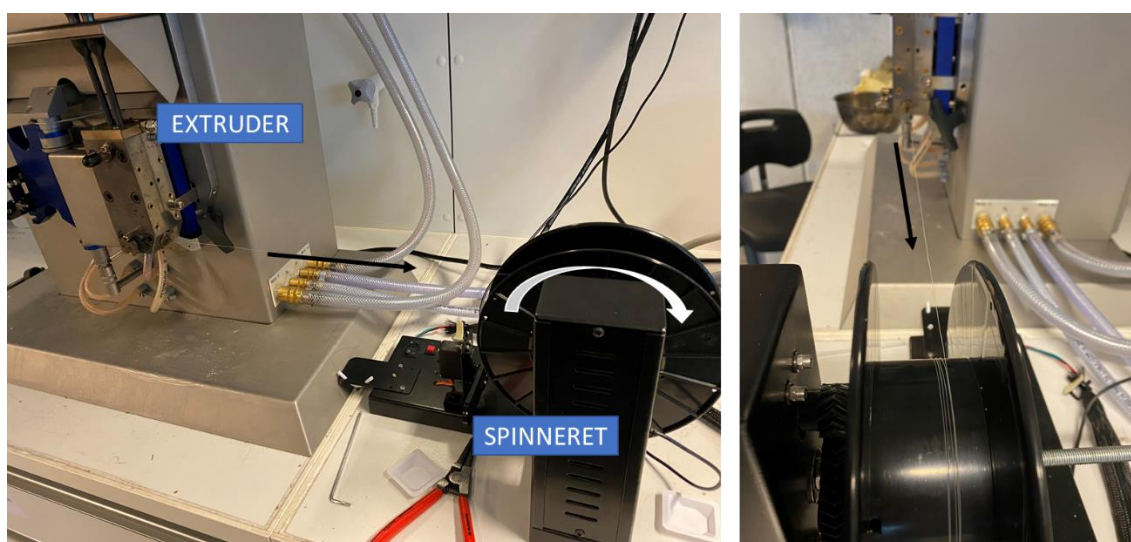
Figure 25. Extruder-spinneret mechanism for the melt-spinning of fibers.

With regards to the drawing conditions, the parameters that were taken into consideration were nozzle extrusion temperature, extrusion speed and spinneret speed.

As for the extrusion temperature, it was chosen based on DSC and rheology results. The fibers were melt-spun at two different temperatures, according to the observed additive transition temperatures and always above the melting temperature of the polymer. In particular, 220°C (above the aggregation temperature of the additive, according to both DSC and rheology) and 190°C (below the aggregation temperature of the additive, according to DSC, but above the G'/G'' crossover temperature, according to rheology) were chosen.

As for the speed of both the extrusion step and the spinneret, they were adapted according to the needs. The extrusion speed could be precisely controlled with the machine, whereas the spinneret speed control

consisted of a regulator that could be turned to increase or decrease the speed. Regarding the dimensional specifications of the fibers, the first aim was to achieve the thinnest possible fiber, as this would increase the chance of having an aligned sample [65]. The second aim was to have similar thicknesses amongst all the sample groups that were being compared, that is, pristine, reference and concept materials so that they are comparable. Due to their different composition, each of them had a slightly different viscosityThis meant that the pristine polymer could be spun at higher draw rates (slow extrusion speed and high spinneret speed) and therefore could be made thinner, as it was the least viscous material. On the other hand, the concept was the most viscous material of the three, and therefore had to be spun at lower draw rates (high extrusion speed and low spinneret speed), resulting in thicker fibers. Therefore, the solution was to first draw the concept materials to their minimum possible thickness, and then adjust the draw ratios of the reference and pristine materials to achieve a similar thickness. Table 5 summarizes this process, indicating the thicknesses obtained for each sample and temperature group, as well as the nomenclature that will be used from here onwards to address the different sample groups.

Table 5. Summary of the parameters involved in the melt-spinning process.

Nozzle temperature	Sample	Extrusion speed	Spinneret speed	Thickness	Nomenclature
220°C (AS220)	Pristine	2 rpm	Maximum	393.88 ± 12.66	AS220P
	Reference	10 rpm	Maximum	369.05 ± 39.81	AS220R
	Concept	2 rpm	Maximum	327.38 ± 32.39	AS220C
190°C (AS190)	Pristine	5 rpm	Minimum	404.76 ± 21.03	AS190P
	Reference	15 rpm	Minimum	336.71 ± 29.45	AS190R
	Concept	10 rpm	Minimum	525.89 ± 29.80	AS190C

Figure 26. Representative appearance of the melt-spun fibers.

The appearance of the fibers is represented in Figure 26. It can be observed that the concept fiber had a slightly yellow color compared to the pristine and reference. We attribute this observation to the fact that the commercial polymer (used in pristine and reference materials) used a stabilizer against oxidation, which the synthesized end-functionalized polymer did not. Therefore, this resulted in slight degradation in the concept polymer, although it was considered negligible in its effect to the results of the project. In

order to be tested, these long fibers were then cut into individual samples. The thickness of the samples was measured using an optical microscope.

COLD-DRAWING OF FIBRES

To make the cold-drawn fibers, sections of the melt-spun fibers were taken and stretched until breakage using the universal testing machine. Table 6 summarizes this process, indicating the thicknesses obtained for each sample, as well as the nomenclature that will be used from here onwards to address the different sample groups.

Table 6. Summary of the parameters involved in the cold-drawing process.

Drawing temperature	Sample	Drawing speed	Thickness	Nomenclature
25°C **(CS190)**	Pristine	25 mm/min	93.45 ± 7.20	CS190P
	Reference	25 mm/min	80.36 ± 7.58	CS190R
	Concept	25 mm/min	142.99 ± 22.00	CS190C

In order to be tested, these long fibers were then cut into individual samples. The thickness of the samples was measured using an optical microscope.

CHARACTERIZATION OF ALIGNED SAMPLES

Once the aligned samples were produced, they were tested to assess their thermomechanical characteristics with DSC and tensile testing. Moreover, their structure was investigated through X-ray experiments.

THERMAL CHARACTERIZATION

The thermal profile of the samples was analyzed in order to investigate the crystallinity and nucleation mechanisms within the material as a consequence of a possible orientation. DSC experiments showed the temperature profile of the oriented (first scan) and relaxed (second scan) samples through Figure 27, Figure 28 and Figure 29, which represent AS220, AS190 and CS190, respectively.
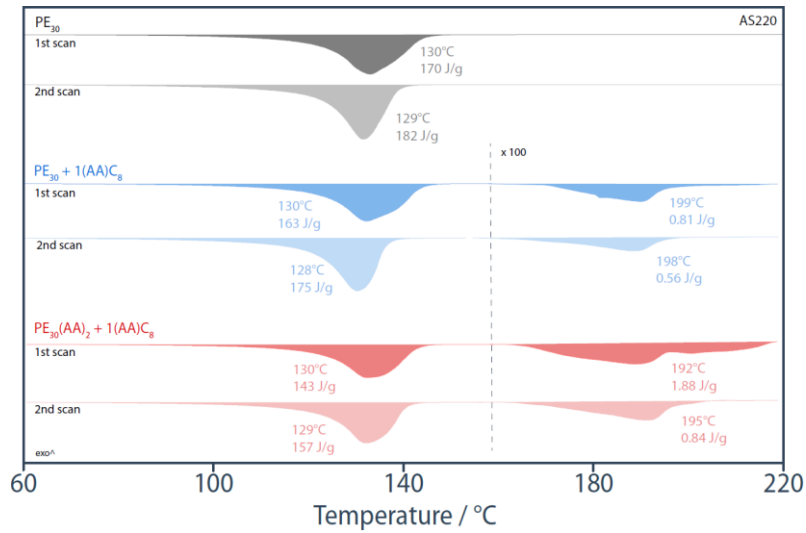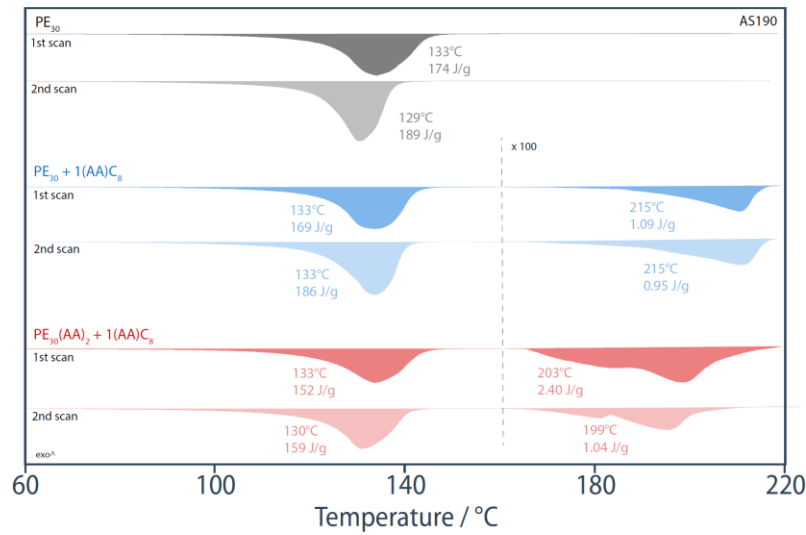
Figure 27. DSC curves of AS220 fibers.
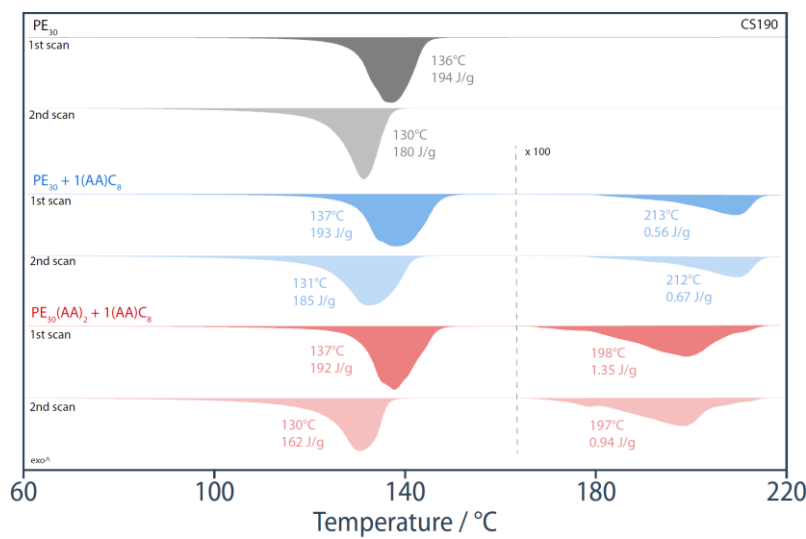

Figure 28. DSC curves of AS190 fibers.

Figure 29. DSC curves of CS190 fibers.

51

Regarding the polymer melting peaks, a first interesting observation came from their shape. In all oriented samples, there appeared to be a shoulder in the first scan. A shoulder would indicate that the polymer peak was formed by two separate peaks, suggesting the coexistence of two different crystalline species. Moreover, in the melt-spun fibers, the predominant shoulder seemed to be the one at higher temperatures, as can be observed in Figure 27 and Figure 28. In the cold-stretched fibers, as shown in Figure 29, the predominant shoulder was the one at lower temperatures. Therefore, a hypothesis for this could be that there were two different predominant crystallization mechanisms occurring with the different processing techniques, resulting in two different types of crystalline microstructures. According to literature [41][43][44], these could be lamellar and fibrillar crystallization of PE. This theory was further reinforced by the melting temperatures revealed in the graphs. Figure 27 and Figure 28 revealed similar polymer melting temperatures for the 1st and 2nd heating cycles in all pristine (PE30), reference (PE30 + 1(AA)C8) and concept (PE30(AA)2 + 1(AA)C8) materials. However, Figure 29 revealed differences of 6°C in the polymer melting peaks for pristine and reference materials, and 7°C (from 137°C to 130°C) for concept materials, suggesting different crystallization mechanisms in the melt-spun versus the cold-stretched fibers [68]. In the case of the pristine and reference samples, this shoulder disappeared in the second scan. In the case of the concept materials, it seemed to be maintained for AS220 fibers and, to lesser extent, in the AS190 fibers. Therefore, the concept material seemed to promote the prevalence of the aforementioned crystalline structures even after a subsequent cooling-heating cycle. This phenomenon seemed to also be affected by the processing temperature, being enhanced by higher processing temperatures (as proved with the AS220 fibers) and diminished with lower ones (as proved with the CS190 fibers).

Another interesting observation regarding the polymer peaks would come from the crystallinity of the samples. As can be observed in Figure 27 and Figure 28, the polymer crystallinity seemed to decrease from the first scan (oriented) to the second scan (relaxed) when the processing was performed at high temperatures (of 220°C and 190°C, respectively). Contrary to this, a cold-stretching processing gave rise to higher polymer crystallinity in the oriented samples, as can be seen in Figure 29. This could expand on the previous hypothesis by suggesting that the crystalline structure resulting from the cold stretching is more constraining for the polymer chains, resulting in a higher enthalpy change when relaxed.

Regarding the additive deaggregation peaks, a first important observation came from the crystallinity. For the melt-spun fibers, shown in Figure 27 and Figure 28, the additive crystallinity in the concept materials was higher in the oriented samples than in the relaxed ones. This, however, was not the case for either the reference materials or the concept materials that were cold stretched. Particularly, the cold-stretching process may have been too aggressive for the additive, causing the rupture of these crystalline structures and therefore not resulting in an increase of the additive crystallinity. Moreover, results on the polymer peaks also suggested a more constrained polymer chain state in the cold stretched fibers, as seen in the increased change in enthalpy for the oriented fibers. This constrained state may have also hampered the crystallization of the additive.

Another observation regarding the additive peaks came from their shape. Whereas the reference materials showed one distinct peak in both oriented and relaxed samples, concept materials in the melt-spun fibers showed two peaks for the oriented-sample additive, which then faded into one peak as the sample relaxed.

STRUCTURE INVESTIGATION

XRD experiments were performed to assess the superstructures within the materials, as well as the alignment. These experiments were performed in both short-angle (SAXS) and wide-angle (WAXS) scattering.

SAXS experiments

Figure 30 shows the 2θ integration of the SAXS experiment in AS220 fibers. Reflections corresponding to distances of 230 Å were observed for both the pristine (PE_{30}) and reference ($PE_{30} + 1(AA)C_8$) materials. This distance is characteristic for the lamellar long period in HDPE, which usually shows a reflection at around 200 Å [66]. As for the concept ($PE_{30}(AA)_2 + 1(AA)C_8$) samples, this reflection was shifted towards a Q value corresponding to a slightly higher lamellar long period of 270 Å. The slight difference in distances may have been due to the fact that, whilst pristine and reference materials both used the commercial PE, concept materials used the synthesized end-modified PE.
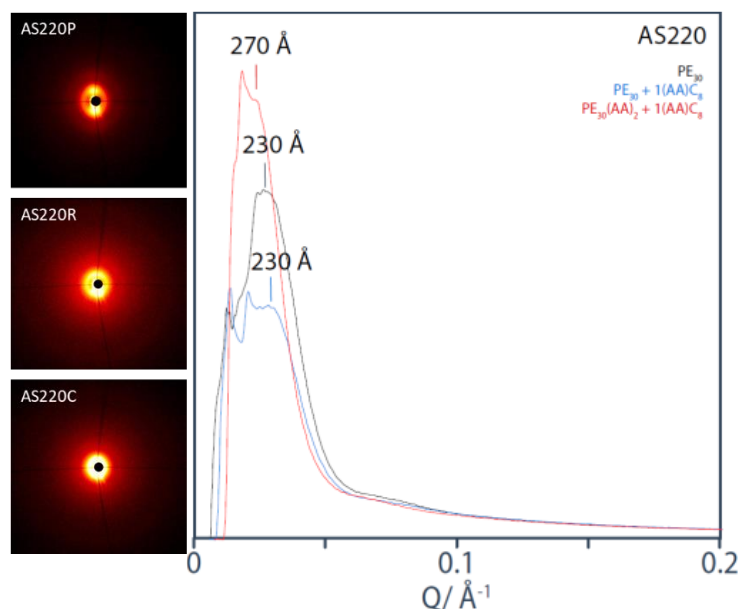

Figure 30. 2-Theta integration of AS220 fibers in SAXS experiment.

Figure 31 shows the 2θ integration of the SAXS experiment in AS190 fibers. Reflections corresponding to spacings of 219 Å can be observed for both the PE_{30} and the $PE_{30} + 1(AA)C_8$ materials, which can once again be assigned to the lamellar long period in PE materials. As for the $PE_{30}(AA)_2 + 1(AA)C_8$ samples, this reflection is shifted towards a lower Q value corresponding to a larger spacing of 306 Å. This could suggest

that the difference between pristine and reference with concept was not, in fact, the different base materials but the end-modification. An increased lamellar long period might indicate that the microstructure was evolving from lamellar to fibrillar crystallization. Moreover, an additional reflection corresponding to a spacing of 20 Å was observed for the reference materials, but not for the concept materials. This reflection has been shown in previous work in the host laboratory to indicate "large", microphase-segregated additive crystals in the reference materials; its absence in the concept materials proves that the additive is well dispersed, supposedly in the form of well-defined, nanophase-segregated, and polymer-tethered aggregates obtained by the co-assembly of additive and polymer end groups.
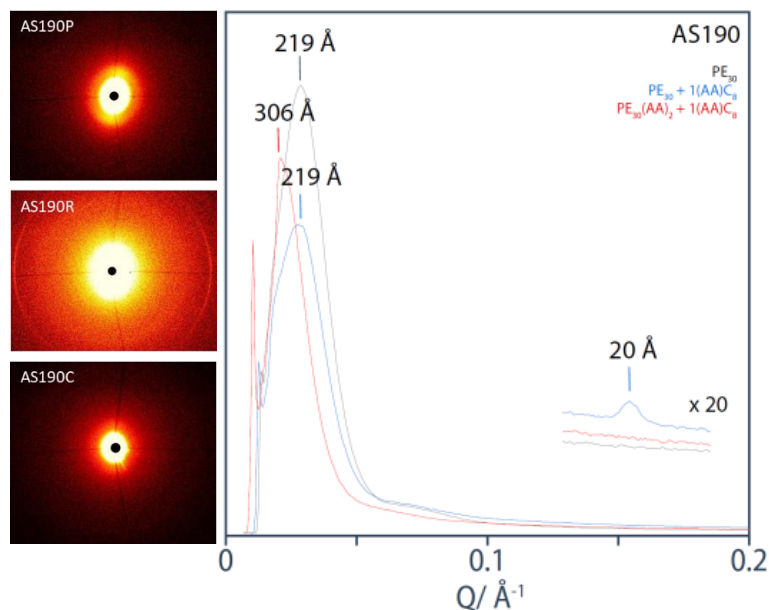
Figure 31. 2-Theta integration of AS190 fibers in SAXS experiment.

Figure 32 shows the azimuthal integration around the reflection of AS220 and AS190 fibers corresponding to the lamellar long period, after being fitted with a Gaussian function to enable the comparison between curves.

The periodicity within both of these fibers was observed parallel to the fiber axis, which is indicative of a lamellar structure, in which the lamellae are oriented perpendicular to the fiber axis. For the AS220 fibers, the highest degree of orientation, as estimated from the FWHM of the azimuthal plots, appeared in pristine materials, followed by concept materials and, finally, reference materials. In the case of AS190 fibers, the highest orientation was observed in the concept materials, followed by the pristine and then reference materials.
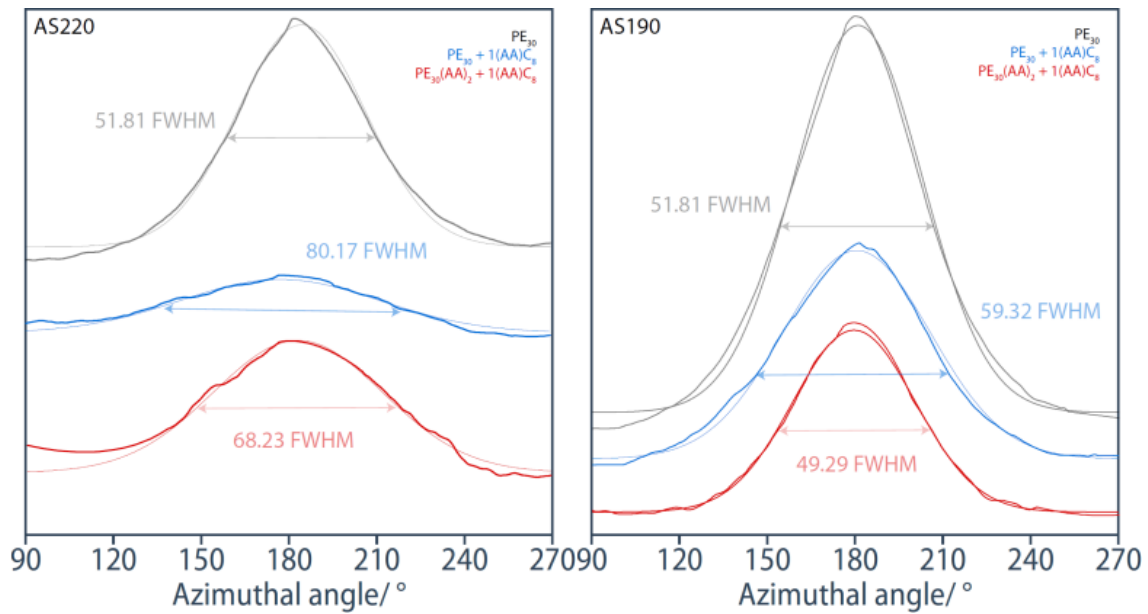
Figure 32. Azimuthal integration of maximum peak in AS220 (left) and AS190 (right), SAXS.

Figure 33 shows the 2θ integration of the SAXS experiment in CS190 fibers. Reflections corresponding to a spacing of 366 Å and 385 Å can be observed for the PE_{30} and PE_{30} + 1(AA)C_8 materials, respectively. In the $PE_{30}(AA)_2$ + 1(AA)C_8 samples, this reflection is shifted towards Q values corresponding to a larger distance of 408 Å.
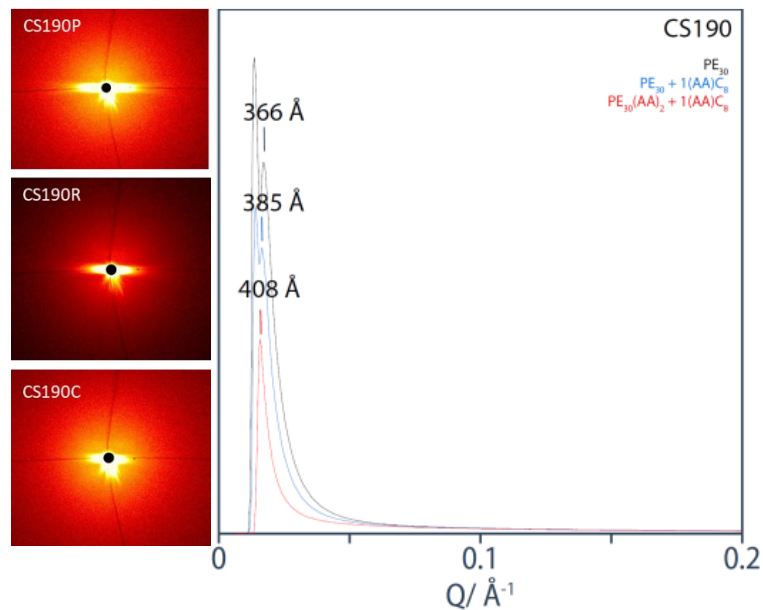

Figure 33. 2-Theta integration of CS190 fibers in SAXS experiment.

Figure 34 shows the azimuthal integration around the maximum peak of CS190 fibers, after being fitted with a Gaussian function to enable the comparison between curves. The maximum at 90º observed in all cases suggests that the microstructure of all materials has most likely changed from predominantly

lamellar to predominantly fibrillar crystalline domains that are aligned parallel to the fiber axis, with a periodicity perpendicular to it.
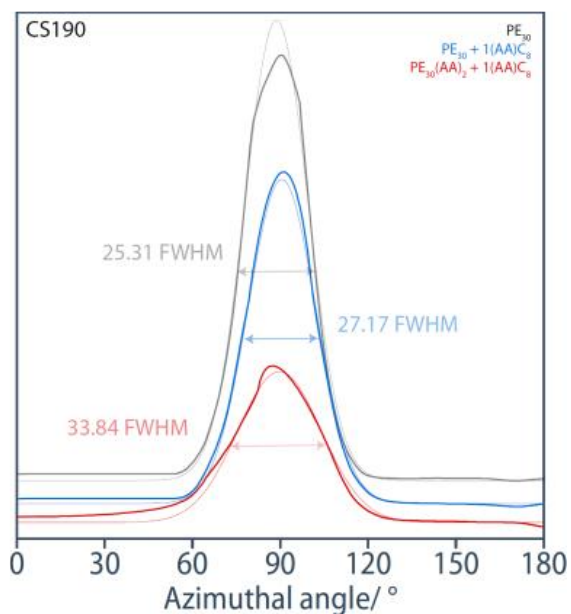

Figure 34. Azimuthal integration of maximum peak in CS190, SAXS.

WAXS experiments

Figure 35 and Figure 36 show the 2θ integration of the WAXS experiment in AS220 and AS190 fibers, respectively, revealing four reflections corresponding to spacings of 4.1 Å, 3.7 Å, 3.0 Å and 2.5 Å. These peaks are all characteristic of PE, according to its lattice parameters [66]. As the WAXS results looked uniform, no azimuthal plots were made for these.
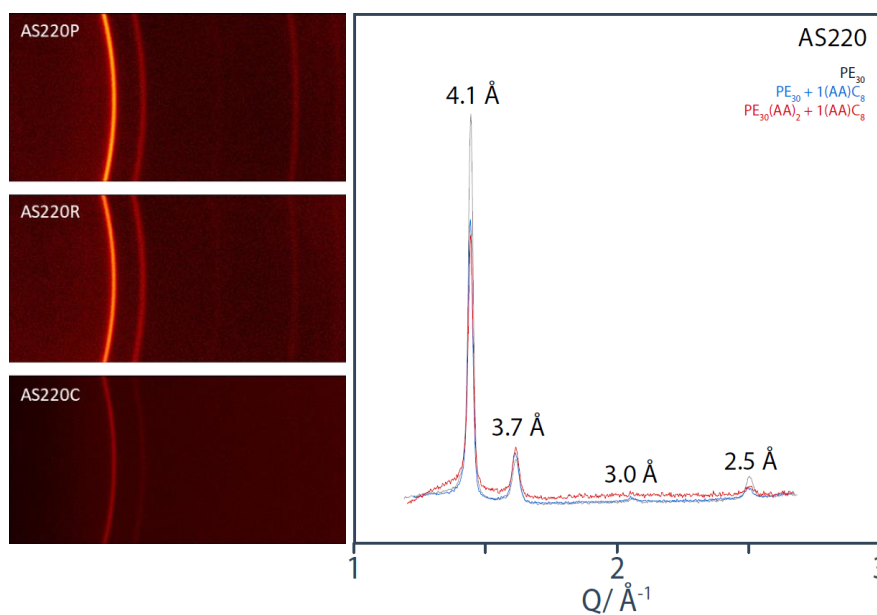

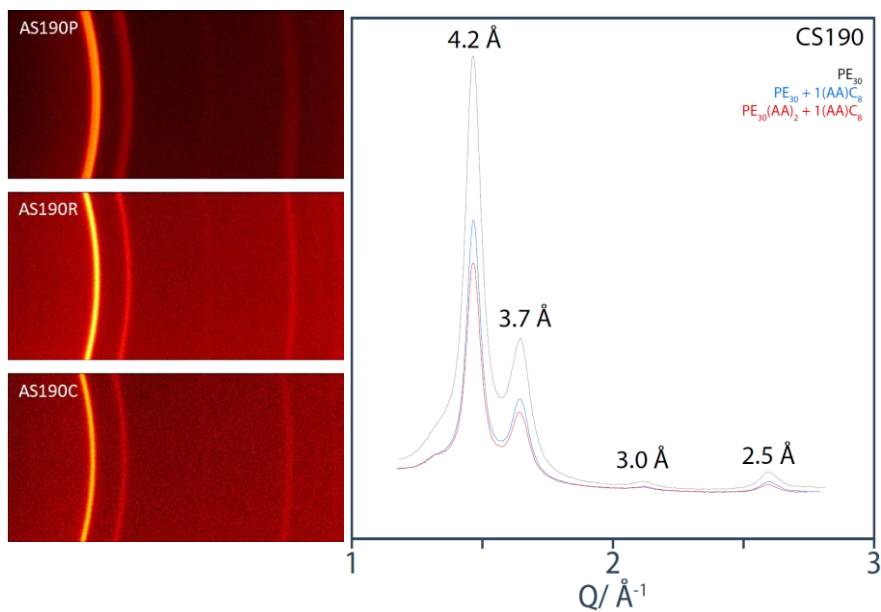*Figure 35. 2-Theta integration of AS220 fibers in WAXS experiment.*

Figure 36. 2-Theta integration of AS190 fibers in WAXS experiment.

Figure 37 shows the 2θ integration of the WAXS experiment in CS190 fibers, revealing four peaks at 4.2 Å, 3.7 Å, 3.0 Å and 2.5 Å.
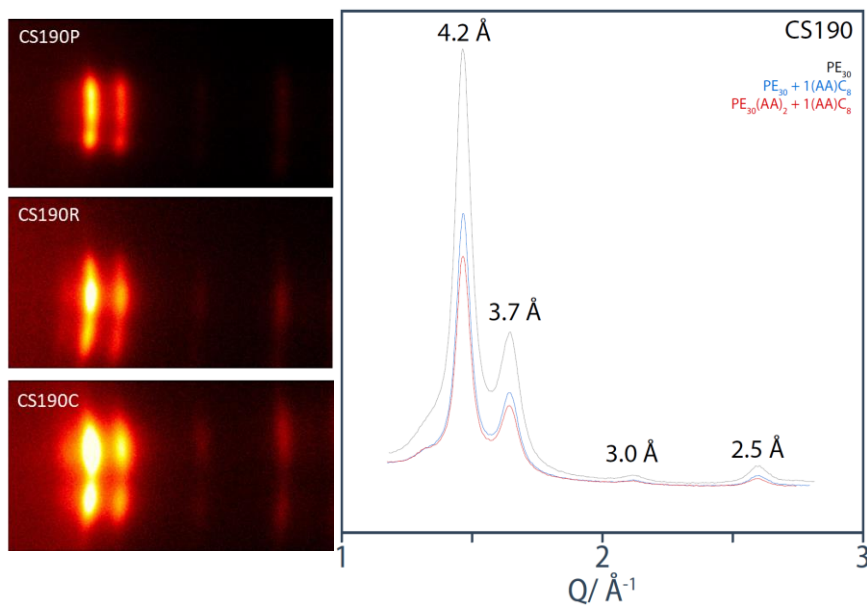

Figure 37. 2-Theta integration of CS190 fibers in WAXS experiment.

Further azimuthal integrations were carried out on the 4.2 Å and 3.7 Å peaks, to assess the orientation at that order of magnitude. Figure 38 represents the azimuthal plot of these peaks, proving that the periodicity occurs along the fiber axis.
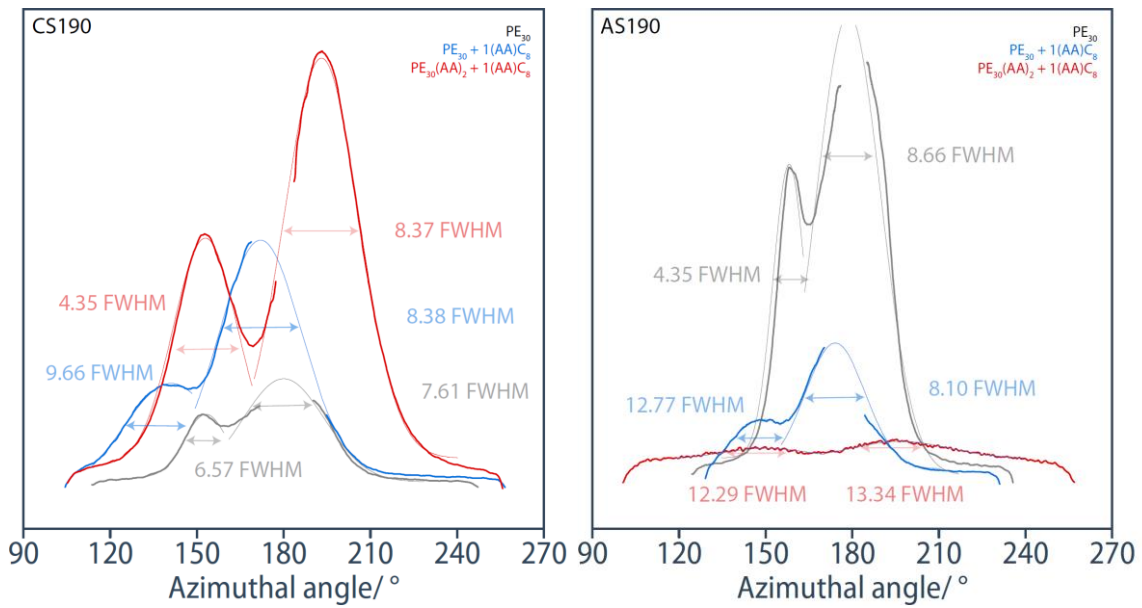
Figure 38. Azimuthal plot of the 4.2 Å (left) and 3.7 Å (right) peaks.

Whilst the melt-spun samples did not show significative orientation in these first two reflections, the CS190 reflections showed azimuthal plots reminiscent of those observed in the case of "chevron-type" morphologies [69]. These are common morphologies that occur in deformed semi-crystalline materials, in structures where lamellar structures are initially oriented perpendicular to the deformation direction [70], as we concluded for the melt-spun fibers AS190 from which the CS190 fibers were obtained by cold stretching. The cold stretching is then postulated to fold the lamellar structures, resulting in a zigzag pattern, referred to as a "chevron-type" morphology. Moreover, such morphologies have attracted great interest in thermoplastic elastomers, as they are usually formed in materials where the crystalline and amorphous phases have a great difference in stiffness [70]. Judging from the previous results, the melt-spun fibers are already materials where the polymer is less stiff than the additive aggregates, so this could promote the creation of these chevron patterns upon cold-stretching. Figure 39 illustrates this chevron morphology.
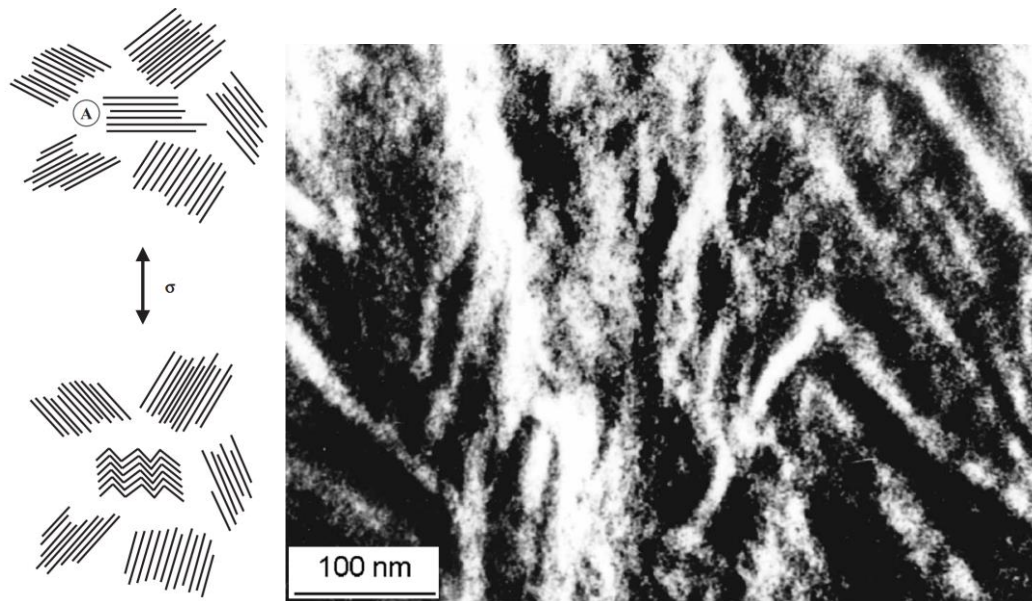
Figure 39. Schematic diagram of a chevron structure formation(left) and micrograph of a chevron structure in a cold-drawn HDPE (right) [70].

MECHANICAL CHARACTERIZATION

The mechanical properties of the samples were analyzed through tensile testing with a universal testing machine. In particular, yield strength and elongation at break, as well as toughness and Young's modulus were assessed and compared amongst samples, obtaining the results represented in Figure 40.
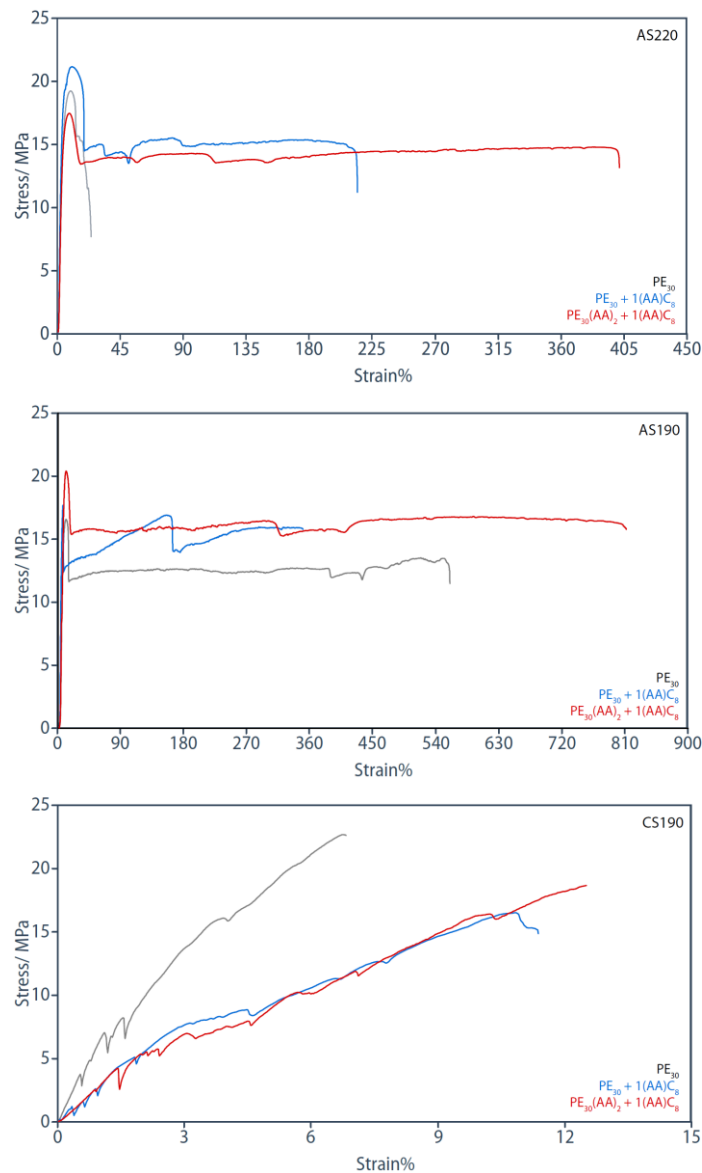
Figure 40. Representative tensile test curves of AS220 (top), AS190 (middle) and CS190 (down) sample groups.

Yield Strength and Elongation at Break

Figure 41 shows the yield strength and elongation at break obtained for the different processing methodologies and sample groups, indicating the statistically significative differences from the pristine sample.

Firstly, elongation at break was increased in the melt-spun samples of the concept materials, compared to the pristine and reference samples. Extrapolating the theory that these are predominantly comprised of stacked lamellae (as opposed to more predominantly fibrillar structures), then the conclusion would be that these stacked lamellae provide higher extensibility. The usual deformation mechanism of polyethylene involves the slipping of the lamellae, causing a reduction in width and an increase in the length of the tie molecules, which in turn get straightened and oriented [55]. SAXS azimuthal integrations of AS220 showed that the concept was the least oriented sample, with respect to pristine and reference.

Consequently, mechanical testing revealed a much higher elongation in this sample, as the tie molecules were not as tensed and therefore had more room to extend. In the AS190 fibers, this increase of the elongation at break was not as pronounced, probably because the concept samples showed greater orientation in the corresponding azimuthal plots. Still, elongation was overall greater in the concept samples. This may be due to the fact that the presence of additive crystals hampered the movement of the polymer chains during the processing, leaving room for further elongation in the testing. In the cold stretched fibers, the elongation at break was minimal because of the difference in the crystalline structure. A fibrillar structure would not permit much extra elongation, as the chains would have technically already stretched in the process.

Judging by the extensibility results, one would expect there to be less yield strength in the samples that showed more elongation, as is usually the case. However, this happened in all but the AS190 fibers, where yield strength showed a statistically significative improvement with regards to the pristine and reference materials. These samples were processed at approximately the aggregation temperature of the additive, and therefore this may have resulted in an improved yield strength because of a load-bearing nature from the additive aggregates during the processing.
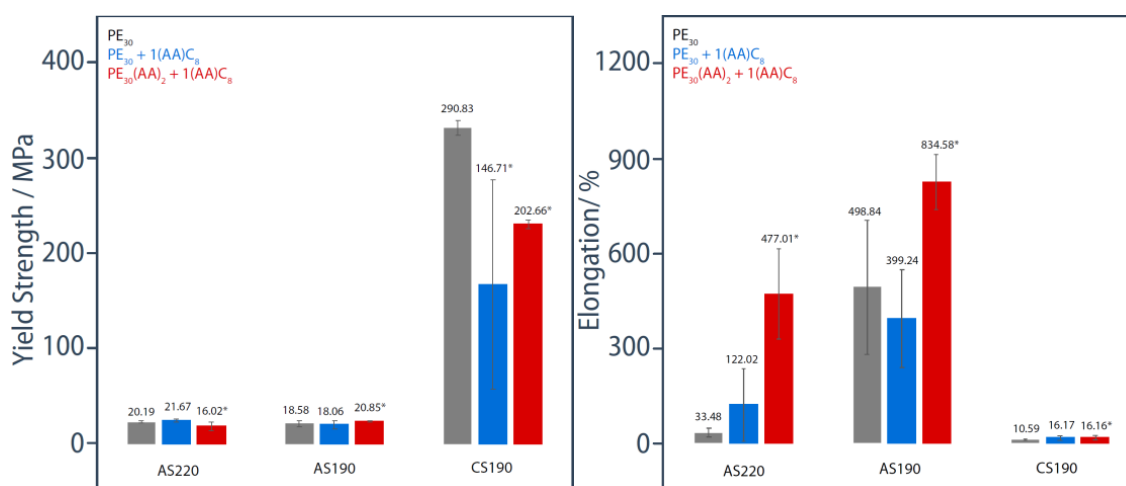

Figure 41. Yield strength (left) and elongation at break (right) of AS220, AS190 and CS190 sample groups.

Toughness and Young's Modulus

Figure 42 shows the toughness and Young's moduli obtained for the different processing methodologies and sample groups.

An interesting observation in the case of these properties concerns the toughness, which increased in the concept material regardless of the processing method. Still, in the AS220 and the CS190 it did so at the expense of the yield strength, and so it was a result mostly of the increased extensibility, which is a normal phenomenon. However, in the case of AS190 fibers, yield strength, elongation at break, and toughness all increased in the concept materials, compared to the pristine and reference ones.

As for the Young's moduli, there was no statistically significative change in the moduli within pristine, reference and concept fibers. However, there was a higher modulus for the cold-stretched fibers, compared to the melt-spun ones.
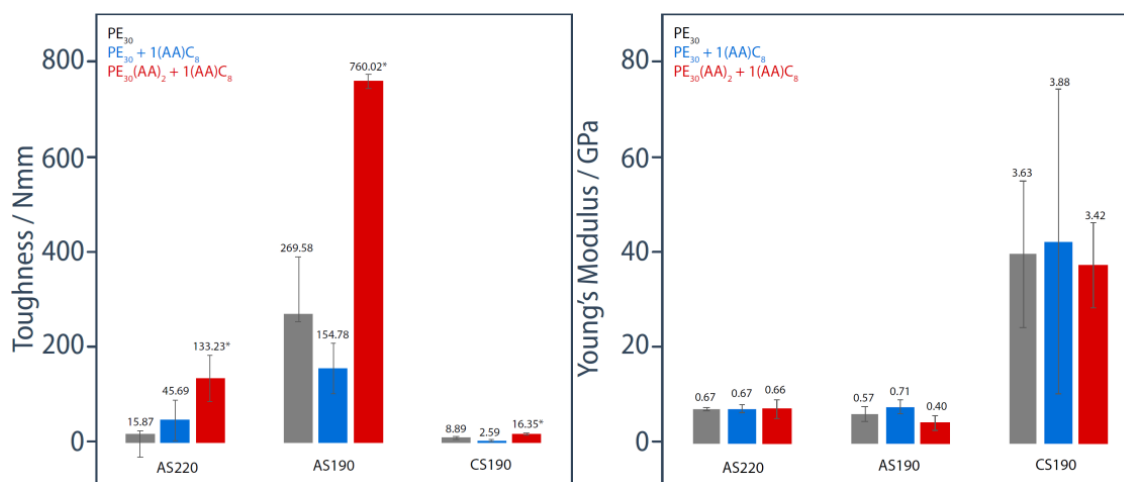

Figure 42. Toughness (left) and Young's modulus (right) of AS220, AS190 and CS190 sample groups.

In conclusion, in fibers melt drawn at approximately the aggregation temperature of the additive, a simultaneous increase in strength, stiffness and toughness was observed, in comparison to the pristine and concept materials. One plausible explanation is that, while the additive aggregates themselves did not directly change the mechanical performance, they allowed the polymer matrix to align in a different manner, which in turn did have an effect on the mechanical performance. The process would start in the melt, with liquid additive drops immiscible in the polymer melt. In the reference materials, these droplets are of macroscopic dimensions, as suggested from the optical microscopy experiments. In the concept materials, these droplets are apparently much smaller than the optical resolution and colloidally dispersed, as a result of the end-modified polymer acting as a surfactant and stabilizing these droplets. As the fibers were drawn from the melt, the polymer matrix was initially load bearing thanks to the entanglement, pulling apart the colloidal droplets in the concept materials due to the attached polymer end groups, which did not happen in the reference materials. This is why, in the SAXS experiments of the AS190 fibers, a 2 nm peak characteristic of additive crystals was observed in the reference materials but not in the concept materials, where the additive was confined to individualized nanofibrils due toits co-assembly with the polymer end groups and the resulting polymer tethering to these nanofibrils. These additive nanofibrils would start aligning in the polymer melt upon continued deformation. Once the nanofibrils were solidify, the physical network of aligned nanofibrils (that can flow in the polymer melt) and polymer segments connecting them would serve as a template to extend and orient the polymer chains. The tethered chains cannot easily relax because they are locked into the aggregates with their end groups. Upon solidification of the polymer matrix, these extended chains may then potentially serve both as nucleation sites and as tie molecules between crystalline lamellae. It is ultimately these tie molecules that provided increased yield strength to the material, while the lamellae provided the increased elongation at break due to lamellar slip.

62

CHAPTER 3

CONCLUSIONS AND FUTURE WORK

CONCLUSIONS

Blends of end-modified polymer with incorporated additive were synthesized and tested, in comparison to pristine HDPE and a reference material that contained the additive but no end-modification.

For the bulk materials, it was confirmed that a new rubbery plateau was formed due to the presence of the end-modification and co-assembly with the additive. This rubbery plateau enabled the material to behave as a soft solid, and was present between the transition temperatures of the polymer and those of the additive. The temperature range of this plateau was extended with increasing additive concentration, but incorporating too much additive resulted in an undesired microphase segregation of an additive-rich and a polymer-rich phase, as proven by optical microscopy.

For oriented materials, DSC results indicated the presence of two competing crystallization mechanisms within the materials, leading to two different crystalline superstructures depending on if the process was performed at high temperatures or at ambient conditions. It was hypothesized that these two structures were lamellar and fibrillar crystalline microstructures, and were represented by a predominant should at lower or higher temperatures, respectively. XRD results confirmed this hypothesis, because the azimuthal plots of the melt-spun samples showed a periodicity parallel to the fiber axis, representative of lamellar stacking, whereas the cold-stretched samples showed a periodicity perpendicular to this axis, which is characterstic of fibrillar crystals. Particularly in the AS190 fibers, the concept materials showed the highest degree of orientation, as estimated from the azimuthal plots. Tensile testing experiments showed increased toughness regardless of the processing method in for the concept materials, with AS190 fibers having the best performance and no trade-off in terms of toughness and yield strength. This enhanced mechanical performance was attributed to the synergistic effect of the end-modification and the processing methodology. In other words, the end-modification and incorporation of additive did not change the mechanical properties of the materials *per se*, but gave rise to processing opportunities that could do so. These processing opportunities involved melt-spinning the material at a temperature close to the aggregation temperature of the additive, so that a sequence of load-bearing roles, first from the polymer entanglement and then from the just solidified additive nanofibrils.

FUTURE WORK

The future work regarding this project could be focused in three directions:

Firstly, there is a need to compare the oriented samples with non-oriented ones. This cannot be done with fibers, as orientation is intrinsic in their processing method. Therefore, samples such as films should be developed, for example, through hot-pressing, to assess these differences. To make the oriented films, two approaches could be followed:

- The same process as in the fiber creation is followed, but using a flat nozzle for the extruder.

- The films can be deformed using a UTM, with the use of a temperature chamber and taking care of flow behavior.

Secondly, a house-made base polymer should be synthesized, as this would eliminate the differences between the commercial PE, used in pristine and reference samples, and the synthesized end-modified PE, used in concept materials.

Finally, other molecular weights could be used to test the mechanism and its influence in the mechanical properties depending on this MW.

CHAPTER 4

MATERIALS AND EXPERIMENTAL METHOD

INTRODUCTION

In this chapter, the work methodology followed to develop the research project will be explained.

On the one hand, information will be given on the materials used for the project, that is, on High-Density Polyethylene and its end-modified version, as well as on the oligopeptides that were used for both this functionalization and the creation of the additive.

On the other hand, the experimental method that was followed for the development of this project will be explained. This method is comprised of:

1. Compound synthesis and polymer blends. This section will provide a detailed description of the different synthesis methods and reactions that were performed in order to obtain the necessary compounds for the creation of the studied polymer blends, as well as the creation of these blends. Also, the characterization of these compounds and blends will be explained.

2. Processing of the samples. This section will explain the processing methods followed to convert the materials into the samples that were further tested and analyzed.

3. Thermomechanical characterization of the samples. This section focuses on the different techniques that were used to determine the thermal and mechanical properties of the samples.

4. Structure investigation of the samples. This section focuses on the different techniques that were used to analyse the internal structure of the samples.

MATERIALS

In this section, the materials used for the development of the research project will be described.

High – Density Polyethylene (HDPE)

The base polymer used for this research project was a DOW^{TM} 25055E High Density Polyethylene Resin in the form of pellets. According to Gel Permeation Chromatography (GPC) previously done at the laboratory, M_n is between 20,000 to 24,000 g/mol, with a dispersion (Đ) of 2.3 to 2.7 (the variability depends on the baselines and calibrations used).

Ala$_2$Ac

The laboratory uses oligopeptides as the reinforcing agent for its materials. In particular, the oligopeptides used in this laboratory were formed from the amino acid Alanine (Ala), combined with an acetyl group (Ac). Ala$_2$Ac was synthesized by previous group members through solution-phase peptide coupling reaction without further purification and characterized through NMR.

EXPERIMENTAL METHOD

All data was graphed using the Origin 2020b data analysis and graphing software for Windows (OriginLab Corp., Northampton, USA) and then exported into the Adobe Illustrator 2020 vector graphics and design software for MacOS (Adobe Inc., San Jose, USA) for final editing.

COMPOUNDS

SYNTHESIS OF END – MODIFIED POLYMER

Telechelic PE was obtained through a ring-opening metathesis polymerization (ROMP) reaction, using Grubb's second-generation catalyst. Then, a peptide reaction was performed to obtain $PE_{30}(AA)_2$. This process is summarized in Figure 43
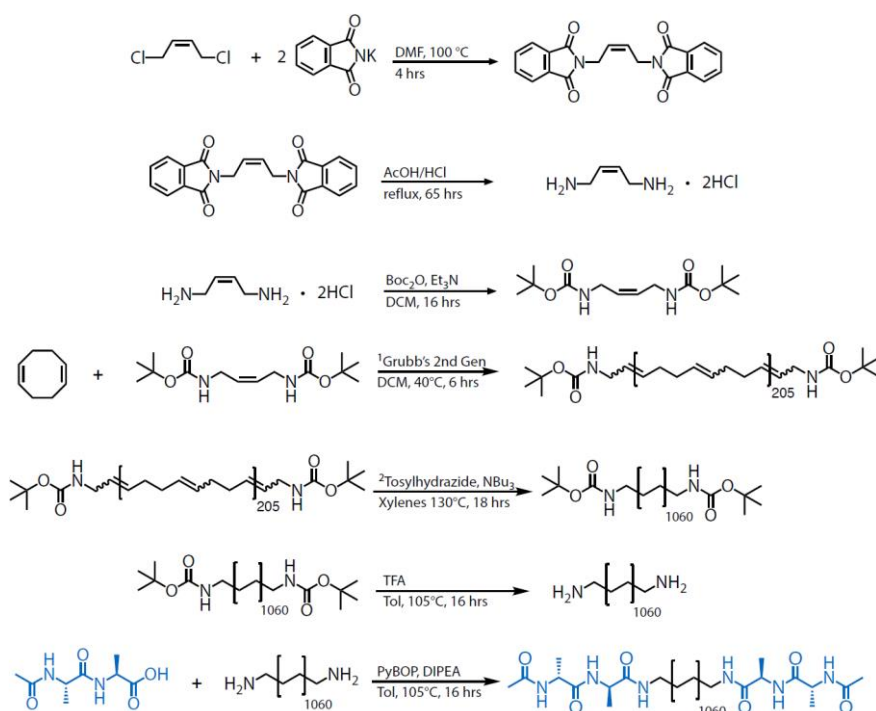
Figure 43. Complete reaction scheme for the synthesis of end-modified PE.

Cis-2-butene 1,4-diamine dihydrochloride (compound 2) was prepared according to a modified literature procedure [71]. Dry DMF (18 mL) and potassium phthalimide salt (4.08 g 22.0 mmol) were added to a flame-dried 50 mL flask under an argon atmosphere. Cis-1,4-dichloro-2-butene (1.24 g, 9.46 mmol) was weighed in a separate vial, and added to the flask. Dry DMF (2 mL) was used to rinse the vial, and this was also added to the flask. The reaction was heated to 100 °C and stirred for 3.5 hours before additional potassium phthalimide salt (0.93 g, 5.0 mmol) was added to the flask, with further stirring at 100 °C for

40 minutes. The reaction was allowed to cool to room temperature before being poured into rapidly stirring water at 0 °C (400 mL). The product was collected via filtration, washed twice with water (50 mL) and dried under vacuum to give the crude product (compound 1) as a pale-yellow powder. The crude product 1 was added to a round-bottom flask with acetic acid (20 mL) and 12M HCl (20 mL), which was then refluxed for 70 hours. The reaction mixture was allowed to cool, and solids were removed via filtration. The filtrate was concentrated in vacuo, and the residue was washed twice with cold ethanol to provide cis-2-butene 1,4-diaminium chloride (1) as a white powder (1.0 g, 66.5%).

Characterization: H NMR (D2O, 400MHz): δ = 5.90 (t, J=4.5 Hz, 2H), 3.76 (d, J=4.9 Hz, 4H).
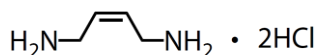
H_2N⎯⎯⎯⎯NH_2 · 2HCl

Figure 44. Molecular structure of compound 2.

Cis-di-tert-butyl 2-butene-1,4-diyldicarbamate (chain-transfer agent, CTA) (compound 3) was prepared according to a modified literature procedure [72]. The hydrochloride salt 2 (1.0 g, 6.3 mmol), triethylamine (5.05 g, 50 mmol) and 125 mL dry DCM were added to a flask at 0 °C. Di-tert-butyl dicarbonate (2.79 g, 12.8 mmol) was added slowly to the mixture and allowed to react for 1 hour before warming to room temperature and stirring for another 15 hours. The reaction was washed twice with each of the following: 0.5N HCl, saturated NaHCO3 solution, brine, and water. The DCM phase was dried over MgSO4 and solvent was removed in vacuo to give 3 as a while solid (1.60 g, 86.8%).

Characterization: H NMR (CDCl₃, 400MHz): δ = 5.54 (t, J = 4.2 Hz, 2H), 4.83 (br s, 2H), 3.77 (dd, J = 5.4 Hz, 4H), 1.44 (s, 18H).
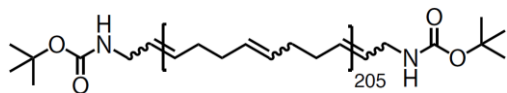

Figure 45. Molecular structure of compound 3.

Boc-amino-telechelic polybutadiene (30K, compound 4) of around 30,000 g/mol was prepared according to the literature procedure [73] using a different CTA and target molecular weight. Cyclooctadiene (COD) was purified by hydroboration via a borane-tetrahydrofuran complex (BH3-THF), followed by distillation as described previously [71]. To a flame-dried 250 mL Schlenk flask under argon, the CTA (3) (234.8 mg, 0.82 mmol), Grubb's second-generation catalyst (24.5 mg, 0.029 mmol), purified COD (2.88 g, 26.6 mmol), and dry, degassed DCM (20 mL) were added. This mixture was stirred at 40 °C for 1 hour, then additional COD (26.0 g, 240.3 mmol) and DCM (75 mL) were added via syringe to the reaction. This was stirred at 40 °C for an additional 6 hours, followed by addition of ethyl vinyl ether (0.3 mL) to terminate the reaction. The reaction was diluted with DCM (300mL) and precipitated into rapidly stirring methanol (1.5 L) at 0 °C. The polymer was washed several times with methanol and dried under vacuum to yield an off-white rubbery solid (24.35 g, 84%).

Characterization: H NMR (CDCl$_3$, 400MHz): δ = 5.41 (br, trans-CH=), 5.37 (br, cis-CH=), 4.48 (br, -NHBoc), 3.68 (br, -CH$_2$-NHBoc), 2.08 (br, cis-CH$_2$-), and 2.03 (br, trans-CH2-). M$_n$, NMR = 29,000 g/mol.
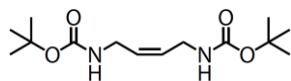

Figure 46. Molecular structure of compound 4.

Boc-amino-telechelic polyethylene (30K, compound 5) was prepared by adding compound 4 (0.5 g, 9.26 mmol double-bonds), xylenes (25 mL), p-toluenesulfonyl hydrazide (3.45 g, 18.5 mmol), tributylamine (3.60 g, 19.4 mmol), and 4,4'-Methylenebis(2,6-di-tert-butylphenol) (10 mg, 2 wt% to 4) to a round-bottom flask equipped with a reflux condenser. This mixture was heated to 135 °C for 18 hours, resulting in a red solution. It was precipitated directly into rapidly stirring methanol (200 mL) at 0 °C, and washed successively with methanol, acetone, and DCM, before being collected and dried under vacuum at 50 °C overnight to afford an off-white solid (0.50 g, 96%). NMR analysis showed over 99% hydrogenation.

Characterization: H NMR (Tol-d8, 400MHz): δ = 2.92 (br, -CH$_2$-NHBoc), 1.42 (s, tBu), and 1.33 (s, -CH$_2$-). GPC: M$_n$ = 22,000 g/mol, M$_w$ = 45,000 g/mol.
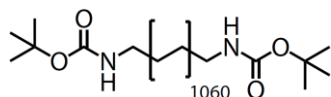

Figure 47. Molecular structure of compound 5.

Amino-telechelic polyethylene (30K, compound 6) was prepared by adding compound 5 (0.5 g, 0.017mmol) to a Schlenk flask and dissolved in o-dichlorobenzene (15 mL) at 70 °C under argon. Trifluoroacetic acid (0.2 mL) was added to the mixture, which was sired for 16 hours, before being precipitated into rapidly stirring methanol (75 mL) at 0 °C, washed with methanol and DCM, and dried under vacuum at 50 °C overnight to afford an off-white solid (0.46 g, 92%).

Characterization: H NMR (TCE-d2, 400MHz): δ = 2.81 (br, -CH$_2$-NH$_2$), and 1.37 (s, -CH$_2$-).
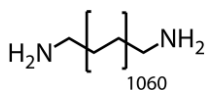

Figure 48. Molecular structure of compound 6.

Polyethylene - (AcAla$_2$)$_2$ (30K, compound 7) was prepared by dissolving compound 6 in Toluene (20 mL) at 100°C in a Schlenk flask under argon, followed by addition of PyBOP (41.g mg, 0.08 mmol). Ala$_2$Ac (16.2 mg, 0.08 mmol), was dissolved in DMSO (1 mL), and added to the reaction mixture, followed by the addition of DIPEA (2 mL). This was heated at 110 °C for 16 hours, before being precipitated into rapidly stirring methanol (75 mL) at 0 °C, washed with in series with methanol, water, methanol and finally DCM, and dried under vacuum overnight to afford an off-white solid (0.44 g, 96%).

Characterization: H NMR (TCE-d2, 400MHz): 4.40 (br, Ala-CH₃), 3.29 (br, -CH₂-NH-), 2.04 (s, Ala-CH₃), 1.37 (s, -CH₂-).
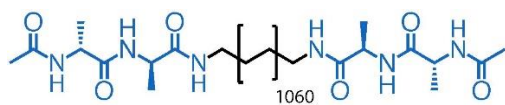

Figure 49. Molecular structure of compound 7.

A higher molecular weight polyethylene of around 100,000 g/mol was synthesized through the same procedure that is described above, but with a different ratio of CTA for the ROMP.

All masses were weighed using a Mettler Toledo XS205 DualRange scale.

Characterization of the end-modified PE

High temperature ^{1}H NMR spectroscopy was carried out on Compound 7 at 373K and 1000 scans using a Bruker Avance NEO 400 spectrometer equipped with heating and a liquid Nitrogen cooling system at a frequency of 400 MHz. The spectrum was calibrated to the residual solvent peaks of Tol-d8 (2.08 ppm).

SYNTHESIS OF ADDITIVE

Acetyl-L-alanyl-L-alanyl-L-alanine (2-ethylhexyl) amide (compound 8) was prepared by adding PyBOP (3.6 g, 6.92 mmol 1.4 equiv.) and DIPEA (3.45 mL, 19.8mmol 4 equiv.) to a solution of Acetyl-L-alanyl-L-alanyl-L-alanine (1 g, 4.95 mmol, 1 equiv.) and 2-ethylhexyl-1-amine (639 mg, 4.95 mmol, 1 equiv.) in 15 mL of THF. After stirring the reaction mixture overnight, it was concentrated to one third of its original volume and poured into water. The solid residue was filtered and redissolved again in THF. The precipitation was repeated twice. The resulting solid was dissolved in DCM, the solution was dried over MgSO₄. After filtration, the solvent was finally evaporated in vacuo, and the resulting solid was dried in high vacuum. Acetyl-L-alanyl-L-alanyl-L-alanine (2-ethylhexyl) amide 8 was obtained as a colorless solid (1.10 g, 4.03 mmol, 68%).

Characterization: H NMR (400 MHz, CDCl₃): δ = 6.99 (s, 1H), 6.37 (d, J = 50.5 Hz, 2H), 4.52 (d, J = 30.8 Hz, 2H), 3.19 (s, 3H), 2.03 (s, 3H), 1.66 (s, 3H), 1.53–1.00 (m, 16H), 1.00–0.70 (m, 6H). C NMR (400 MHz, DMSO-d6): δ = 172.43, 169.66, 48.75, 48.60, 41.65, 30.70, 28.77, 23.99, 22.96, 18.87, 18.50, 14.42, 11.19.
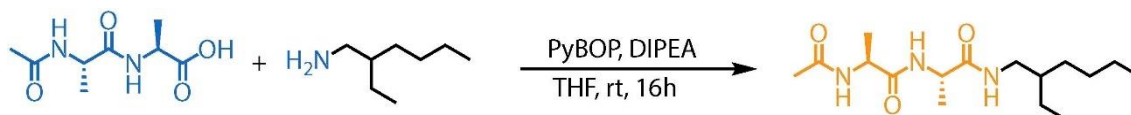

Figure 50. Reaction scheme for the synthesis of compound 8.

^{1}H NMR spectroscopy was carried out on Compound 8 at 324K and 1000 scans using a Bruker Avance III 400 spectrometer at a frequency of 400 MHz. The spectrum was calibrated to the residual solvent peaks of $CDCl_3$ (7.26 ppm).

POLYMER BLENDS

SYNTHESIS OF POLYMER BLENDS

For the reference material, the amounts of commercial PE and additive were weighed using a Mettler Toledo XS205 DualRange scale according to the required wt%. The weighed compounds were then added to 7 mL of Toluene and stirred at 100 °C until dissolved. The resulting solution was let to cool down for 10 min, after which it was attached to a Heidolph Instruments Hei-VAP Core rotary evaporator until the solvent was completely evaporated. Finally, the resulting product was dried overnight under vacuum to afford a white solid.

For the concept material, the same procedure was performed, but using compound 7 instead of the commercial PE. The resulting product was dried under vacuum overnight to afford a pale-yellow solid.

CHARACTERIZATION OF POLYMER BLENDS

Differential Scanning Calorimetry (DSC)

DSC measurements were performed on a Mettler Toledo DSC 3+ for a total of 3 cycles. All cycles except the last one comprised a heating of the sample from 50°C to 230°C at a rate of 20 K/min, after which it was left isothermally for 1 min and then cooled down to 50°C. The last cycle was done according to the same structure, but with a rate of 10 K/min. A mass of 5 to 15 mg of material was used for these tests.

The data obtained from the software was imported into the Origin 2020b software, where a baseline correction was performed for both the polymer and the additive peaks, following the equation:

$$Y = \frac{y_2 - y_1}{x_2 - x_1} \cdot T + \frac{x_2 \cdot y_1 - x_1 \cdot y_2}{x_2 - x_1}$$

Where x_1 and x_2 are the temperatures between which the baseline correction is to be made, y_1 and y_2 are the corresponding initial heat flow values.

Then, these two peaks were placed into the same graph using the Adobe Illustrator 2020 software, adjusting the scale accordingly.

Dynamic Shear Rheology

Dynamic shear rheology was performed on a parallel plate TA Instruments rheometer, model ARES 2. Aluminum plates of 8 mm were used, and a gap of 1 to 1.5 mm was set. The samples were loaded at a temperature of 150°C, and the starting temperature of the test was 200°C, from which a temperature sweep was performed at a rate of 5°C/min, a fixed radial frequency of 1rad/s and a variable strain rate dependent on the temperature.

The data was imported to the Origin 2020b software, where it was plotted and exported into the Adobe Illustrator 2020 software for final aesthetic touches.

Temperature-dependent Optical Microscopy

Temperature-dependent optical microscopy was performed using an Olympus BX60 optical microscope and a Linkam TMS600 heating stage. Samples of the bulk material were compressed between two crystal plates and heated up to 150°C to obtain a melt. Then, the temperature was increased to 230°C at a rate of 1°C/min. Then, the cooling cycle was performed by cooling the sample to 190°C at a rate of 10°C/min, then cooling from 190°C to 140°C at a rate of 30°C/min and then from 140°C to 110°C at a rate of 10°C/min. Then, a heating cycle was performed by following these same temperatures and rates but in heating. This cooling-heating cycle was repeated twice. Throughout the performance of the test, the sample was observed through the computer screen, and pictures were taken of the critical or transition moments.

PROCESSING OF SAMPLES

An Xplore Instruments, model MC 5 micro compounder was used for the melt-spinning of the fibers, as well as a custom-made spinneret. The processing methodology was the same for all of the materials (pristine, reference and concept), but adjusting the extrusion and spinneret speeds for each of them to obtain comparable thicknesses. An amount of approximately 5 mL of material was hot-pressed using a XX hot press. The process was done at a temperature of 140°C and a heating rate of 20°C/min, holding these conditions for 10 min at a pressure of $40N/m^2$. The resulting film was cut into small pieces with scissors and fed to the extruder at 50 rpm. Then, the speed was increased to 100 rpm and the mixture was left mixing for 3 min. After the time lapsed, the extruder speed was adjusted to the desired value and the valve was open. With the help of aluminum tweezers, the molten material was guided from the extruder nozzle to the spinneret, that would already be spinning, and was stuck to it using adhesive tape. The spinneret would then pull from this end, helping form a fiber. The fiber was then collected by coiling it around a glass vial. Individual samples were made by cutting this into 60 mm segments, and their thickness was measured using an Olympus BX60 optical microscope.

CHARACTERIZATION OF SAMPLES

Differential Scanning Calorimetry (DSC)

DSC measurements were performed on the obtained fibers using a Mettler Toledo DSC 3+ for a total of 2 cycles. These comprised a heating of the sample from 50 °C to 230°C at a rate of 20 K/min, after which it was left isothermally for 1 min and then cooled down to 50 °C. A mass of 5 to 15 mg of material was used for these tests. The melting points were obtained from the second heating curve, whereas the crystallization temperatures were obtained from the first cooling curve.

The processing of the curves was done as explained for the previous DSC methodology on characterization of the polymer blends.

Mechanical Testing

Tensile tests were performed on the obtained fibers using a Zwick Roell XX universal testing machine. A load cell of 50N was used, and 60 mm fibers were clamped to self-tightening grips. To avoid slippage, the ends of the fibers were coiled two times around a 1 cm wide sandpaper strip, therefore having an end length of the tested sample (gap between clamps) of approximately 25 mm. The pre-load was set to 0.2 N. The tests were performed at a speed of 10 mm/min, and breakage was investigated at a drop of 80% in strain.

Yield strength and elongation were obtained directly from the software. Toughness was calculated as a result of the obtained curves, also by the machine software. Young's Modulus was calculated from the obtained data, through eh following equation:

$$E = \frac{\sigma}{\varepsilon}$$

Where σ is the uniaxial stress, measured in MPa, and ε is the strain, dimensionless.

The obtained tensile test data was processed by performing statistical analysis on the data points. Firstly, for each sample type, an analysis of outliers was performed to understand how representative each of the values were within the same group. To do so, Z-scores of the different values were computed to reveal the significative differences of these values with the average, as formulated in Equation 3, where X is the value, $\bar{X}$ is the average and σ is the standard deviation. If a significative difference was observed, the sample was deemed as an outlier and discarded. A P-value of 0.05 was taken as an indication of significative difference.

$$Z = \frac{x - \bar{X}}{\sigma}$$

Equation 3. Formula to compute the Z-score.

After the outliers were identified and discarded, a one-factor ANOVA analysis was performed to assess the significative differences between sample groups. This was done using the SPSS 24.0 statistical software for Windows (IBM SPSS, Chicago, USA). A P-value of 0.05 was taken as an indication of significative difference.

X-Ray Diffraction (XRD)

In-situ SAXS and WAXS analysis were carried out on a EIGER2R-500K HPAD detector. The technical details of the scattering experiments are summarized in Table 7.

Table 7.Parameters of X-ray experiments.

Parameter	Value
Energy	50 KeV
Wavelength	0.154 nm
Beam size	0.2 mm
Step width	100 mm

For the 1D plots, primary data was processed using the DIFFRAC.EVA interface (Bruker, Billerica, USA), by performing circular integration and identifying the corresponding peaks. Data was expressed in terms of wave vector, as described in Equation 4, where 2θ is the scattering angle and ν is the wavelength.

$$q = \frac{4 \cdot \sin \theta}{\nu}$$

Equation 4. Formula for the wave vector.

The distances, according to Bragg's law, were evaluated through Equation 5.

$$d = \frac{2\pi}{q}$$

Equation 5. Bragg's law for evaluation of distances from wave vector.

The obtained plots were then exported into the Origin 2020b software, where the curves were smoothed by using the Savitzky-Golay method of polynomial order 2.

For the Azimuthal plots, primary data was processed using the DIFFRAC.EVA interface, by performing Azimuthal integration. Then, the obtained curves were exported into Origin 2020b and smoothed out using the same smoothing method as in the 1D plots. To eliminate the artifacts caused by the Kapton that kept the beamstop in place, a Bezier interpolation was performed on the area of interest. The curve was then fitted with a Gaussian to determine the full width at half maximum (FWHM).

EXPERIMENT MATRIX

As a result of the aforementioned procedures, the resulting experiment matrix is shown in Table 8 as a summary of the process and experiments that were carried out during the research project.

Table 8. Experimental matrix.

	Sample	S	Type	Process	DSC	R	OM	XRD	UTM
Additives	$(AA)C_8$	✓	Bulk	-	✓	✓			
	$(AA)C_{20}$	✓	Bulk	-	✓	✓			
Polymers	HDPE		Bulk	-	✓	✓			
			Fiber	AS220	✓			✓	✓
				AS190	✓			✓	✓
				CS190	✓			✓	✓
	$PE_{30}(AA)_2$	✓	Bulk	-	✓	✓			
	$PE_{100}(AA)_2$	✓	Bulk	-	✓	✓			
Blends	$PE_{30} + 0.25(AA)C_8$	✓	Bulk	-	✓		✓		
	$PE_{30} + 0.5(AA)C_8$	✓	Bulk	-	✓	✓	✓		
	$PE_{30} + 1(AA)C_8$	✓	Bulk	-	✓	✓	✓		
		✓	Fiber	AS220	✓			✓	✓
		✓		AS190	✓			✓	✓
		✓		CS190	✓			✓	✓
	$PE_{30} + 2(AA)C_8$	✓	Bulk	-	✓	✓	✓		
	$PE_{30} + 4(AA)C_8$		Bulk		✓		✓		
	$PE_{30} + 8(AA)C_8$		Bulk		✓		✓		
	$PE_{30} + 0.25(AA)C_{20}$	✓	Bulk	-	✓	✓	✓		
	$PE_{30} + 0.5(AA)C_{20}$	✓	Bulk	-	✓	✓	✓		
	$PE_{30} + 1(AA)C_{20}$	✓	Bulk	-	✓	✓	✓		
	$PE_{30} + 2(AA)C_{20}$	✓	Bulk	-	✓	✓	✓		
	$PE_{30}(AA)_2 + 0.25(AA)C_8$	✓	Bulk	-	✓		✓		
	$PE_{30}(AA)_2 + 0.5(AA)C_8$	✓	Bulk	-	✓	✓	✓		
	$PE_{30}(AA)_2 + 0.75(AA)C_8$	✓	Bulk	-	✓		✓		
	$PE_{30}(AA)_2 + 1(AA)C_8$	✓	Bulk	-	✓	✓	✓		
		✓	Fiber	AS220	✓			✓	✓
		✓		AS190	✓			✓	✓
		✓		CS190	✓			✓	✓
	$PE_{30}(AA)_2 + 1.5(AA)C_8$	✓	Bulk	-	✓		✓		
	$PE_{30}(AA)_2 + 2(AA)C_8$	✓	Bulk	-	✓	✓	✓		
	$PE_{30}(AA)_2 + 4(AA)C_8$		Bulk		✓	✓			
	$PE_{30}(AA)_2 + 8(AA)C_8$		Bulk		✓				
	$PE_{30}(AA)_2 + 0.25(AA)C_{20}$	✓	Bulk	-	✓	✓	✓		
	$PE_{30}(AA)_2 + 0.5(AA)C_{20}$	✓	Bulk	-	✓	✓	✓		
	$PE_{30}(AA)_2 + 1(AA)C_{20}$	✓	Bulk	-	✓	✓	✓		
	$PE_{30}(AA)_2 + 2(AA)C_{20}$	✓	Bulk	-	✓	✓	✓		
	$PE_{100}(AA)_2 + 0.5(AA)C_8$	✓	Bulk	-	✓		✓		
	$PE_{100}(AA)_2 + 1(AA)C_8$	✓	Bulk	-	✓		✓		
	$PE_{100}(AA)_2 + 2(AA)C_8$	✓	Bulk	-	✓		✓		
	$PE_{100}(AA)_2 + 0.25(AA)C_{20}$	✓	Bulk	-	✓		✓		
	$PE_{100}(AA)_2 + 0.5(AA)C_{20}$	✓	Bulk	-	✓		✓		
	$PE_{100}(AA)_2 + 1(AA)C_{20}$	✓	Bulk	-	✓		✓		
	$PE_{100}(AA)_2 + 2(AA)C_{20}$	✓	Bulk	-	✓		✓		

* S = synthesis, DSC = differential scanning calorimetry, R = rheology, OM = optical microscopy, XRD = X-ray diffraction, UTM = tensile testing

CHAPTER 5

REFERENCES

REFERENCES

[1].   Nerland, I. L., Halsband, C., Allan, I., & Thomas, K. V. (2014). *Microplastics in marine environments: occurrence, distribution and effects*. Norwegian Institute for Water Research

[2].   The Freedonia Group. (2014). *World Polyethylene*. The Freedonia Group. Study #3210

[3].   PlasticsEurope. (2020). *Plastics – The Facts 2020*. PlasticsEurope [Online] Available at: www.plasticseurope.org/application/files/8016/1125/2189/AF_Plastics_the_facts-WEB-2020-ING_FINAL.pdf

[4].   Al-Sammerrai, D., & Al-Nidawy, N. K. (1989). Polyethylene: Synthesis, Properties, and Uses. Marcel Dekker, Inc., Handbook of Polymer Science and Technology., 2, 341-365.

[5].   Treenate, P., Limphitakphong, N., & Chavalparit, O. (2017, July). *A complete life cycle assessment of high density polyethylene plastic bottle*. In IOP Conference series: materials science and engineering (Vol. 222, No. 1, p. 012010). IOP Publishing.

[6].   Vega, J. F., Rastogi, S., Peters, G. W. M., & Meijer, H. E. H. (2004). *Rheology and reptation of linear polymers. Ultrahigh molecular weight chain dynamics in the melt*. Journal of Rheology, 48(3), 663-678.

[7].   Spiegelberg, S., Kozak, A., & Braithwaite, G. (2016). *Characterization of physical, chemical, and mechanical properties of UHMWPE*. In UHMWPE Biomaterials Handbook (pp. 531-552). William Andrew Publishing.

[8].   Tam, T., & Bhatnagar, A. (2016). *High-performance ballistic fibers and tapes*. In Lightweight Ballistic Composites (pp. 1-39). Woodhead Publishing.

[9].   Stadler, R., & de Lucca Freitas, L. (1986). Thermoplastic elastomers by hydrogen bonding 1. Rheological properties of modified polybutadiene. Colloid and polymer science, 264(9), 773-778.

[10].   Holden, G. (1987). *Thermoplastic elastomers*. In Rubber technology (pp. 465-481). Springer, Boston, MA.

[11].   de Greef, T. F., & Meijer, E. W. (2008). *Supramolecular polymers*. Nature, 453(7192), 171-173.

[12].   Holden, G., Bishop, E. T., & Legge, N. R. (1969). *Thermoplastic elastomers*. In Journal of Polymer Science Part C: Polymer Symposia (Vol. 26, No. 1, pp. 37-57). New York: Wiley Subscription Services, Inc., A Wiley Company.

[13].   Bonart, R. (1979*). Thermoplastic elastomers*. Polymer, 20(11), 1389-1403.

[14].   Holden, G. (2011). *Thermoplastic elastomers*. In Applied Plastics Engineering Handbook (pp. 77-91). William Andrew Publishing.

[15].   Burnett, D. J., Thielmann, F., & Ryntz, R. A. (2007). *Correlating thermodynamic and mechanical adhesion phenomena for thermoplastic polyolefins*. Journal of Coatings Technology and Research, 4(2), 211-215.

[16].   Boyce, M. C., Kear, K., Socrate, S., & Shaw, K. (2001). *Deformation of thermoplastic vulcanizates*. Journal of the Mechanics and Physics of Solids, 49(5), 1073-1098.

[17].   Qi, H. J., & Boyce, M. C. (2005). *Stress–strain behavior of thermoplastic polyurethanes*. Mechanics of materials, 37(8), 817-839.

[18].   Nitta, K. H., & Kuriyagawa, M. (2016). *12 Thermoplastic Polyurethanes*. Handbook of Thermoplastics, 41, 387.

[19].   Kollman, P. A., & Allen, L. C. (1972). *Theory of the hydrogen bond*. Chemical Reviews, 72(3), 283-303.

[20].   Buckingham, A. D., Del Bene, J. E., & McDowell, S. A. C. (2008). *The hydrogen bond*. Chemical Physics Letters, 463(1-3), 1-10.

[21].   McRee, D. E. (1999). *Practical protein crystallography*. Elsevier.

[22].   Kresge, E. N. (1991). *Polyolefin thermoplastic elastomer blends*. Rubber chemistry and technology, 64(3), 469-480.

[23].   Gessler, A. M., & Haslett, W. H. (1962). 7.(to Esso Research and Engineering Co.). US Pat, 3037954.

[24].   Coran, A. Y. (1995). *Vulcanization: Conventional and dynamic*. Rubber chemistry and technology, 68(3), 351-375.

[25].   Hartman, P. F., Eddy, C. L., & Koo, G. P. (1970). *A report on new elastomeric thermoplastics*. SPE JOURNAL, 26(5), 62.

[26].   Tobolsky, A. V. (1959). *Trends in rubber research*. Rubber world, 139, 857.

[27].   Kontos, E. G., Easterbrook, E. K., & Gilbert, R. D. (1962). *Block copolymers of α-olefins prepared from macromolecules with long chain lifetimes*. Journal of Polymer Science, 61(171), 69-82.

[28].   Kontos, E. G. (1968). (to Uniroyal Inc.), US Pat, 3378606.

[29].   Puett, D., Smith Jr, K. J., Ciferri, A., & Kontos, E. G. (1964). *Elasticity of Block Copolymers*. The Journal of Chemical Physics, 40(1), 253-254.

[30].   Dai, S., Li, S., Xu, G., & Chen, C. (2020). *Direct synthesis of polar functionalized polyethylene thermoplastic elastomer*. Macromolecules, 53(7), 2539-2546.

[31].   Chum, P. S., & Swogger, K. W. (2008). *Olefin polymer technologies—History and recent progress at The Dow Chemical Company*. Progress in Polymer Science, 33(8), 797-819.

[32].   Leone, G., Mauri, M., Bertini, F., Canetti, M., Piovani, D., & Ricci, G. (2015). *Ni (II) α-diimine-catalyzed α-olefins polymerization: thermoplastic elastomers of block copolymers*. Macromolecules, 48(5), 1304-1312.

[33].   O'Connor, K. S., Watts, A., Vaidya, T., LaPointe, A. M., Hillmyer, M. A., & Coates, G. W. (2016). *Controlled chain walking for the synthesis of thermoplastic polyolefin elastomers: synthesis, structure, and properties*. Macromolecules, 49(18), 6743-6751.

[34].   Lian, K., Zhu, Y., Li, W., Dai, S., & Chen, C. (2017). Direct synthesis of thermoplastic polyolefin elastomers from nickel-catalyzed ethylene polymerization. Macromolecules, 50(16), 6074-6080.

[35].   Fang, J., Sui, X., Li, Y., & Chen, C. (2018). Synthesis of polyolefin elastomers from unsymmetrical α-diimine nickel catalyzed olefin polymerization. Polymer Chemistry, 9(30), 4143-4149.

[36].   Roumeli, E., Markoulis, A., Kyratsi, T., Bikiaris, D., & Chrissafis, K. (2014). Carbon nanotube-reinforced crosslinked polyethylene pipes for geothermal applications: From synthesis to decomposition using analytical pyrolysis–GC/MS and thermogravimetric analysis. Polymer degradation and stability, 100, 42-53.

[37].   Tamboli, S. M., Mhaske, S. T., & Kale, D. D. (2004). *Crosslinked polyethylene*.

[38].   Caminiti, R., Pandolfi, L., & Ballirano, P. (2000). *Structure of polyethylene from X-ray powder diffraction: Influence of the amorphous fraction on data analysis*. Journal of Macromolecular Science, Part B, 39(4), 481-492.

[39].   Severin, N. (1999). Molecular Dynamics Simulations of Polymers and Micelles at Interfaces.

[40].   Vaughan, A. S., & Bassett, D. C. (1989). *Crystallization and morphology*. Pergamon Press plc, Comprehensive Polymer Science: the Synthesis, Characterization, Reactions & Applications of Polymers., 2, 415-457.

[41].   Hosemann, R., & Bagchi, S. N. (1962). *Direct analysis of diffraction by matter*. North-Holland Publishing Company.

[42].   Ottani, S., Ferracini, E., Ferrero, A., Malta, V., & Porter, R. S. (1996). *SAXS investigations on uniaxially drawn fibers obtained from polyethylene reactor powder*. Macromolecules, 29(9), 3292-3299.

[43].   Brady, J. M., & Thomas, E. L. (1989). *Deformation of oriented high density polyethylene shish-kebab films*. Journal of materials science, 24(9), 3311-3318.

[44].   Pennings, A. J., Van der Mark, J. M. A. A., & Kiel, A. M. (1970). *Hydrodynamically induced crystallization of polymers from solution*. Kolloid-Zeitschrift und Zeitschrift für Polymere, 237(2), 336-358.

[45].   Dargazany, R., Khiêm, V. N., Poshtan, E. A., & Itskov, M. (2014). *Constitutive modeling of strain-induced crystallization in filled rubbers*. Physical Review E, 89(2), 022604.

[46].   Richards, R. B. (1951). *Polyethylene‐structure, crystallinity and properties*. Journal of Applied Chemistry, 1(8), 370-376.

[47].   Gent, A. N., & Vickroy Jr, V. V. (1967). *Elastic behavior, birefringence, and swelling of amorphous polyethylene networks*. Journal of Polymer Science Part A-2: Polymer Physics, 5(1), 47-61.

[48].   Gräfen, H. (Ed.). (2013). Lexikon Werkstofftechnik: Berichtigter Nachdruck. Springer-Verlag.

[49].   Roberts, D. E. (1950). Heats of polymerization. A summary of published values and their relation to structure. J. Res. Natl. Bur. Stand, 44, 221-232.

[50].   Hosemann, R., & Bagchi, S. N. (1962). *Direct analysis of diffraction by matter*. North-Holland Publishing Company.

[51].   Young, R. J., Bowden, P. B., Ritchie, J. M., & Rider, J. G. (1973). *Deformation mechanisms in oriented high-density polyethylene*. Journal of Materials Science, 8(1), 23-36.

[52].   Dasari, A., & Misra, R. D. K. (2003). *On the strain rate sensitivity of high density polyethylene and polypropylenes*. Materials Science and Engineering: A, 358(1-2), 356-371.

[53].   Andrews, J. M., & Ward, I. M. (1970). *The cold-drawing of high density polyethylene*. Journal of Materials Science, 5(5), 411-417.

[54].   Jiang, Z., Tang, Y., Rieger, J., Enderle, H. F., Lilge, D., Roth, S. V., ... & Men, Y. (2009). Structural evolution of tensile deformed high-density polyethylene at elevated temperatures: Scanning synchrotron small-and wide-angle X-ray scattering studies. Polymer, 50(16), 4101-4111.

[55].   Wang, Z., An, M., Xu, H., Lv, Y., Tian, F., & Gu, Q. (2017). Structural evolution from shish-kebab to fibrillar crystals during hot-stretching process of gel spinning ultra-high molecular weight polyethylene fibers obtained from low concentration solution. Polymer, 120, 244-254.

[56].   Vega, J. F., Rastogi, S., Peters, G. W. M., & Meijer, H. E. H. (2004*). Rheology and reptation of linear polymers. Ultrahigh molecular weight chain dynamics in the melt*. Journal of Rheology, 48(3), 663-678.

[57].   Tam, T., & Bhatnagar, A. (2016). *High-performance ballistic fibers and tapes*. In Lightweight Ballistic Composites (pp. 1-39). Woodhead Publishing.

[58].   Bhatnagar, A. (Ed.). (2016). Lightweight ballistic composites: military and law-enforcement applications. Woodhead Publishing.

[59].   Folmer, B. J., Sijbesma, R. P., Versteegen, R. M., Van der Rijt, J. A. J., & Meijer, E. W. (2000). *Supramolecular polymer materials: chain extension of telechelic polymers using a reactive hydrogen-bonding synthon*. Advanced Materials, 12(12), 874-878.

[60].   Sijbesma, R. P., Beijer, F. H., Brunsveld, L., Folmer, B. J., Hirschberg, J. K., Lange, R. F., ... & Meijer, E. W. (1997). *Reversible polymers formed from self-complementary monomers using quadruple hydrogen bonding*. Science, 278(5343), 1601-1604.

[61].   Roosma, J., Mes, T., Leclère, P., Palmans, A. R., & Meijer, E. W. (2008). *Supramolecular materials from benzene-1, 3, 5-tricarboxamide-based nanorods*. Journal of the American Chemical Society, 130(4), 1120-1121.

[62].   Croisier, E., Liang, S., Schweizer, T., Balog, S., Mionić, M., Snellings, R., ... & Frauenrath, H. (2014). *A toolbox of oligopeptide-modified polymers for tailored elastomers*. Nature communications, 5(1), 1-10.

[63].   Lacombe, J., Pearson, S., Pirolt, F., Norsic, S., D'agosto, F., Boisson, C., & Soulié-Ziakovic, C. (2018). *Structural and mechanical properties of supramolecular polyethylenes*. Macromolecules, 51(7), 2630-2640.

[64].   Litvinov, V. M., Ries, M. E., Baughman, T. W., Henke, A., & Matloka, P. P. (2013). *Chain entanglements in polyethylene melts. Why is it studied again?*. Macromolecules, 46(2), 541-547.

[65].   Park, J. H., & Rutledge, G. C. (2018). *Ultrafine high performance polyethylene fibers*. Journal of Materials Science, 53(4), 3049-3063.

[66].   Schmacke, S. (2010). *Investigations of polyethylene materials by means of X-ray Diffraction*. Technical University of Dortmund: Dortmund, Germany.

[67].   Zhao, Y., Inbar, P., Chokshi, H. P., Malick, A. W., & Choi, D. S. (2011). Prediction of the thermal phase diagram of amorphous solid dispersions by Flory–Huggins theory. Journal of pharmaceutical sciences, 100(8), 3196-3207.

[68]. Gupta, A. K., Rana, S. K., & Deopura, B. L. (1992). *Crystallization behavior of high-density polyethylene/linear low-density polyethylene blend*. Journal of applied polymer science, 44(4), 719-726.

[69]. Srinivas, S., Brant, P., Huang, Y., & Paul, D. R. (2003). Structure and properties of oriented polyethylene films. Polymer Engineering & Science, 43(4), 831-849.

[70]. Krumova, M., Henning, S., & Michler, G. H. (2006). Chevron morphology in deformed semicrystalline polymers. Philosophical Magazine, 86(12), 1689-1712.

[71]. Okabayashi, R., Ohta, Y., & Yokozawa, T. (2017). Control of Molecular Weight and End-Functional Groups of Polyester from A2+ B2 Polycondensation via Cross-Metathesis of Cyclic Unsaturated Polyester with Difunctional Olefin. Macromolecules, 50(24), 9589-9597.

[72]. Ji, S., Hoye, T. R., & Macosko, C. W. (2004). Controlled synthesis of high molecular weight telechelic polybutadienes by ring-opening metathesis polymerization. Macromolecules, 37(15), 5485-5489.

[73]. Todd, A. D., McEneany, R. J., Topolkaraev, V. A., Macosko, C. W., & Hillmyer, M. A. (2016). Reactive compatibilization of poly (ethylene terephthalate) and high-density polyethylene using amino-telechelic polyethylene. Macromolecules, 49(23), 8988-8994.

[74]. United Nations (2015). Transforming our World: The 2030 Agenda for Sustainable Development [Online] Available at: https://sdgs.un.org/goals

[75]. WCED (World Commission on Environment and Development). (1987). Our Common Future. Oxford University Press, Oxford.

ANNEX I

LINK TO SDGs

INTRODUCTION

This chapter will discuss the Sustainable Development Goals that this research project addresses. Consequently, it will heavily rely on the information provided by the United Nations' Agenda 2030 [74].

The Sustainable Development Goals are a set of 17 interconnected goals established in 2015 by the United Nations General Assembly, through the Agenda 2030, and intended to be achieved by 2030 [74]. Their aim is to promote sustainable development at a global scale by defining specific targets as well as indicators to measure the progress towards these, although they are mostly interdependent.

According to the Brundtland Report, established in 1987 by the United Nations, sustainable development is a development that "meets the needs of the present without compromising the ability of future generations to meet their own needs" [74]. It comprises three pillars: economic viability, environmental protection and social equity. In response to the challenges that this transition involved, the SDGs were designed to provide a more comprehensive plan of action for the worldwide application of these fundamental pillars.

In particular, this project addresses 8 out of the 17 Sustainable Development Goals, which will be further explained in the following sections.

ADDRESSED SDGs

In this section, the SDGs that will be addressed with the completion of this research project will be outlined and discussed, namely [74]:

8. Decent Work and Economic Growth

Decent work and economic growth focuses on "promoting sustained, inclusive and sustainable economic growth, full and productive employment and decent work for all" [74]. Being the world's most used polymer[2], polyethylene has a huge impact on the world's economy. Still, its production is linked to environmental impact, as it is not biodegradable, and therefore the current solutions involve the reprocessing of this polymer to obtain new products from used material. Therefore, the development of a process that improves this processability is key to promoting a more sustainable economic growth. In particular, polymers applied to industry are even less reprocessable because of their high mechanical performance, which often comes hand in hand with high entanglement, as is the case for UHMWPE [56]. A breakthrough in this area is key to obtaining more sustainable polymeric materials for these applications.

9. Industry, Innovation and Infrastructure

Industry, innovation and infrastructure focuses on "building resilient infrastructure, promoting inclusive and sustainable industrialization and fostering innovation" [74]. This project is focused on expanding the use of a generally commodities-applied polymer to engineering applications, therefore innovating through, in this case, supramolecular modification of polyethylene. What is more, this modification enables a more sustainable use of the polymer at hand, and offers a good substitution to the current approaches, which involve non-reprocessable polymers, such as UHMWPE, or other materials.

12. Responsible Consumption and Production

Responsible consumption and production focuses on "taking urgent action to combat climate change and its impacts". An important step towards responsible consumption and production is the promotion of circular use of materials. With this project, the aim is to obtain a high-performance polymer that is still easily reprocessable, in order to tackle the challenge that is usually involved in this property-processability tradeoff.

ANNEX II

SUPPLEMENTARY RESULTS

SUPPLEMENTARY DATA

This Annex will contain additional primary data that was obtained, and that may serve to better understand the procedure and discussions in this project.

SYNTHESIS AND CHARACTERIZATION OF MATERIALS

NMR DATA

The synthesized compounds were characterized using NMR experiments.

NMR of PE$_{30}$(AA)$_2$

Figure 51 shows the NMR characterization of the PE$_{30}$(AA)$_2$ synthesized materials, indicating all the relevant peaks with red letters.
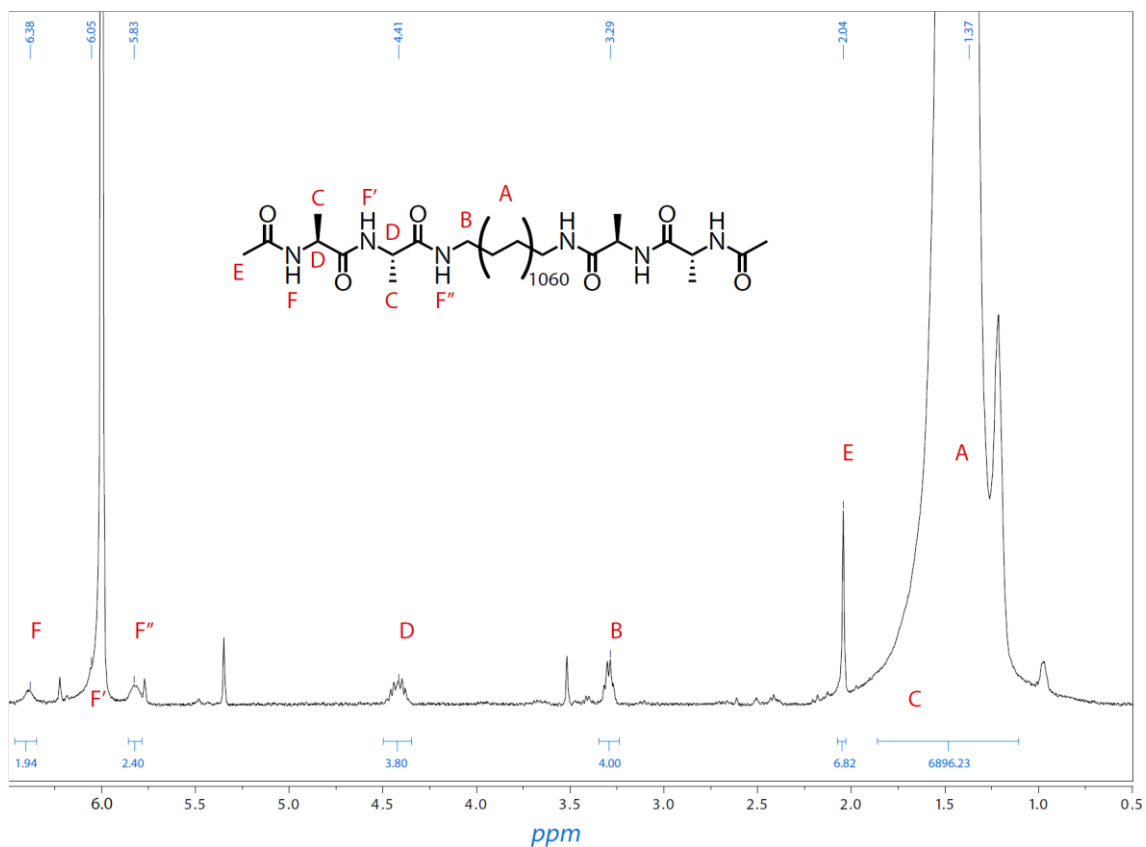
Figure 51. NMR characterization of PE$_{30}$(AA)$_2$.

NMR of PE$_{100}$(AA)$_2$

Figure 52 shows the NMR characterization of the PE$_{100}$(AA)$_2$ synthesized materials, indicating all the relevant peaks with red letters. The peaks at 4 and 7.7 ppm are probably due to chlorination byproducts from the TCE. The peak at 7.4 is residual Toluene.
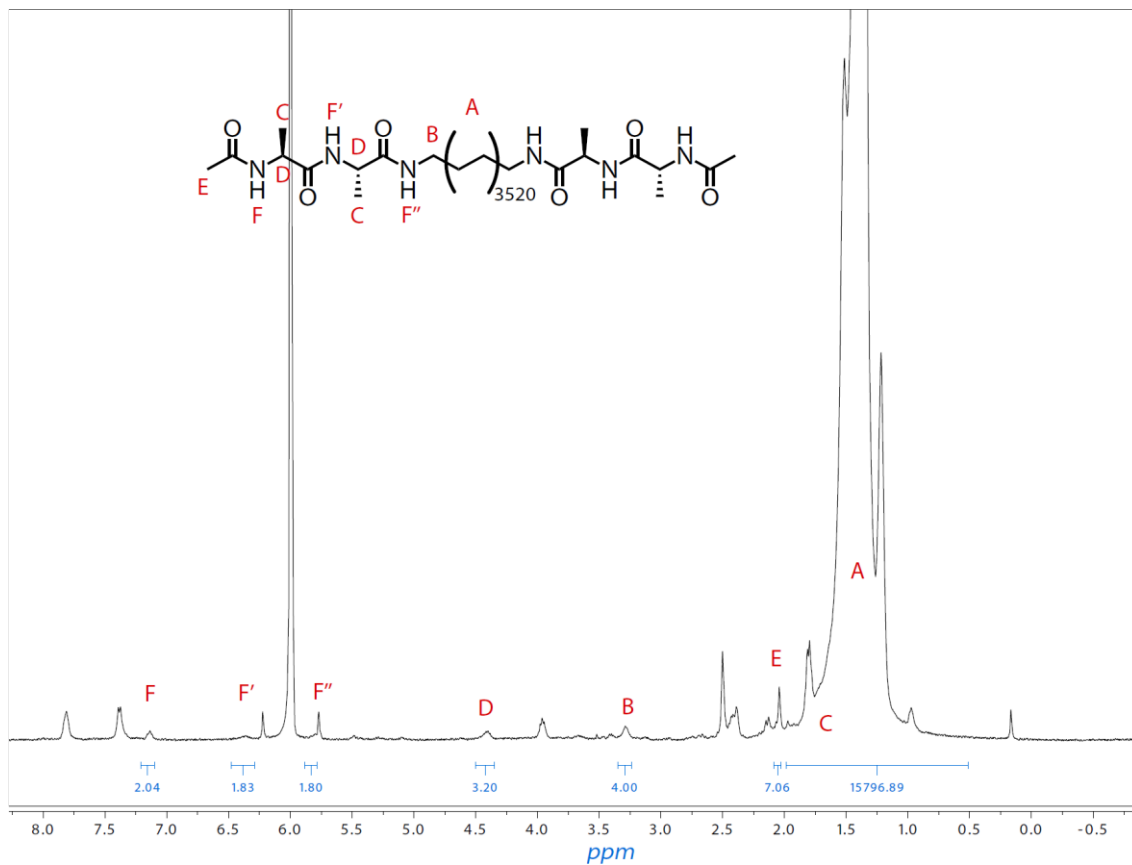
Figure 52. NMR characterization of PE$_{100}$(AA)$_2$.

NMR of (AA)C$_8$

Figure 53 shows the NMR characterization of the (AA)C$_8$ synthesized additives, indicating all the relevant peaks with red letters.
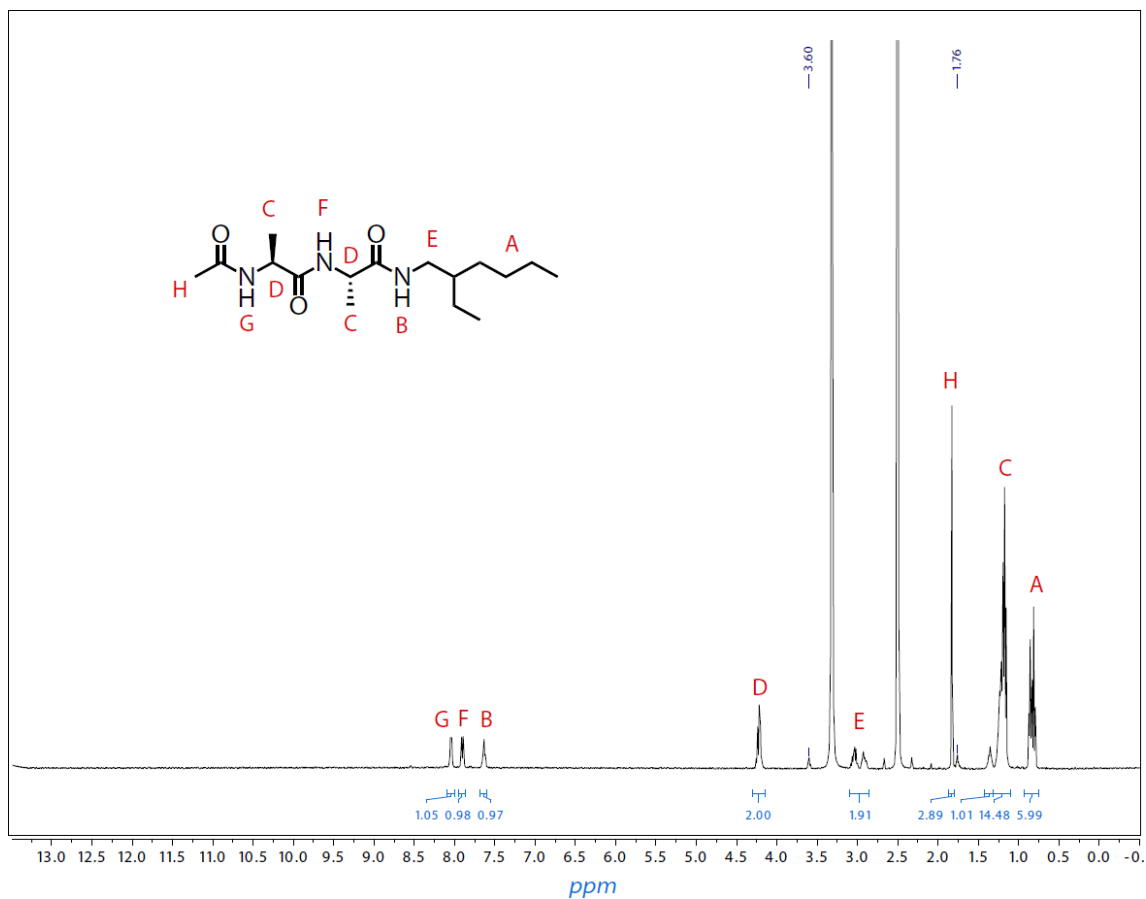
Figure 53. NMR characterization of (AA)C$_8$.

NMR of (AA)C$_{20}$

Figure 54 shows the NMR characterization of the (AA)C$_{20}$ synthesized additives, indicating all the relevant peaks with red letters.
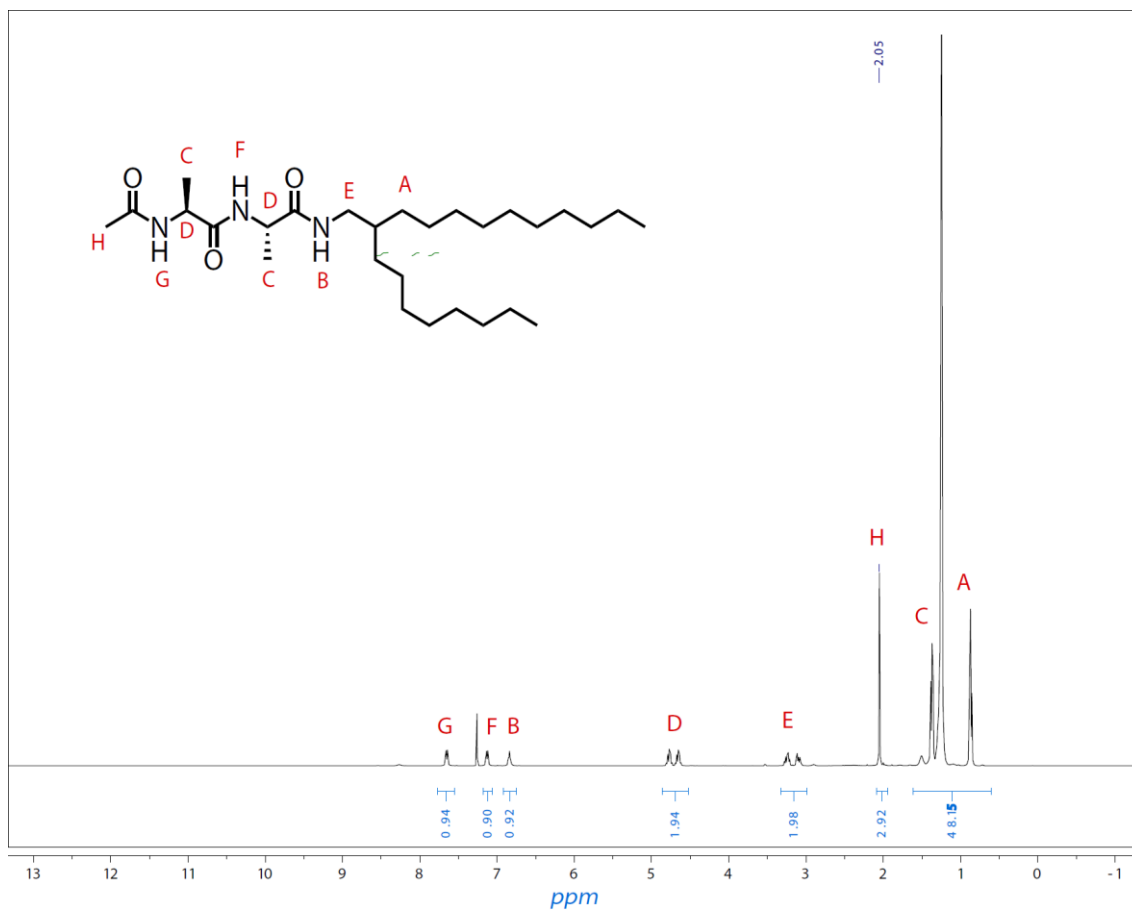
Figure 54. NMR characterization of (AA)C$_{20}$.

OPTICAL MICROSCOPY DATA

Apart from the micrographs showed in the main text, temperature-dependent optical microscopy experiments were performed on both concept and reference materials for 1, 2, 4 and 8 wt% blends, cooling from the fully molten state.
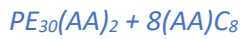
PE$_{30}$(AA)$_2$ + 1(AA)C$_8$

Figure 55 shows the micrographs obtained during the cooling of both reference and concept materials of the 1 wt% blends from the fully molten state.
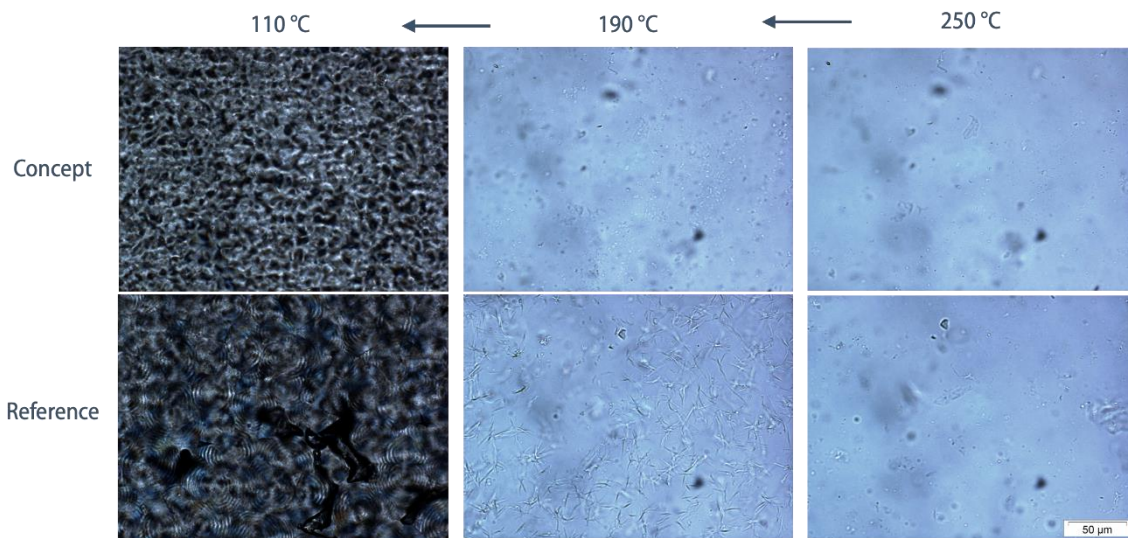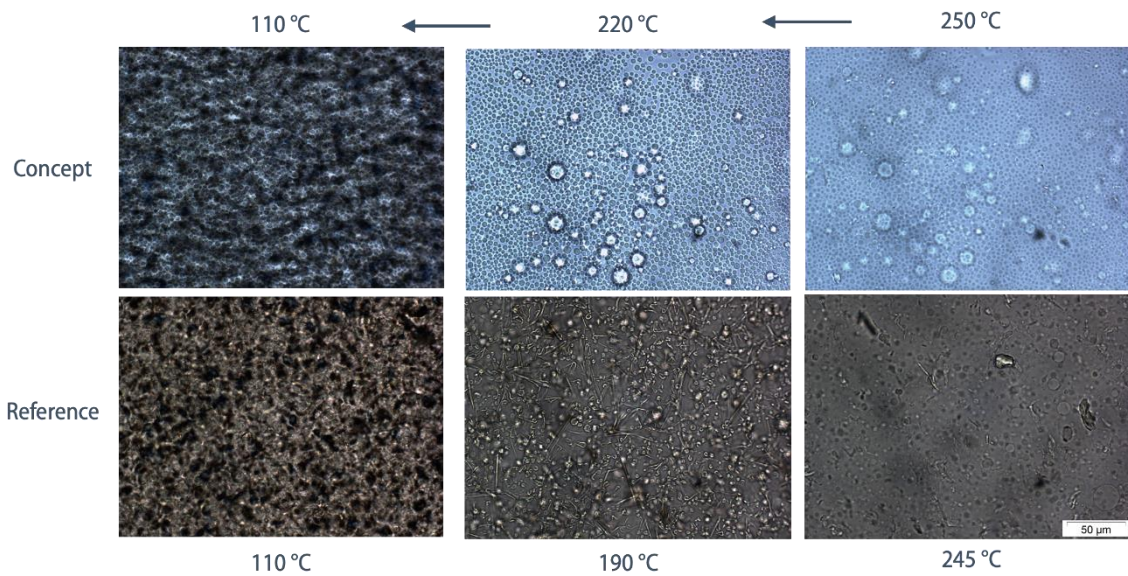
Figure 55. Micrographs of the 1 wt% blends.

PE$_{30}$(AA)$_2$ + 2(AA)C$_8$
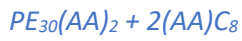
Figure 56 shows the micrographs obtained during the cooling of both reference and concept materials of the 2 wt% blends from the fully molten state.
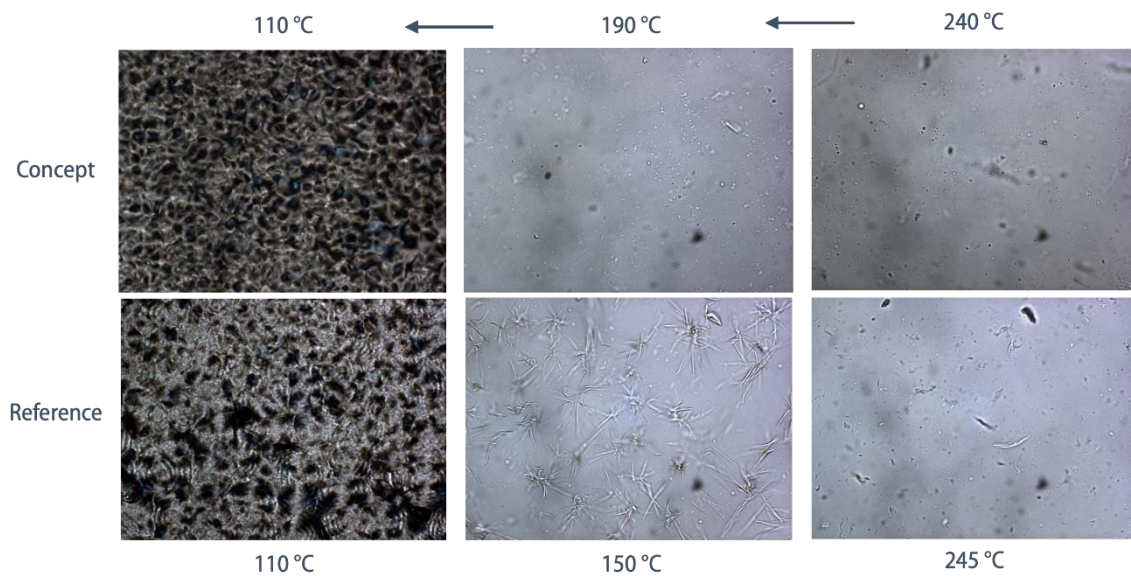
Figure 56. Micrographs of the 2 wt% blends.

PE$_{30}$(AA)$_2$ + 4(AA)C$_8$
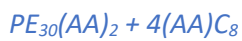
Figure 57 shows the micrographs obtained during the cooling of both reference and concept materials of the 4 wt% blends from the fully molten state.
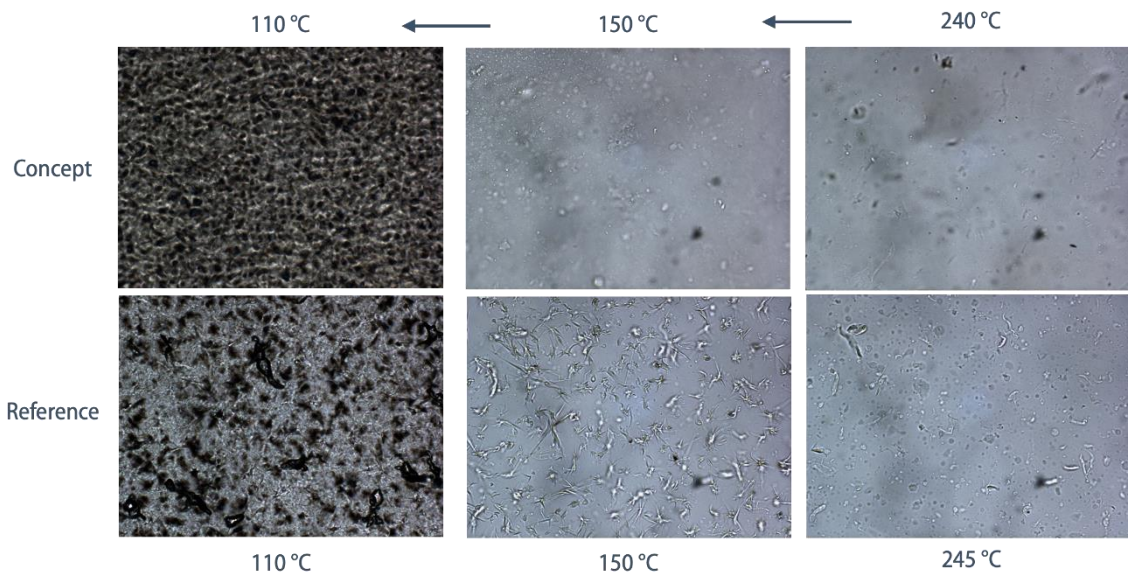
Figure 57. Micrographs of the 4 wt% blends.

PE$_{30}$(AA)$_2$ + 8(AA)C$_8$

Figure 58 shows the micrographs obtained during the cooling of both reference and concept materials of the 8 wt% blends from the fully molten state.

Figure 58. Micrographs of the 8 wt% blends.

CHARACTERIZATION OF ALIGNED SAMPLES

XRD DATA

As previously explained, the XRD data was processed to obtain comparable curves that could be fitted to a Gaussian. This section will show the original curves.

94

Azimuthal integration of AS220 SAXS experiment

Figure 59 shows the original curves for the azimuthal integration of the maximum peaks in the SAXS experiments of AS220 fibers. The pronounced dips in the curve correspond to the fixation points of the sample to the experimental set, and therefore they were eliminated for the correct analysis of the results.
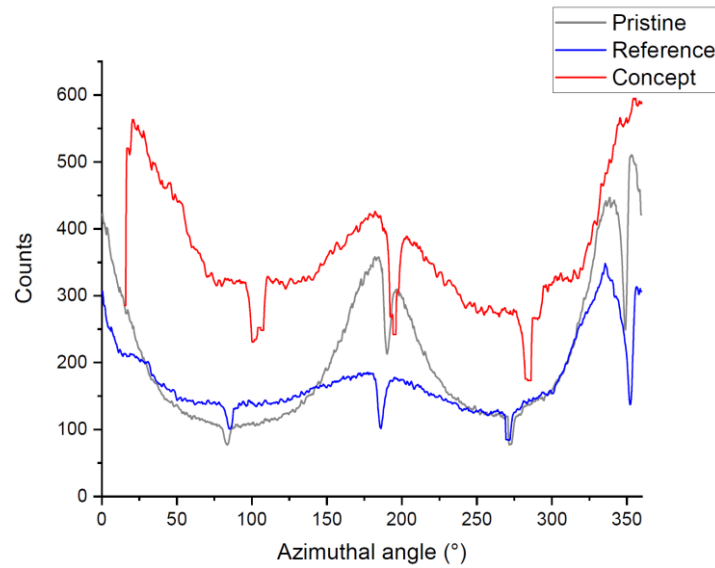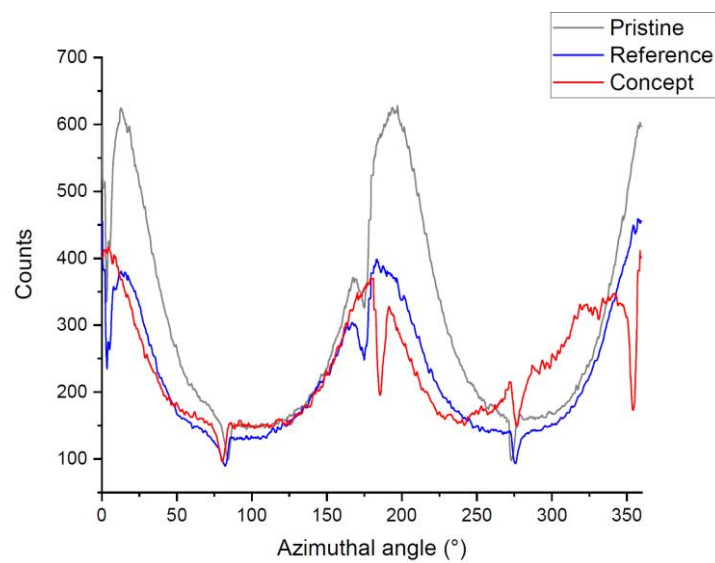

Figure 59. Original curve for the azimuthal integration of the XRD SAXS experiments for the AS220 fibers.

Azimuthal integration of AS190 SAXS experiment

Figure 60 shows the original curves for the azimuthal integration of the maximum peaks in the SAXS experiments of AS190 fibers. The pronounced dips in the curve correspond to the fixation points of the sample to the experimental set, and therefore they were eliminated for the correct analysis of the results.
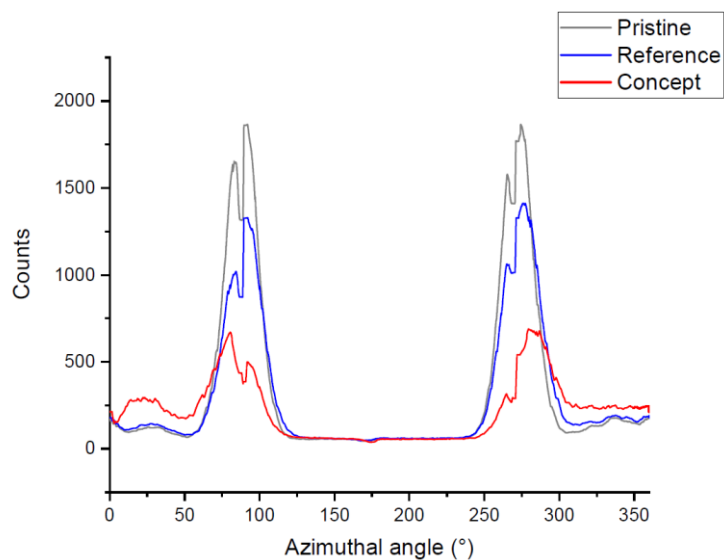

Figure 60. Original curve for the azimuthal integration of the XRD SAXS experiments for the AS190 fibers.

Azimuthal integration of CS190 SAXS experiment

Figure 61 shows the original curves for the azimuthal integration of the maximum peaks in the SAXS experiments of CS190 fibers. The pronounced dips in the curve correspond to the fixation points of the sample to the experimental set, and therefore they were eliminated for the correct analysis of the results.
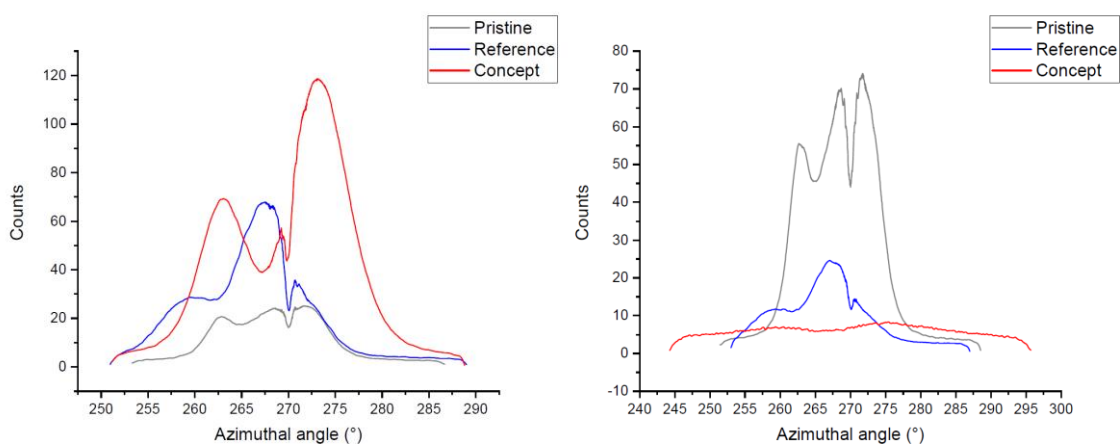

Figure 61. Original curve for the azimuthal integration of the XRD SAXS experiments for the CS190 fibers.

Azimuthal integration of CS190 WAXS experiment

Figure 62 shows the original curves for the azimuthal integration of the maximum peaks in the WAXS experiments of CS190 fibers. The pronounced dips in the curve correspond to the fixation points of the sample to the experimental set, and therefore they were eliminated for the correct analysis of the results.

Figure 62. Original curve for the azimuthal integration of the XRD WAXS experiments for the CS190 fibers.

TENSILE TESTING DATA

The tensile testing results are a product of statistical analysis of the raw data. This data is represented in the following curves.

Stress-strain curves of AS220

Figure 63 represents the original tensile test curves for the AS220 fibers. The dips that appear throughout the length of the curves are due to the various necking points within the fiber.
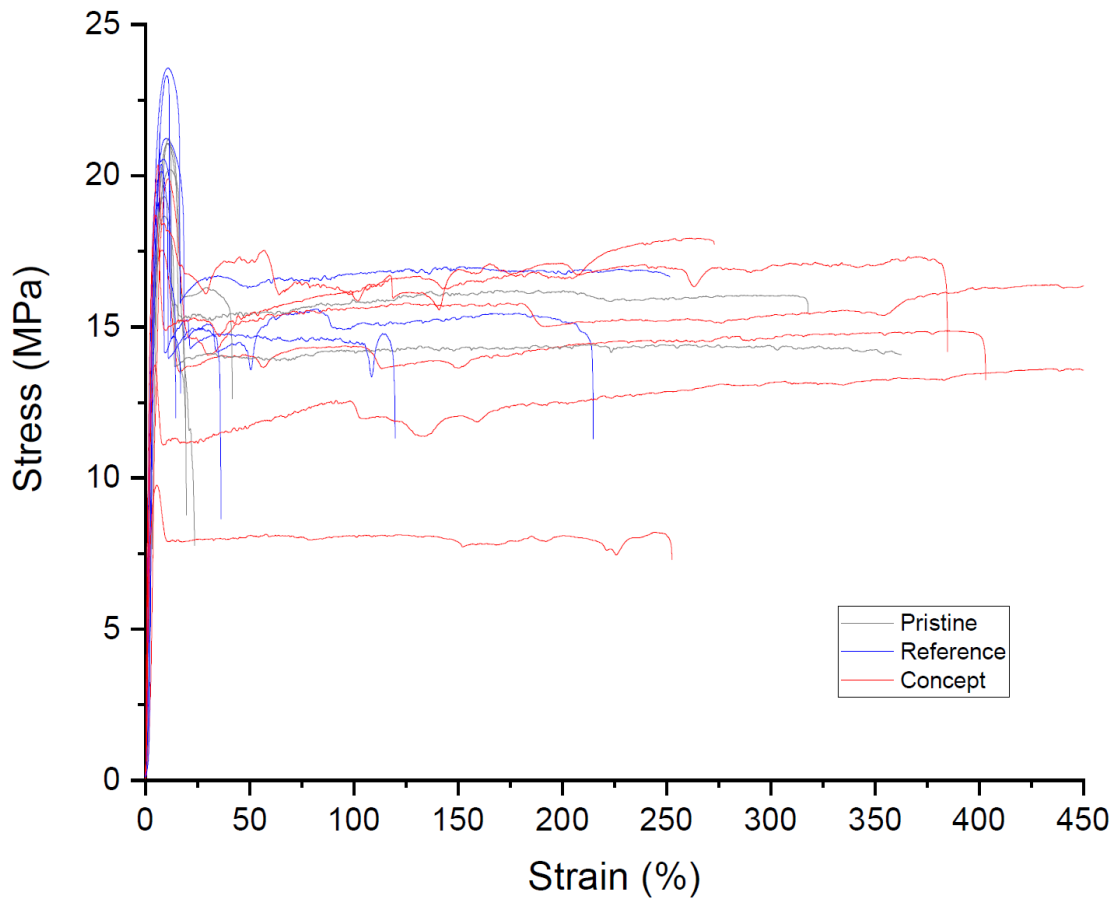

Figure 63. Original tensile curves for the AS220 fibers.

Stress-strain curves of AS190

Figure 64 represents the original tensile test curves for the AS190 fibers. The dips that appear throughout the length of the curves are due to the various necking points within the fiber.
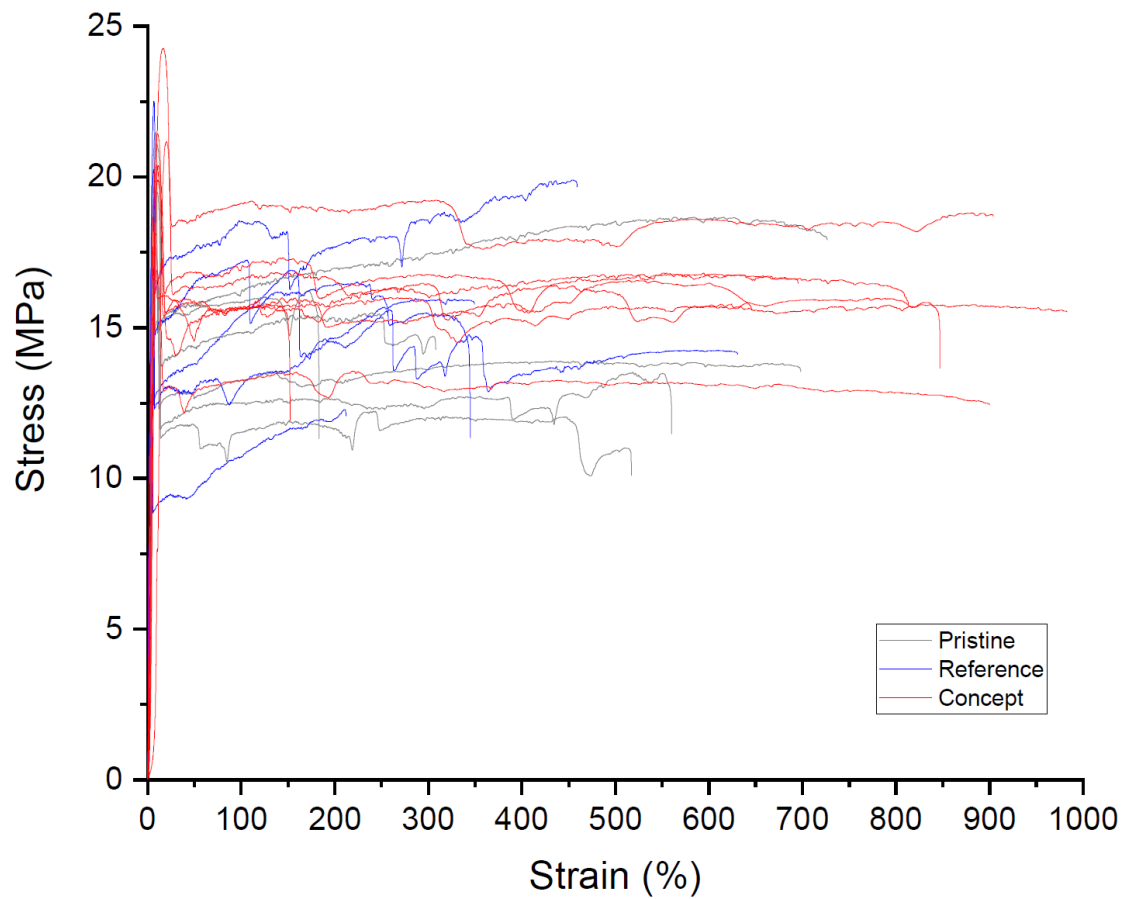
Figure 64. Original tensile curves for the AS190 fibers.

Stress-strain curves of CS190

Figure 65 represents the original tensile test curves for the CS190 fibers. The dips that appear throughout the length of the curves are due to the various necking points within the fiber.
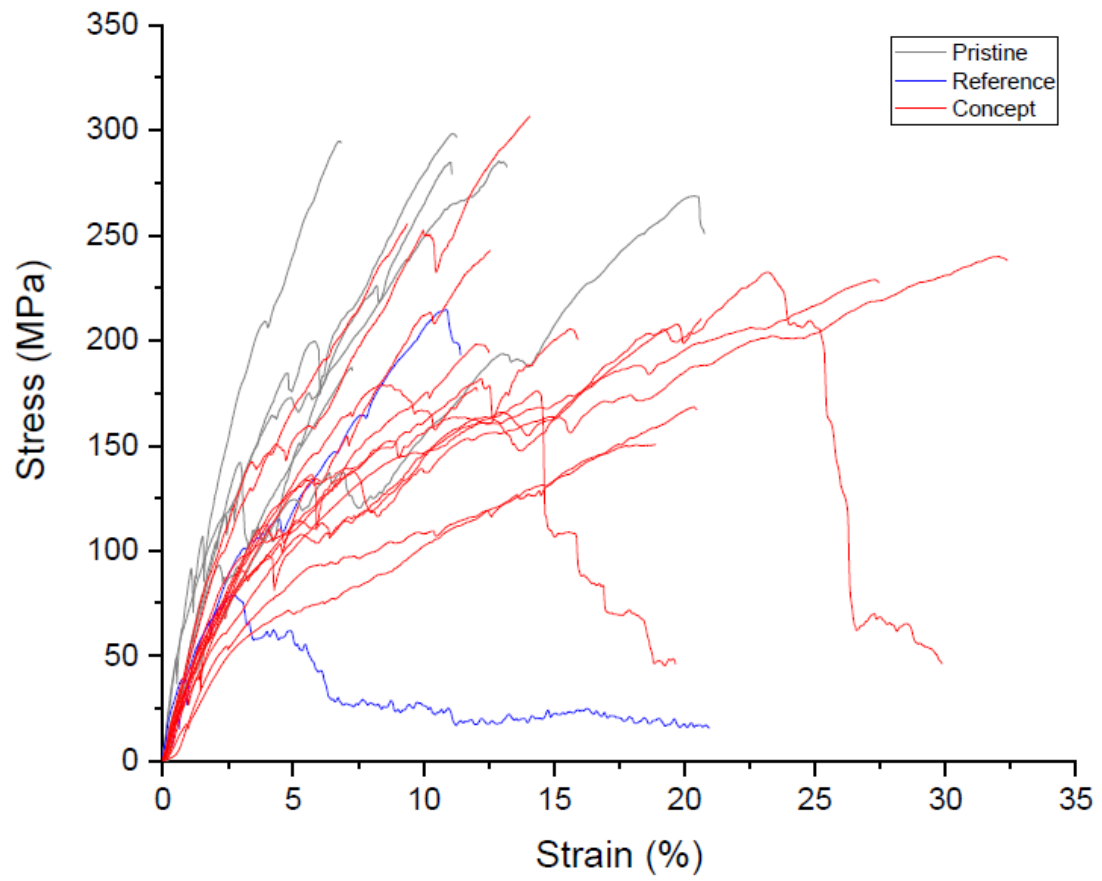
Figure 65. Original tensile curves for the CS190 fibers.